2014

Modeling of Foam Flow in Porous Media for Subsurface Environmental Remediation

Seungjun Lee
Louisiana State University and Agricultural and Mechanical College, slee95@lsu.edu

MODELING OF FOAM FLOW IN POROUS MEDIA FOR SUBSURFACE ENVIRONMENTAL REMEDIATION

A Dissertation

Submitted to the Graduate Faculty of the
Louisiana State University and
Agricultural and Mechanical College
in partial fulfillment of the
requirements for the degree of
Doctor of Philosophy

in

The Craft & Hawkins Department of Petroleum Engineering

by
Seungjun Lee
B.S., Hanyang University, South Korea, 2006
M.S., The University of Texas at Austin, 2009
August 2014

ACKNOWLEDGEMENTS

My deepest thanks should go to my supervisor, Dr. Seung Ihl Kam, for continually challenging me and always answering my questions kindly. I have been very fortunate to study and learn under his kind and insightful supervision. Working with him, I have gained a lot of valuable knowledge in organizing and solving problems.

I am also very thankful to my committee members, Dr. Arash Dahi Taleghani, Dr. Karsten Thompson, Dr. Frank Tsai, and Dr. Shahab Mehraeen, for their valuable comments and suggestions which have led this study in the right direction.

I would like to express my gratitude to Rural Research Institute (RRI), SK innovation, and Craft and Hawkins Department of Petroleum Engineering for financial support for my research. In particular, I would like to thank Dr. Gyu Sang Lee at RRI for helping me visit the remediation sites in South Korea. Without their support, this study could not have been initiated and continued.

Although some coreflood experiments I carried out during my study are not a part of this dissertation, I am thankful to Mr. Fenelon Nunes for helping me set up and perform flow tests. Also, I would like to thank to all foam group members I have worked with.

Finally, much love to my parents and two sisters who have always encouraged and believed in me; and very special thanks to my sweet wife, Minjung Kim, for her patience, understanding, and love!

TABLE OF CONTENTS

LIST OF TABLES

LIST OF FIGURES

ABSTRACT

Among numerous foam applications in a wide range of disciplines, foam flow *in porous media* has been spotlighted for improved/enhanced oil recovery processes in petroleum-bearing geological formations and shallow subsurface in-situ NAPL (non-aqueous phase liquid) environmental remediation in contaminated soils and aquifers. In those applications, foams are known to reduce the mobility of gas phase by increasing effective gas viscosity and improve sweep efficiency by mitigating subsurface heterogeneity.

This study investigates how surfactant/foam process works fundamentally for environmental remediation purpose by using MoC (Method of Characteristics) based foam modeling and simulation techniques. It consists of two main parts: Part 1, developing foam model using three-phase fractional flow theory accounting for foam flow rheology such as foam strength and stability at different phase saturations; and Part 2, extending the model to investigate the mechanisms of surfactant/foam displacement in multi-layer systems.

Part 1 investigates six scenarios such as different levels of foam strength (i.e., gas mobility reduction factors), different initial conditions (i.e., initially oil/water or oil/water/gas present), foam stability affected by water saturation (S_w), oil saturation (S_o), and both together, and uniform vs. non-uniform initial saturations. The process is analyzed by using ternary diagrams, fractional flow curves, effluent histories, saturation profiles, time-distance diagrams, and pressure and recovery histories. The results show that the three-phase fractional flow analysis presented in this study is robust enough to analyze foam-oil displacements in various conditions, as validated by an in-house numerical simulator built in this study. The use of numerical simulation seems crucial when the foam modeling becomes complicated and faces multiple possible solutions.

Part 2 first shows how to interpret theoretically the injection of surfactant preflush and following foams into a single-layer system at pre-specified rock and fluid properties, and then extends the knowledge gained into multi-layer systems where the properties vary in different layers. The results in general show that the mechanisms of foam displacement strongly depend on foam properties such as gas-phase mobility reduction factors (MRF), limiting water saturation (S_w*), critical oil saturation (S_o*), and so on as well as petrophysical properties of individual layers such as porosity (ϕ), permeability (k), relative permeability and so on. The overall sweep efficiency in a multi-layer system is very difficult to predict because of the complexity, but the mathematical framework presented in this study is shown to be still reliable. The in-house foam simulator is also extended to compare with modeling results.

CHAPTER 1
INTRODUCTION

1.1 Background

Subsurface contamination has been a significant concern as the number of surface/subsurface storage tanks increases. The use of storage tanks is a common method to manage liquid-based chemicals and wastes. Those tanks may fail over the years, however, causing a leakage of contaminants and resulting in soil and ground water pollution above and/or below water table. Hydrocarbon liquid-based contaminants, often called NAPLs (non-aqueous phase liquids), are most typical, consisting of various types of oils such as gasoline, diesel, TCE (trichloroethylene), and PCE (tetrachloroethylene or perchloroethylene). Depending on the density, NAPLs can be further classified into LNAPLs (light non-aqueous phase liquids) and DNAPLs (dense non-aqueous phase liquids). Figure 1.1 and Figure 1.2 schematically show different types of contaminant sources encountered and their mechanisms of subsurface trapping and migration.

A number of different types of remedial methods have been developed to resolve these subsurface environmental issues: pump and treat, soil vacuum extraction, soil flushing, surfactant flooding, and foam injection to name a few (U.S. EPA, 1990 and 2004; Rothmel et al., 1998). Each remediation technique has its own difficulties and limitations, however.

This study is a part of collaborative research with Rural Research Institute (RRI), a research organization under Korea Rural Community Corporation, which handles the majority of the in-situ subsurface remediation projects in South Korea. Initially dealing with shallow contaminated area mainly using ex-situ excavation remediation method, RRI moves into in-situ remediation

methods which can be applicable to deeper formations and zones under existing structures (residential and commercial buildings, roads, levies, and so on). Overcoming subsurface heterogeneity during in-situ remediation treatments using foam/surfactant injection is regarded as a potential and promising solution in actual field-scale applications.

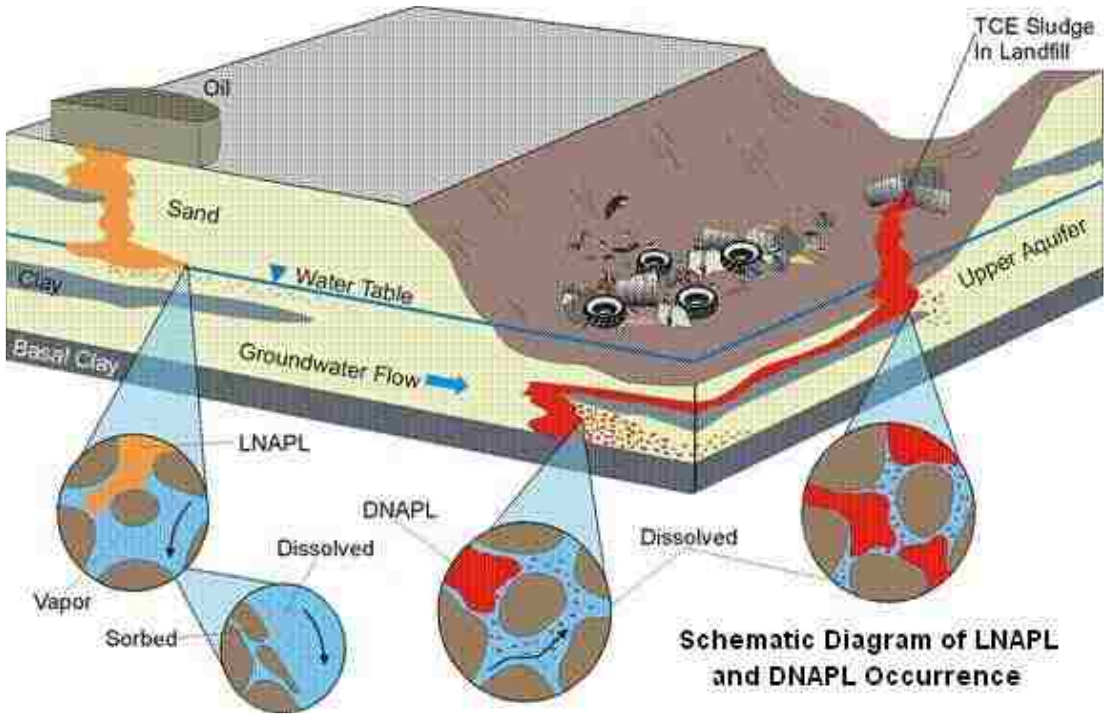

Figure 1.1: A schematic diagram of subsurface contamination (www.afcee.af.mil)

The entire scope of this collaborative work with RRI is made up of three major components: (1) understanding the mechanisms of surfactant/foam processes in the presence of NAPL contaminants; (2) extending the foam model and simulation techniques developed into the geological system with heterogeneity (i.e., a systems with non-communicating layers with different permeability); and (3) applying the gained knowledge into the field-scale multi-dimensional remediation treatments. As a first step, this study focuses on the first two components dealing with fundamentals of surfactant/foam processes as described more in the following section.

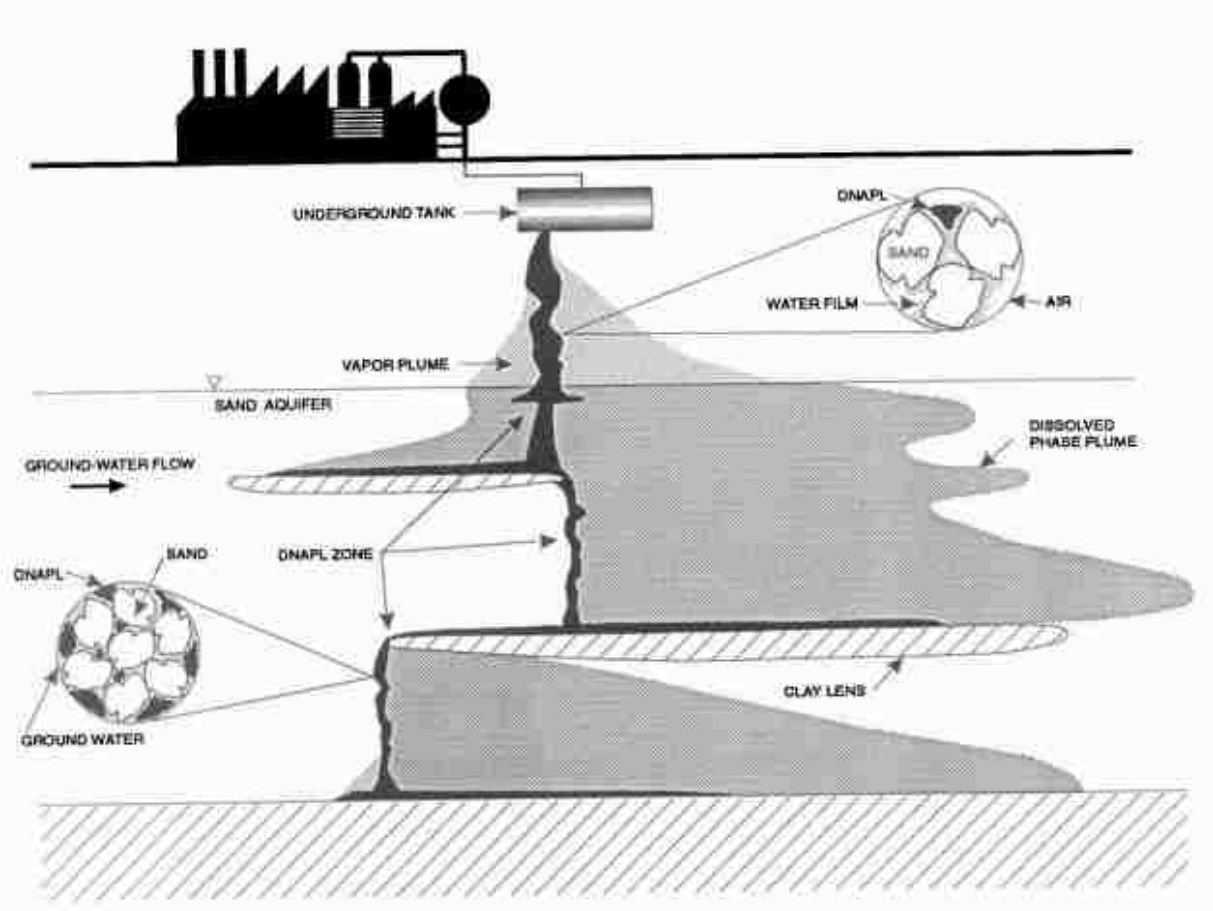

Figure 1.2: A typical migration and distribution of DNAPL (Jackson, 1993)

1.2 Objectives of this study

The objectives of this study are aligned with the first two components of the RRI's scope as explained earlier. More specifically, there are two main tasks: (1) Task 1, establishing the mathematical framework about how surfactants and foams propagate in porous media interacting with contaminants with different properties and evaluating the displacement performance of the process in one-dimensional space, in order to investigate the wide range of interactions between foams and NAPLs in remediation treatments, and (2) Task 2, developing models to describe how such a process works in a system with non-communicating multiple geological layers, in order to

evaluate foam/surfactant flow experiments in the similar conditions within the RRI's field-scale laboratory. In all these tasks, a mathematical tool called Method of Characteristics (MoC) is applied, and its analytical solutions are compared with the results from in-house developed foam simulator written in Fortran language.

Modeling and simulation of surfactant/foam processes require a wide range of input parameters: initial conditions in terms of phase saturations, injection conditions in terms of flowing phase fractions, foam properties (i.e., mobility reduction factor (MRF), limiting water saturation (S_w*), and critical oil saturation (S_o*)) and other rock and fluid properties (i.e., porosity, permeability, relative permeability, surfactant adsorption, etc.). Analyzing the displacement mechanism can be carried out by using three-phase fractional flow analysis based on Method of Characteristics (MoC). The results are present in terms of saturation paths in ternary diagram and so-called Walsh diagram consisting of fractional flow curves, effluent history, saturation profile, and time-distance diagram.

1.3 Chapter description

The contents of this study are summarized as follows:

Chapter 1 describes an introduction of the problem investigated in this study followed by objectives.

Chapter 2 provides the background and previous studies related to foam flow in porous media, especially those associated with surfactant/foam remediation techniques.

Chapter 3 presents the first main part of this study, that is, analytical and numerical solutions developed for foam flow in porous media in presence of NAPLs. A significant portion

in the chapter is dedicated to understanding the roles of foam characteristic on displacement process. Chapter 4 presents the second main part of the study, that is, foam flow in a non-communicating multi-layered system where subsurface heterogeneity is represented by a combination of multiple horizontal layers with differing properties. The focus of this chapter is made on how fluid injectivity into each layer changes with time during surfactant preflush and subsequent foam injection.

Chapter 5 covers a sensitivity study for some of the modeling and simulation parameters, including relative permeabilities and foam stability.

Chapter 6 provides major conclusions from this study and recommendations for future studies.

CHAPTER 2
LITERATURE REVIEW

Foams have been used in a wide range of applications. Among those, foam propagation in complex pore structures has been of great interest for decades to improve and enhance oil recovery in petroleum industry (Schramm, 1994; Prud'Homme and Khan, 1996; Rossen, 1996). An extension of such a technique can also be found in subsurface environmental remediation. Once present in porous media, foams are shown to effectively clean up the media with reduced gas mobility and improved sweep efficiency.

Previous studies show that numerous subsurface contaminants can be originated from various sources, for example, a leakage from pipelines, failure of surface and underground storage tanks, an inappropriate disposal of wastes and so on (Mackay and Cherry, 1989, Londergan et al., 2001). Many different types of contaminants are reported such as gasoline, diesel, trichloroethylene (TCE), perchloroethene (PCE), benzene, metals, radioactive wastes, to name a few, which should be treated or removed properly. These liquid types of contaminants are categorized into two groups: light non-aqueous phase liquids (LNAPLs), such as gasoline and diesel, and dense non-aqueous phase liquids (DNAPLs), such as chlorinated solvents, wood preservative wastes, coal tar wastes and pesticides. The chemical structure of chlorine-containing compounds helps them to dissolve organic materials efficiently and to be used as raw materials or intermediates in the production of other chemicals. Therefore, majority of DNAPL contaminants is those chlorinated solvents.

In order to clean up the contaminated soils and groundwater by those NAPLs, many different types of techniques have been developed and used. Typically, these methods could be largely grouped into two types: ex-situ and in-situ remediation methods.

An ex-situ method is usually considered if contaminated area is relatively small or shallow and easy to access, and if the concentration of the contaminants is high. This method takes the soils out of the contaminated area and then transports them to the processing facilities or sites for physical and chemical treatments. The transported soils are flushed with cleaning chemicals to wash them by chemical reaction or physical disturbance. Mulligans et al. (2001) showed that ex-situ remediation is better for sands with less amount of clay-mineral and organic substance, typically 10 to 20%. Ex-situ remediation techniques can be very inefficient and challenging, however, if the contaminated area is large or deep or the contaminants with low concentration covers a relatively wide area. These limitations of ex-situ methods have led the development and application of in-situ remediation methods.

In general, in-situ methods are categorized by three types: volatilization techniques, flushing methods, and thermal processes (U.S. EPA., 1990; Fountain, 1998). Since thermal techniques such as steam injection, electrical heating or in-situ vitrification involve modification of formation temperature, only volatilization and flushing methods are described in this study.

First, typical volatilization methods are soil vapor extraction (SVE), air sparging and in-well stripping (Staudinger et al., 1997; Lundergard and LaBrecque, 1995; Miller, 1996). Crow et al. (1987) evaluated soil vapor extraction (SVE) to control and remove hydrocarbon vapors from a subsurface formation. This method uses vacuum pumps at extraction well to withdraw air from wells so that it allows atmospheric air to enter the subsurface formation. Air may, or may not, be

injected in other wells. A combination with thermal enhancement or biodegradation can improve the process. Also, it is noted that this technique may be used for conventional liquid recovery. Air sparging is simply air injection below water table and typically cooperated with SVE to clean both vadose and saturated zones. In-well stripping involves pumping of contaminated water from the target area into a well, and then pumping atmospheric air from the surface to sparge the water in the well. Therefore, the contaminants are cleaned by volatilization within the well casing, then the water is pumped back out of the well through screens.

Second, flushing technology includes water injection (so-called pump-and-treat), alcohol or cosolvent injection, surfactant injection and in-situ oxidation (Fountain, 1998). Pump-and-treat is the most widely applied method for in-situ subsurface remediation because it simply injects water to displace subsurface contaminants. It is now known, however, that remediation of contaminated areas by pump-and-treat may take a significant amount of time, as much as decades to centuries, because NAPLs are trapped by capillary forces in porous media with often negligible solubility to water (NRC, 1994; Taber, 1969; Haley et al., 1991). Such a limitation of pump-and-treat can be greatly enhanced by using surfactant injection, so-called surfactant-enhanced aquifer remediation (SEAR), which reduces residual contaminants by lowering capillary force and improving NAPL's solubility (Jackson, 1993; Oolman et al., 1995; Londergan et al., 2001). For example, Oolman et al. (1995) considered a pump-and-treat system with surfactant solution to clean up a pool of DNAPL containing TCE and other chlorinated solvents from the subsurface at Hill Air Force Base, Utah. Their coreflooding experiments, however, showed that approximately one-third of the DNAPL initially present was not recovered by water injection. With 2 pore volume of subsequent surfactant injection, the remaining oil saturation was reduced down to one order of magnitude less. Their field test was reported to be successful by recovering more than 23,000

gallons of DNAPL in one million gallons of contaminated ground water by using both pump-and-treat and SEAR. Cosolvent/alcohol flooding is similar to SEAR. It lowers interfacial tension with DNAPL and provides efficient recovery. In-situ oxidation can be applicable for those contaminants readily oxidized such as chlorinated solvents and gasoline-related compounds, but its performance may be limited by the difficulties of handling acids and by the presence of oxidation-resistant contaminants.

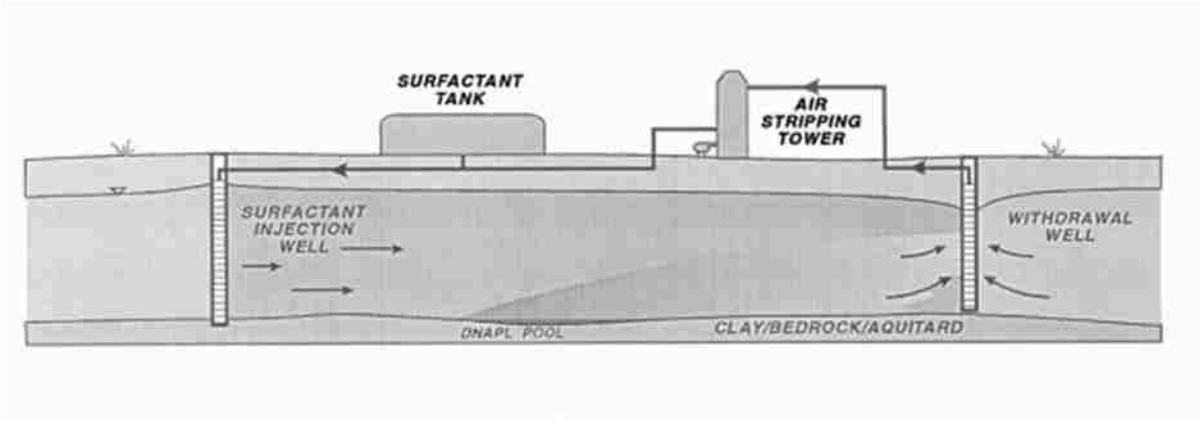

Figure 2.1: A schematic design of a surfactant enhanced aquifer remediation (SEAR) operation (Jackson, 1993)

Figure 2.1 shows a schematic of SEAR operation showing a single surfactant injection well and a single extraction well. A similar design can equally be accommodated for cosolvent/alcohol flooding as well as pump-and-treat. These various in-situ remediation methods unfortunately have been shown to be applied with limited success in actual field treatments. Among many, subsurface heterogeneity has been regarded as a major impediment, because it hinders the injected fluids from contacting the contaminants in less permeable areas.

A literature review reveals successful foam-assisted remediation treatments for both LNAPLs and DNAPLs (Peters et al., 1996; Hirasaki et al., 1997; Hirasaki et al., 2000; Mamum et

al., 2002) even in the presence of permeability contrasts. The benefit of using foams for NAPL remediation comes from its versatility (Lee and Kam, 2013): first, by mixing both gas phase and surfactant-laden aqueous phase, the resulting mixture forms dispersed bubbles isolated by thin foam films, essentially alleviating gravity segregation (i.e., the gas phase that tends to migrate upward is blocked); second, although aqueous phase flows into smaller pores and gas phase flows into large pores, as is the case of conventional two-phase flow, the gas phase moving together with foam films experiences a dramatic increase in viscosity due to the drag of films at the pore wall. This increase in effective gas viscosity (or, decrease in gas mobility, equivalently) greatly enhances the stability of the displacement front preventing viscous fingering; third, although foam flows into the high-permeability region preferentially at the beginning of foam injection, the low capillary pressure environment contributes to the formation of more stable foams, diverting subsequent foams into the low permeability region where capillary pressure is high. In other words, foam diversion into the low permeability regions is endowed by foam's sensitivity to capillary pressure which counteracts with permeability.

Hirasaki et al. (1997) demonstrated field application of surfactant/foam for DNAPL remediation in heterogeneous formation at Hill Air Force Base in Utah. The injected surfactant solution was intended to mobilize and solubilize the contaminants at the bottom of aquifer, and subsequently injected foam was designed to divert following surfactant solution to low permeability zones by blocking high permeability zones. After surfactant/foam process, the average DNAPL saturation in the field was reduced from 0.3% down to 0.03%. Figure 2.2 shows a similar example from foam deep-vadose-zone remediation showing how foam works in the presence of high permeability streaks in highly heterogeneous porous media.

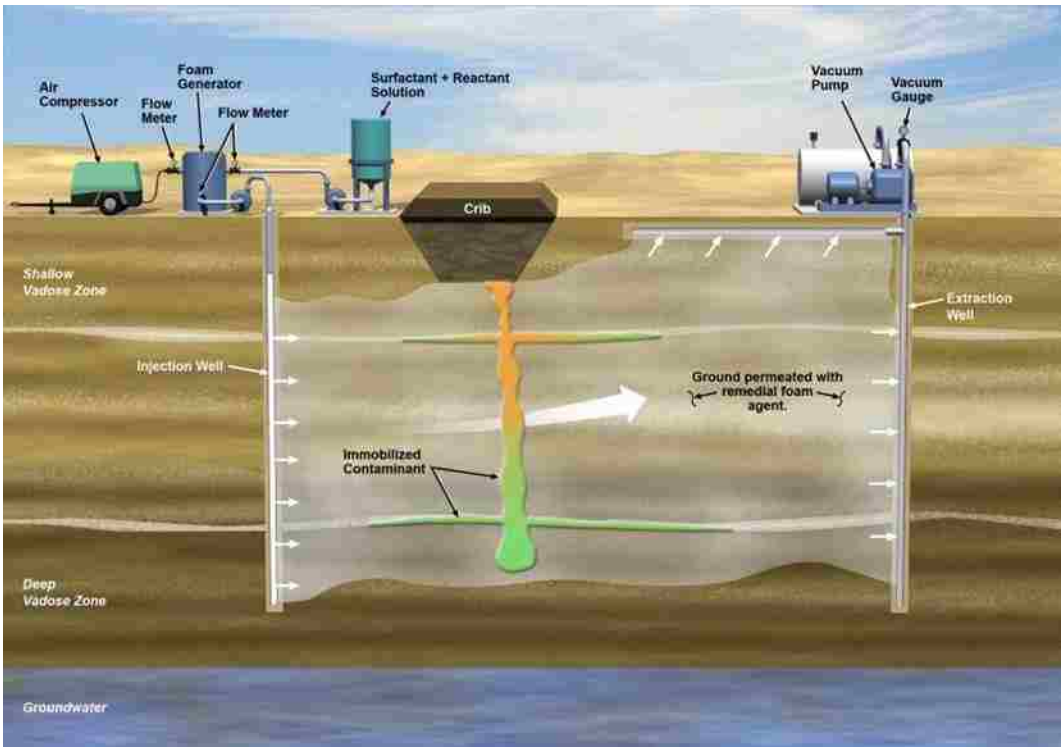

Figure 2.2: In-situ foam-assisted remediation operations in deep-vadose zones (www.pnl.gov)

It is necessary to define what foam is in order to understand what foam does and how foam flows in porous media. Foam is a dispersion of gas bubbles in a continuous liquid phase while gas bubbles are disconnected by thin liquid films, so-called lamellae (Rossen, 1996). Therefore, thin liquid films, or foam films, are surrounded by gas from both sides and surfactant molecules in the liquid help those films to be stable. Typically, foam film thickness ranges from only few nano meters to micro meters (Bergeron et al., 1993; Farajzadeh et al., 2008). Unlike "bulk" foam in open space (e.g., within a pipe, in a cup, etc.), foam in "porous media" has a gas-bubble size smaller than the characteristic length of the flow conduits (i.e., pore body size). In water-wet system, the surfactant-dissolved liquid phase tends to coat grain surfaces and be connected as wetting films, while the gas phase tends to be dispersed and isolated by the liquid films, as schematically shown in Figure 2.3.

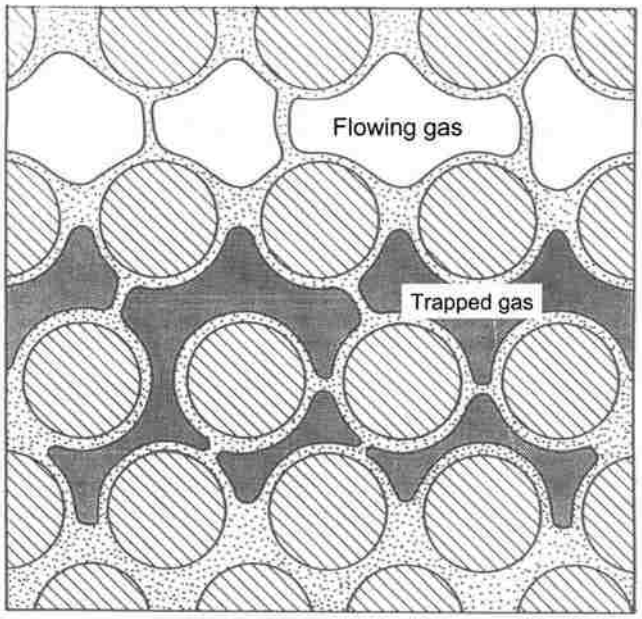

Figure 2.3: A schematic of foam structure in porous media (Kovscek and Radke, 1994)

While flowing in porous media, foam films may generate and collapse, which is, often to be referred as dynamic in-situ mechanisms of lamella creation and coalescence. Typically, foams are created by snap-off, lamella division and leave-behind mechanisms (Kovscek and Radke, 1994). Roof (1970) first identified snap-off, a repetitive bubble generation process that depends on the level of fluctuation in capillary pressure. It happens when gas phase first enters a narrow pore throat initially filled with water and subsequently the gas phase comes out of the pore throat (i.e., an increase in capillary pressure first, followed by a sufficient decrease in capillary pressure). Lamella division takes place when existing foam films are mobilized by enough pressure gradient and divided into multiple films at the downstream pore junctions. Leave-behind mechanism describes liquid lenses (which may thin down to foam films in the presence of surfactant molecules when capillary pressure rises) left behind when non-wetting gas phase is introduced into initially water-saturated media.

On the other hand, among many, foams are destructed by capillary-suction force. Capillary suction causes foam film to become thinner and the two surfaces of the film to interact each other more. The concept of capillary-suction for foam coalescence was firstly introduced by Derjaguin and coworkers (1936, 1939a, 1939b) by using disjoining pressure which is a combination of electrostatic repulsive force and van der Waals attractive force.

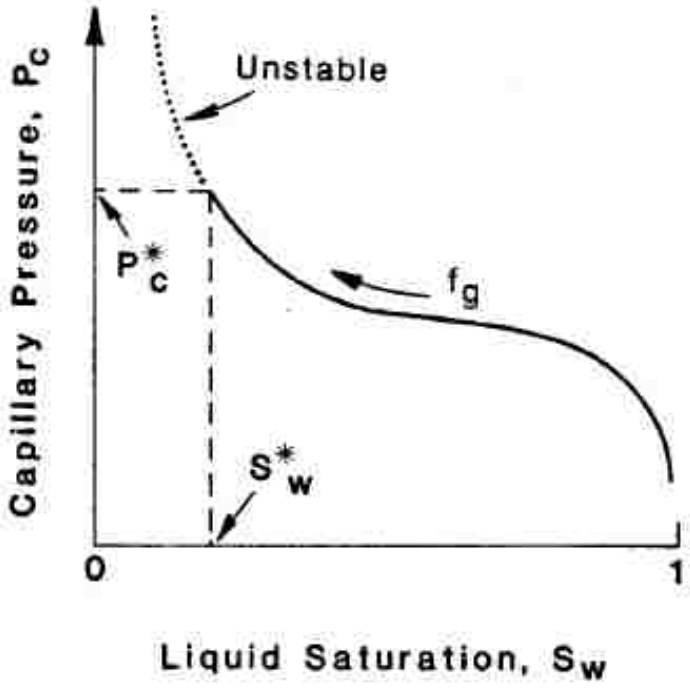

Figure 2.4: Foam stability across P_c* or S_w* (Khatib et al., 1988)

How active lamella creation and coalescence mechanisms are within porous media depends on numerous factors such as surfactant chemistry and concentration, salt type and concentration, adsorption kinetics, interfacial tension, capillary pressure, rock mineralogy and so on (Aronson et al., 1994), and they all affect foam rheological properties. Putting lamella creation and coalescence

mechanisms together, the resulting steady-state foam texture (often unknown) can be related to apparent foam viscosity or gas phase mobility reduction in foam modeling.

The sensitivity of foam stability to capillary pressure is related to water saturation (S_w) within porous media. As Khatib et al. (1988) observed, there exists a threshold P_c value, called "limiting capillary pressure (P_c*)", above which foams cannot sustain in the media, and this capillary pressure value can be translated into "limiting water saturation (S_w*)", a threshold S_w value below which foams cannot survive. This abrupt change in foam stability across P_c* or S_w*, as shown in Figure 2.4, has been well supported by following studies (Jimenez and Radke, 1989; Aronson et al., 1994; Rossen and Zhou, 1995). A small value of S_w* means that the particular surfactant solution in use is a good former creating relatively stable foams even at lower water saturation.

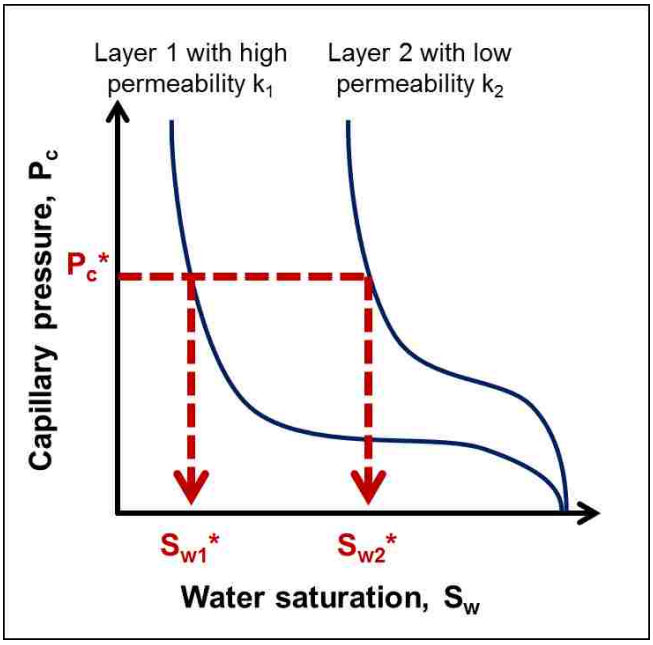

Figure 2.5: Effect of rock permeability on limiting water saturation (Lee and Kam, 2013)

The fact that foam's sensitivity is related to P_c^* (or S_w^*) enables foam to overcome subsurface heterogeneity. It is because foam films are more stable in the high-permeability zone due to smaller S_w^* than in the low-permeability zone, and therefore the subsequent fluid can be diverted into the low-permeability zone, if P_c^* are comparable as shown in Figure 2.5. Of course, how effectively this diversion process takes place depends on medium properties as well as foam characteristics.

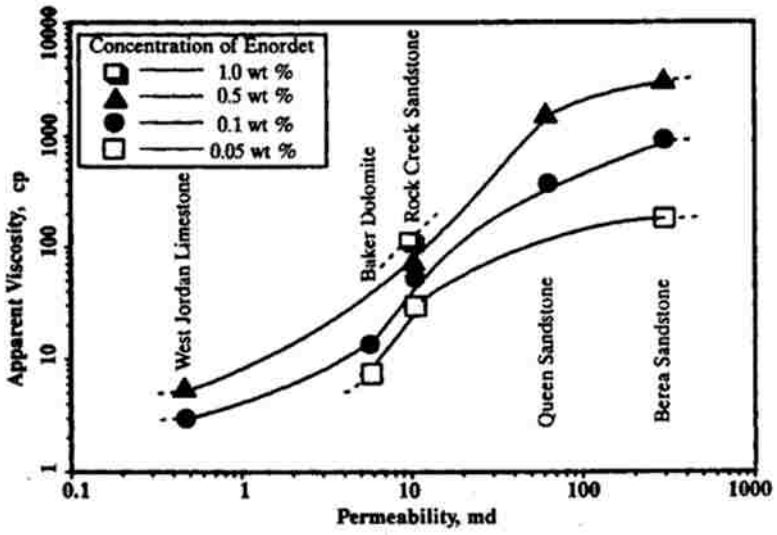

Figure 2.6: Effect of rock permeability on apparent foam viscosity (Lee et al., 1991)

The capability of foams to overcome formation heterogeneity has been proved by many experimental studies. Lee et al. (1991) studied the relationship between apparent viscosity of foam and rock permeability. As shown in Figure 2.6, foam tends to have higher apparent viscosity as rock permeability increases. Bertin et al. (1999) investigated foam diversion using a sandstone core inserted in sandpack system with permeability contrast of 67. Li et al. (2010) carried out foam flooding in two-layered system with permeability contrast 19. During both experiments, foam swept the heterogeneous system evenly by overcoming permeability contrasts.

Foam stability is also shown to be sensitive to oil saturation (S_o), because oil phase can enter the interface between gas and surfactant solution and spread, resulting in a significant reduction in limiting capillary pressure (Nikolov et al., 1986; Koczo et al., 1992; Svorstøl et al., 1996). Experimental data from difference sources (Law et al., 1992; Mannhardt and Svorstøl, 1999) show that foam is not created easily, or once present, foam breaks down abruptly, if S_o is higher than a "critical oil saturation (S_o*)" as shown in Figure 2.7. This implies that those oils deteriorating foam stability to a higher degree tend to have a smaller value of S_o*.

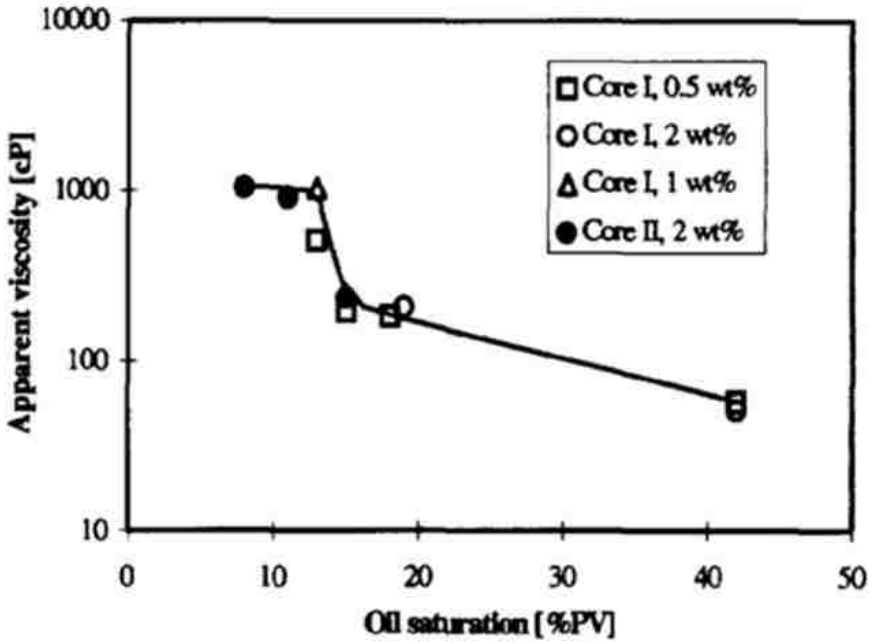

Figure 2.7: Foam apparent viscosity as a function of oil saturation (Svorstøl et al., 1996)

To analyze and model multiphase flow in porous media with foams, understanding the role of foam films or bubble population is a must. Previous studies show that the relative permeability to liquid phase (i.e., water and oil) is not affected while the relative permeability to gas phase is. The presence of foams is also shown to affect gas viscosity significantly due to the drag of foam

films at the rock surface (Bernard et al., 1965; Kovscek et al., 1997). Separating these two components (i.e., change in gas relative permeability vs. change in gas viscosity), however, is complex.

In general, two types of foam modeling techniques are widely used: bubble-population-balance model and local-equilibrium (or local-steady-state) model. Bubble-population-balance model explicitly describes the dynamics of lamella generation and coalescence to obtain the number of foam films (or foam texture) and model foam flow in porous media (Falls et al., 1988; Friemann et al., 1991; Kovscek et al., 1995; Myers and Radke, 2000; Kam and Rossen, 2003; Chen et al., 2010; Zitha and Du, 2010), while local-equilibrium model uses a pre-defined local steady-state foam resistance, in terms of apparent gas viscosity or gas mobility, which may change as a function of water and oil saturations (Patzek and Myhill, 1989; Mohammadi et al., 1993; Lau and Coombe, 1994; Surguchev et al., 1995; Shrivastava et al., 1999; Rossen et al., 1999; Cheng et al., 2000).

The local-equilibrium modeling can be combined with fractional flow theory to analyze how foam migrates in porous media. Buckley and Leverett (1942) first developed fractional-flow theory for two phases (water and oil). Helfferich (1981) extended this theory to multi-component, multi-phase displacement in porous media with coherence theory, which is later followed by other studies such as Pope (1980), Lake (1989), and Falls and Schulte (1992a, b) for chemical enhanced oil recovery (EOR). For foam transport in porous media, Mayberry et al. (2008) applied three-phase fractional flow theory to foam displacement in presence of oil, where the effective gas viscosity is kept constant irrespective of phase saturations. A similar model with two phases (gas and water) was developed for deep vadose zone remediation (Roostapour and Kam, 2012), a

layered geological system (Rosman and Kam, 2009), miscible CO2 foam floods (Ashoori et al., 2010), and three-phase immiscible foam EOR (Zanganeh et al., 2011; Lee et al., 2013). Although it is more complicated, bubble-population-balance modeling technique can also be combined with fractional flow analysis, if dynamic mechanisms of lamella creation and coalescence are of importance (Kam and Rossen, 2003; Dholkawala et al., 2007; Afshapoor et al., 2010; Roostapour and Kam, 2013).

Foams can be introduced into the media by injecting gas and surfactant solution together (so-called "co-injection") or by alternating surfactant and gas in multiple cycles (so-called "surfactant-alternating-gas (SAG)"). In either case, the use of surfactant preflush (i.e., injecting slugs of surfactant solution prior to foam injection) is a common practice to satisfy surfactant adsorption. Unless surfactant adsorption is satisfied prior to foam injection, the loss of surfactant molecules from the injected foams limits foam propagation in porous media. The adsorption rate of surfactant molecules onto the rock surface depends on the properties of surfactant and rock/soils. Generally, a Langmuir-type isotherm model is used to describe the adsorption rate (Grigg and Bai, 2005; Goloub et al., 1996; Trogus et al., 1977). In multi-dimensional systems, several physical mechanisms such as diffusion, tortuosity, and mechanical dispersion also affect the transport of a surfactant through porous media. Diffusion is a spreading of solutes (or surfactant molecules in this case) due to the concentration gradient within aqueous phase, while mechanical dispersion is a mixing that occurs due to local variations in velocity. The dispersion coefficient (or dispersivity) to quantify these mechanisms can be determined by coreflooding experiments (Ramirez et al., 1980).

CHAPTER 3
MODELING OF FOAM FLOW IN ONE-DIMENSIONAL POROUS MEDIA BY USING METHOD OF CHARACTERISTICS (MoC)

This chapter is devoted to the development of foam model which can analyze how foam propagates in a one-dimensional medium initially saturated with different phases such as water, gas and oil. The nature of displacement is investigated in terms of initial conditions as well as other input parameters associated with injection conditions, foam strength, sensitivity of foams to water and oil saturations, etc.

3.1 Methodology

3.1.1 Formulation of MoC for foam fractional flow analysis

Three-phase fractional flow theory, which is a subset of Method of Characteristics (MoC) for the flow of three immiscible phases in porous media, is employed as a major modeling tool in this study (see Dake (1978) and Lake (1989) for more details about mathematical background and derivation procedures). Assuming that the flow is horizontal and one-dimensional with negligible capillary pressure gradient, gravity, and mass exchange between different phases, the governing partial differential equation from material balance is

$$\phi \frac{\partial S_j}{\partial t} + u_t \frac{\partial f_j}{\partial x} = 0, \quad \text{j = w, o, or g} \tag{3.1}$$

where ϕ is porosity, S_j is saturation of phase j, t is time, u_t is the total superficial velocity, f_j is the fractional flow of phase j, and x is distance or length. In dimensionless differential equation form,

$$\frac{\partial S_j}{\partial t_D} + \frac{\partial f_j}{\partial x_D} = 0, \quad \text{j = w, o, or g} \tag{3.2}$$

where the dimensionless time (t_D) and the dimensionless distance (x_D) are given by

$$t_D = \frac{qt}{A\phi L} \quad \text{and} \quad x_D = \frac{x}{L} \tag{3.3}$$

respectively, where q represents flow rate, and A and L represent the cross-sectional area and length of the medium.

The fractional flow of phase j (f_j) during conventional three phase flow (water, oil and gas) can be written as

$$f_j = \frac{u_j}{u_t} = \frac{u_j}{u_w + u_o + u_g} = \left(\frac{k_{rj}}{\mu_j}\right) \Big/ \left(\frac{k_{rw}}{\mu_w} + \frac{k_{ro}}{\mu_o} + \frac{k_{rg}}{\mu_g}\right), \quad \text{j = w, o, or g} \tag{3.4}$$

where u_j, μ_j are the superficial velocity and viscosity of phase j, k_{rj} is the relative permeability to phase j, and subscripts w, o, and g represent phase j such as aqueous phase (water with surfactant chemicals), oleic phase (oil), and gaseous phase (gas). Note that $u_t = u_w + u_o + u_g$, and Darcy's law is applied for transport equation, i.e.,

$$u_w = \frac{q_w}{A} = \frac{kk_{rw}}{\mu_w}\nabla P \tag{3.5}$$

$$u_o = \frac{q_o}{A} = \frac{kk_{ro}}{\mu_o}\nabla P \tag{3.6}$$

$$u_g = \frac{q_g}{A} = \frac{kk_{rg}}{\mu_g} \nabla P \tag{3.7}$$

for water, oil and gas, where q_j is the flow rate of phase j, k is absolute permeability of the medium, and the pressure gradient, ∇P, is the pressure drop (ΔP) across the medium over the length of L.

One common technique to accommodate the presence of foams is to reduce gas mobility by a certain magnitude in gas transport equation, often called mobility reduction factor (MRF), without altering the transport equations for water and oil. For example,

$$u_g = \frac{kk_{rg}}{\mu_g MRF} \nabla P \tag{3.8}$$

Note that MRF = 1 for conventional three phase flow (i.e., no foams), and MRF > 1 for the flow with foams. Although there are no clear cuts, MRF is typically greater than thousands, or as high as hundreds of thousands, for fine-textured low-mobility foams (so called "strong foams"), and is less than tens or hundreds for coarse-textured high-mobility foams (so called "weak foams"). The fractional flow of phase j (f_j) in the presence of foams is then expressed by

$$f_j = \left(\frac{k_{rj}}{\mu_j} \right) \Bigg/ \left(\frac{k_{rw}}{\mu_w} + \frac{k_{ro}}{\mu_o} + \frac{k_{rg}}{\mu_g MRF} \right), \quad \text{j = w, o, or g} \tag{3.9}$$

The solutions obtained from MoC by solving Eq. (3.2) have the nature that the condition inside the medium is changing from one constant state (so called "initial condition (I)") to another constant state (so called "injection condition (J)") over time during which the waves representing different saturation values are propagating from the inlet to the outlet. The saturation velocity of phase j, given by df_j/dS_j, represents the dimensionless velocity (x_D/t_D) of a particular saturation of

interest (i.e., $df_j/dS_j = x_D/t_D$ for any arbitrary S_j). Based on the coherence theory (Helfferich and Klein, 1970), the saturation velocity along the path from I to J must be the same for all three phases and thus can be expressed by σ, i.e.,

$$\frac{df_w}{dS_w} = \frac{df_o}{dS_o} = \frac{df_g}{dS_g} = \sigma \tag{3.10}$$

Note that σ is not a fixed value but varies as a function of x_D and t_D along the saturation path. Although there are three governing equations (cf. Eq. (3.2)), one for each phase, the displacement problem has only two degrees of freedom because of the material balance equations as follows:

$$S_w + S_o + S_g = 1 \text{ and } f_w + f_o + f_g = 1 \tag{3.11}$$

which lead to the following eigenvalue problem (Helfferich and Klein 1970; Lake 1989):

$$\begin{pmatrix} f_{ww} & f_{wo} \\ f_{ow} & f_{oo} \end{pmatrix} \begin{pmatrix} dS_w \\ dS_o \end{pmatrix} = \sigma \begin{pmatrix} dS_w \\ dS_o \end{pmatrix} \tag{3.12}$$

where $f_{ww}=df_w/dS_w$, $f_{wo}=df_w/dS_o$, $f_{ow}=df_o/dS_w$ and $f_{oo}=df_o/dS_o$. The two resulting eigenvalues are

$$\sigma^{\pm} = 0.5\left\{ (f_{ww} + f_{oo}) \pm \left[(f_{ww} - f_{oo})^2 + 4 f_{wo} f_{ow} \right]^{0.5} \right\} \tag{3.13}$$

where σ^+ and σ^- are fast and slow moving saturation waves, respectively. Resulting eigenvectors, which can be calculated by putting Eqs. (3.12) and (3.13) together, do not play a major role in the problem-solving process. The two terms in Eq. (3.10), dS_w and dS_o, can be obtained by rearranging the above equations:

$$\frac{dS_o}{dS_w} = \frac{\sigma^{\pm} - f_{ww}}{f_{wo}} = \frac{f_{ow}}{\sigma^{\pm} - f_{oo}} \tag{3.14}$$

In general, fractional flow solutions can be spreading waves, shock waves, or a combination of both. The dimensionless velocity (v_D) for a spreading wave is expressed by

$$v_D = \frac{df_j}{dS_j} \tag{3.15}$$

and for a shock wave,

$$v_D = \frac{\Delta f_j}{\Delta S_j} \tag{3.16}$$

where Δ denotes the difference across the shock wave. The shock, or the discontinuity in saturation, occurs when the saturation velocity cannot increase monotonically from injection condition (J) to initial condition (I) (Buckley and Leverett, 1942).

3.1.2 Construction of solution paths in ternary diagram and fractional flow curve

Finding fractional flow solutions to MoC equations, as demonstrated by the eigenvalue problem (Eq. (3.12) to (3.14)), is equivalent to obtaining the saturation velocities of all saturations involved. An example is shown in Figure 3.1 by using a ternary diagram (Figure 3.1(a)) and three fractional flow curves (Figure 3.1(b)), where the initial condition (I) is given by I:(S_w, S_o, S_g) = (0.8, 0.2, 0) and the injection condition is given by J:(f_w, f_o, f_g) = (0.2, 0, 0.8). Note that this J in terms of injection fractions (i.e., J:(f_w, f_o, f_g)) is then converted into J in terms of phase saturations (i.e., J:(S_w, S_o, S_g)) by using Eq. (3.9) for all three phases involved.

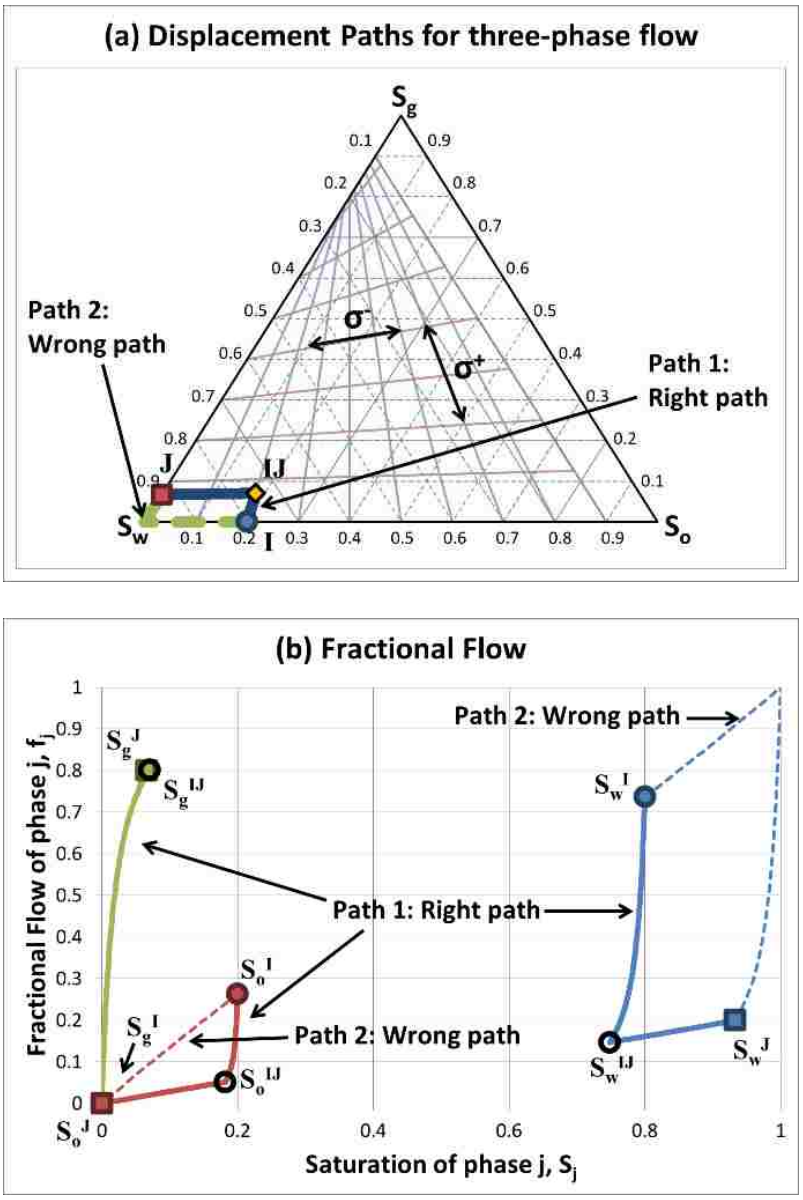

Figure 3.1: Three-phase displacement solution from fractional flow theory with: $I(S_w,S_o,S_g) = (0.8,0.2,0)$ and $J(f_w,f_o,f_g) = (0.2,0,0.8)$

Once I and J are decided, the next step is to determine how to go from I to J. In general, there are two possible paths from I to J based on two calculated eigenvalues (σ^+ and σ^- in Eq. (3.13)) with two intersection points in between (i.e., one intersection point for each path). These intersection points, so-called intermediate state and denoted by IJ in Figure 3.1(a), together with

two different saturation paths are represented by Path 1 and Path 2 in Figure 3.1(a). The presence of IJ is always guaranteed because of two different mobility values associated at that single point, and furthermore the size of IJ increases with time proportionally. Between the two paths (i.e., σ^+ followed by σ^-, or σ^- followed by σ^+), the final solution is the one which satisfies the velocity constraint (i.e., saturation velocity must increase from J to I monotonically), that is, Path 1 in this particular case. Path 1 and Path 2 are also shown in the domain of f_j vs. S_j in Figure 3.1(b), by thick solid lines and thin dashed lines respectively, for individual phases. It should be noted that each of three phases has its own three constant states (I, J and IJ) and saturation paths (eg. for aqueous water phase, the path connects S_w^I, S_w^{IJ}, and S_w^J); one can use the fractional flow curve of any of those three phases to solve for wave propagation, however, because the solutions are guaranteed to be the same as defined by coherence theorem explained earlier. The change in saturation velocity can be checked more conveniently with Figure 3.1(b) because saturation velocity is no other than the slope at the saturation of interest.

More details on the construction of saturation path during three-phase flow are available elsewhere (Lake, 1989; Mayberry et al., 2008; Zanganeh et al., 2011).

3.1.3 Modeling foam sensitivity to water and oil saturations

Although the easiest way of handling the reduction in gas mobility is to apply a fixed value of MRF (Mayberry et al., 2008), it is obviously an oversimplification because MRF is a function of S_w and S_o. A better way to deal with it is, first, to identify the full-strength MRF value corresponding to the fine-textured foams (MRF_{full}) when there is a sufficient amount of water and a negligible amount of oil (i.e., $MRF = MRF_{full}$ for $S_w > S_w^*$ and $S_o < S_o^*$), which typically comes from laboratory flow experiments. Then, the next step is to assign a reduced value for MRF (for

example, MRF = 1 if foam completely collapses down), if the medium is too dry ($S_w < S_w^*$) or contains too much oil ($S_o > S_o^*$). Because such a discontinuity at S_w^* or S_o^* cannot be handled easily in numerical calculations, incorporating a transition from full-strength foams to no foams over the length of $2\varepsilon_w$ (for S_w) or $2\varepsilon_o$ (for S_o) is helpful for modeling and simulation purpose. Therefore, if S_w^* is considered

$$\begin{aligned} \text{MRF} &= \text{MRF}_{\text{full}} \text{ (full strength foam)} && \text{if } S_w \geq (S_w^* + \varepsilon_w), \\ &= 1 \text{ (no foam)} && \text{if } S_w \leq (S_w^* - \varepsilon_w), \\ &= \frac{MRF_{full} - 1}{2\varepsilon_w}\left(S_w - S_w^* + \varepsilon_w\right) + 1 && \text{if } (S_w^* - \varepsilon_w) < S_w < (S_w^* + \varepsilon_w), \end{aligned}$$

and if S_o^* is considered

$$\begin{aligned} \text{MRF} &= \text{MRF}_{\text{full}} \text{ (full strength foam)} && \text{if } S_o \leq (S_o^* - \varepsilon_o), \\ &= 1 \text{ (no foam)} && \text{if } S_o \geq (S_o^* + \varepsilon_o), \\ &= \frac{MRF_{full} - 1}{2\varepsilon_o}\left(S_o^* + \varepsilon_o - S_o\right) + 1 && \text{if } (S_o^* - \varepsilon_o) < S_o < (S_o^* + \varepsilon_o) \end{aligned}$$

as illustrated in Figure 3.2. The effect of S_w^* and S_o^* can be expressed as F_w and F_o, respectively. If MRF changes sharply around S_w^* and S_o^*, solving for the saturation paths may suffer from convergence and instability issues.

Therefore, if both S_w^* and S_o^* are considered

$$MRF = 1 + (MRF_{full} - 1) \cdot F_w \cdot F_o \tag{3.17}$$

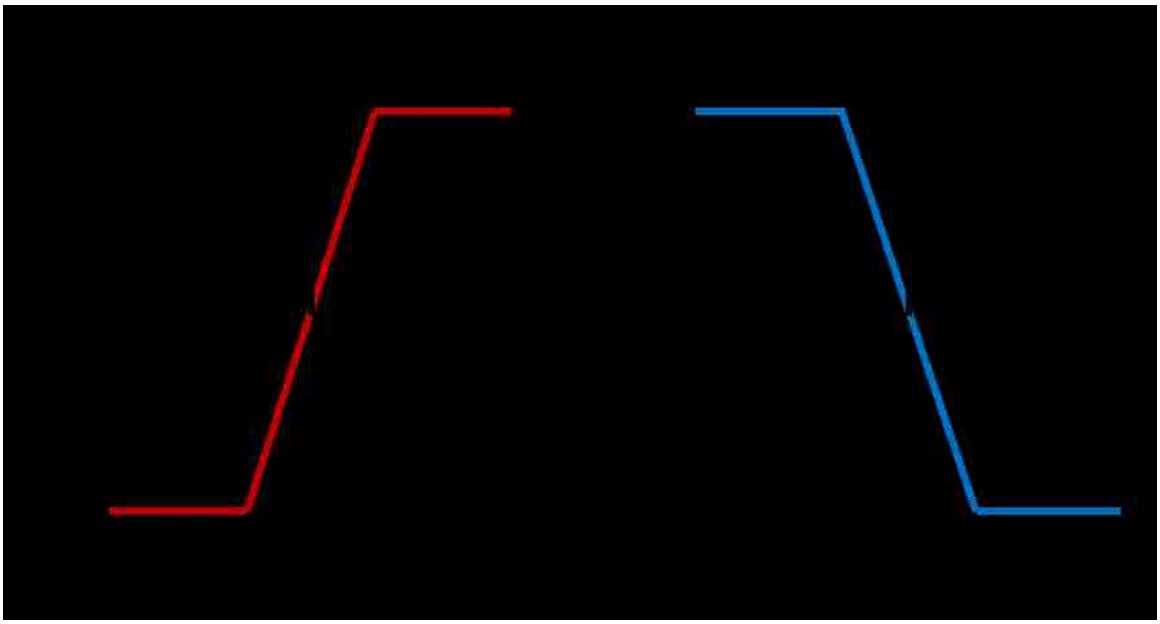

Figure 3.2: Foam model with effect of water and oil saturation

The transport equations (cf. Eqs. (3.5), (3.6), and (3.7)) require relative permeability functions. This study assumes the simplest forms as follows:

$$k_{rw} = k_{rw}^{o}\left(\frac{S_w - S_{wr}}{1 - S_{wr} - S_{or} - S_{gr}}\right)^{n_w} \tag{3.18}$$

$$k_{ro} = k_{ro}^{o}\left(\frac{S_o - S_{or}}{1 - S_{wr} - S_{or} - S_{gr}}\right)^{n_o} \tag{3.19}$$

$$k_{rg} = k_{rg}^{o}\left(\frac{S_g - S_{gr}}{1 - S_{wr} - S_{or} - S_{gr}}\right)^{n_g} \tag{3.20}$$

where k_{rw}^{o}, k_{ro}^{o}, and k_{rg}^{o} are the end-point relative permeability values for water, oil and gas respectively; S_{wr}, S_{or}, and S_{gr} the residual saturations; and n_w, n_o, n_g the exponents. The parameter

and viscosity values are summarized in Table 3.1. These simple shapes of relative permeability functions allow the interpretation of the outputs easier, numerical calculations more stable, and convergence improved. Note that the aqueous phase in this study is assumed to always have surfactant chemicals because of surfactant pre-flush.

Table 3.1: Parameters for foam model study

Input Parameters							
μ_w =	1	k_{rw}^o =	1	S_{wr} =	0.1	n_w =	1
μ_o =	0.8	k_{ro}^o =	1	S_{or} =	0	n_o =	1
μ_g =	0.02	k_{rg}^o =	1	S_{gr} =	0	n_g =	1

All calculations to solve MoC equations and saturation velocities are conducted by using Microsoft Excel Visual Basic for Applications (VBA). The simulator developed for comparison is based on 1D finite difference method, implicit in time and forward difference in space. Similar versions are available elsewhere (Mayberry et al., 2008; Afsharpoor et al., 2010).

3.2 Results

Six different cases are presented in this study. In first two cases (Case 3.1 and Case 3.2), foam is assumed to be at its full strength irrespective of water and oil saturations, i.e., MRF = MRF_{full}. Case 3.1 has an initial condition with water and oil only, without gas (mimicking DNAPL below the groundwater level), whereas Case 3.2 has an initial condition with all three phases (mimicking LNAPL above the groundwater level). Various MRF values, ranging from 1 to 1000, are examined.

In the next two cases, the effects of S_w* and S_o* are investigated individually (not together) for Case 3.3 and Case 3.4 respectively, by keeping other conditions the same. Note that a low S_w* means a strong foamer which creates and maintains stable and low-mobility foams, while a high S_w* means a poor foamer which has a hard time in creating, or maintaining if created already, fine-textured foams. S_w* does not only reflect surfactant formulations and concentrations, but also many other parameters affecting foam stability such as medium wettability, water composition, temperature, pore structures, and so on. Similarly, a low S_o* means a foam very sensitive to even a small amount of oil, while a high S_o* means a foam tolerating oil saturation to some degree.

The last two cases demonstrate how foam simulator guided by fractional flow analysis, as shown in and verified by Case 3.1 through Case 3.4, can deal with more realistic situations. More precisely, Case 3.5 shows both modeling and simulation results when S_w* and S_o* are imposed together, and Case 3.6 shows the case where the initial saturation is not uniform but varies such that oil saturation is relatively high in the middle and diminishes towards the inlet and outlet progressively. In both cases, fractional flow analysis cannot be applied easily because of the complexities (i.e., two discontinuities caused by S_w* and S_o* in Case 3.5, and possible collisions of saturation waves caused by non-uniform saturations in Case 3.6) where foam simulation can be of great help.

In all cases examined in this study, the injection condition (J) is set at 80% foam quality (i.e., $f_g = 0.8$ and $f_w = 0.2$), and the initial condition (I) is either (S_w, S_o, S_g) = (0.8, 0.2, 0.0) or (S_w, S_o, S_g) = (0.3, 0.2, 0.5). For those calculations requiring transitions near S_w* and S_o* (Case 3.3 through Case 3.6), ε_w and ε_o are set at 0.05. The medium has a linear geometry with the cross sectional area of 0.5 m^2 and the length of 5 m (Except for pressure calculations, actual medium

length does not play a role in this study because of the use of dimensionless variables and parameters).

The selection of model parameters, initial conditions, and injection conditions in Case 3.1 through Case 3.6 is somewhat arbitrary at this point, but intends to cover the range that one can observe in actual field applications. For example, MRF value of 1 represents a simple air-water injection with no foam; MRF value of 10 to 100 represents coarsely-textured weak foam; and MRF value of 1000 represents fine-textured strong foams. In addition, S_w* values of 0.0, 0.4, and 0.6 represent three types of foam stability to water saturation such as high stability (insensitive to S_w), moderate stability (moderately sensitive to S_w), and low stability (very sensitive to S_w), while S_o* values of 0.0 (should it be 1.0 rather than 0.0??) and 0.1 represent two types of foam stability to oil saturation such as high stability (insensitive to S_o) and low stability (very sensitive to S_o). The ranges of these parameters, of course, can be narrowed down further, as the conditions in field treatments become available.

3.2.1 Translation of injection condition from fractional flow to saturation

The use of MoC for multiphase flow analysis specifies initial conditions (I) with phase saturations and injection conditions (J) with flowing fractional flows. As a result, the use of ternary diagram for multiphase flow analysis (cf. Figure 3.1(a)) requires that the injection conditions given by fractional flows be translated into saturation domain.

An example is shown in Figure 3.3 which illustrates how gas-water two-phase fractional flow curve changes as a function of full-strength foam MRF, MRF_{full}, (Figure 3.3(a)) and how the injection condition locates in the ternary diagram in terms of injection saturations (Figure 3.3(b)). As expected, as MRF increases from MRF_{full} = 1 to MRF_{full} = 1000, the fractional flow curve shifts

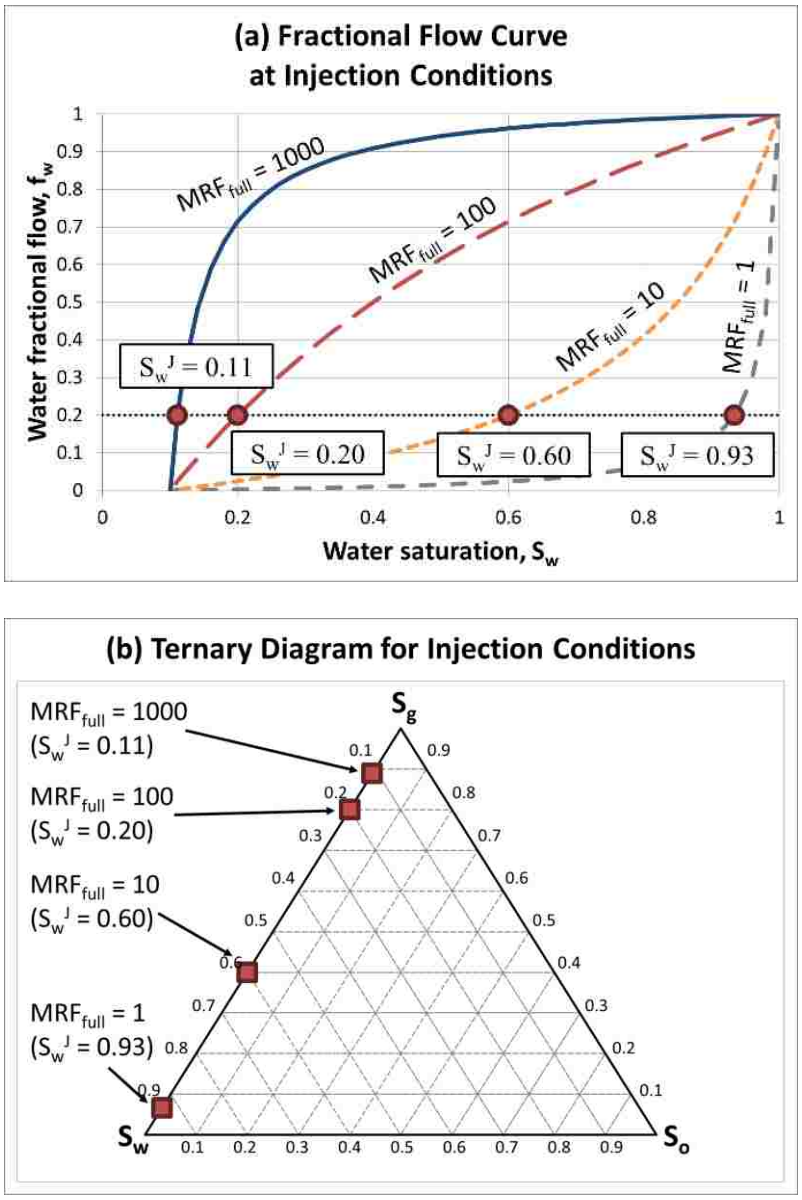

Figure 3.3: Effect of MRF on two-phase fractional flow (injection condition) with 80% foam quality

to the upper left corner (Figure 3.3(a)) and the resulting injection water saturation (S_w^J) in response to 80 % injection foam quality (f_w^J=0.2 or f_g^J=0.8) decreases dramatically from about 0.93 (for MRF_{full} = 1) to 0.11 (for MRF_{full} = 1000) (see those filled circle marks in Figure 3.3(a)). These S_w^J values can also be mapped in the ternary diagram lined up at the value of $S_o = S_{or}$ (see filled square

marks along the side line in the left-hand side of the ternary diagram in Figure 3.3(b)) where the position of S_w^J varies significantly depending on MRF_{full} values.

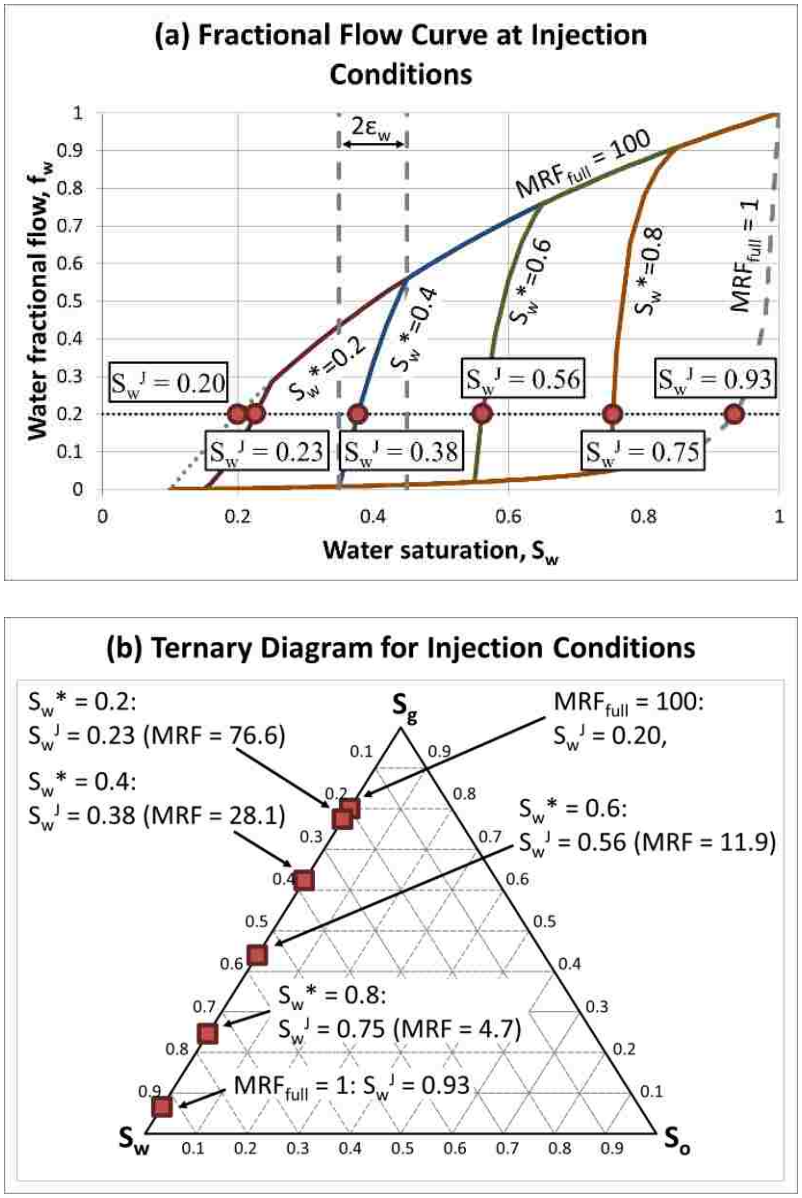

Figure 3.4: Effect of S_w* on injection condition with 80% foam quality (MRF_{full} = 100 and ε_w = 0.05)

Determination of injection saturation (S_w^J) becomes more complicated if S_w* is applied. Figure 3.4 shows an example illustrating how S_w* impacts the fractional flow curve when MRF_{full}

= 100 and how S_w^J values are influenced accordingly in the ternary diagram at the S_w^* value of 0.2, 0.4, 0.6, and 0.8. As expected, for any value of S_w^*, MRF value for $S_w > S_w^*+\varepsilon_w$ is the same as MRF_{full} (meaning full-strength foams), MRF value for $S_w < S_w^*-\varepsilon_w$ is the unity (meaning no foams), and liner interpolation in between. In general, the injection condition of $f_w^J = 0.2$ coincides with S_w range between $S_w^*-\varepsilon_w$ and $S_w^*+\varepsilon_w$ (i.e., within the very steep portion of the curves) in all cases of $S_w^* = 0.2$, 0.4, 0.6, and 0.8 (Figure 3.4(a)). Figure 3.4(b) shows the position of S_w^J values in the ternary diagram. Although MRF_{full} values are all the same ($MRF_{full} = 100$), S_w^J for a larger value of S_w^* has a significantly lower MRF at the injection condition (for example, $S_w^J = 0.23$ when $S_w^* = 0.2$ vs. $S_w^J = 0.75$ when $S_w^* = 0.8$) and is therefore positioned closer to the lower and left-hand side corner of the ternary diagram. Physically, this happens because a poor foamer (large S_w^*) does not effectively reduce gas mobility, leading to a relatively low gas saturation and high water saturation.

3.2.2 Case 3.1: Full strength foams (MRF = MRF_{full}) with water and oil initially

Figure 3.5 shows ternary diagrams at MRF = 1, 10, 100 and 1000 when 80% quality foams are injected into the medium initially at (S_w, S_o, S_g) = (0.8, 0.2, 0.0). As discussed earlier, although the initial conditions remain at the same locations, the injection conditions vary significantly – S_g^J increases dramatically (or S_w^J decreases dramatically, equivalently) as MRF increases and thus more gas phase becomes trapped due to the increase in gas viscosity. The intermediate state (IJ) is positioned within the diagram when MRF values are 1 and 10, while it is located at the corner when MRF values are 100 and 1000. Note that as shown in Figure 3.5, the direction of the solution paths is distinctly different between the first two cases and the second two cases, which is solely caused by MRF. The details of these differences are described in the following figures.

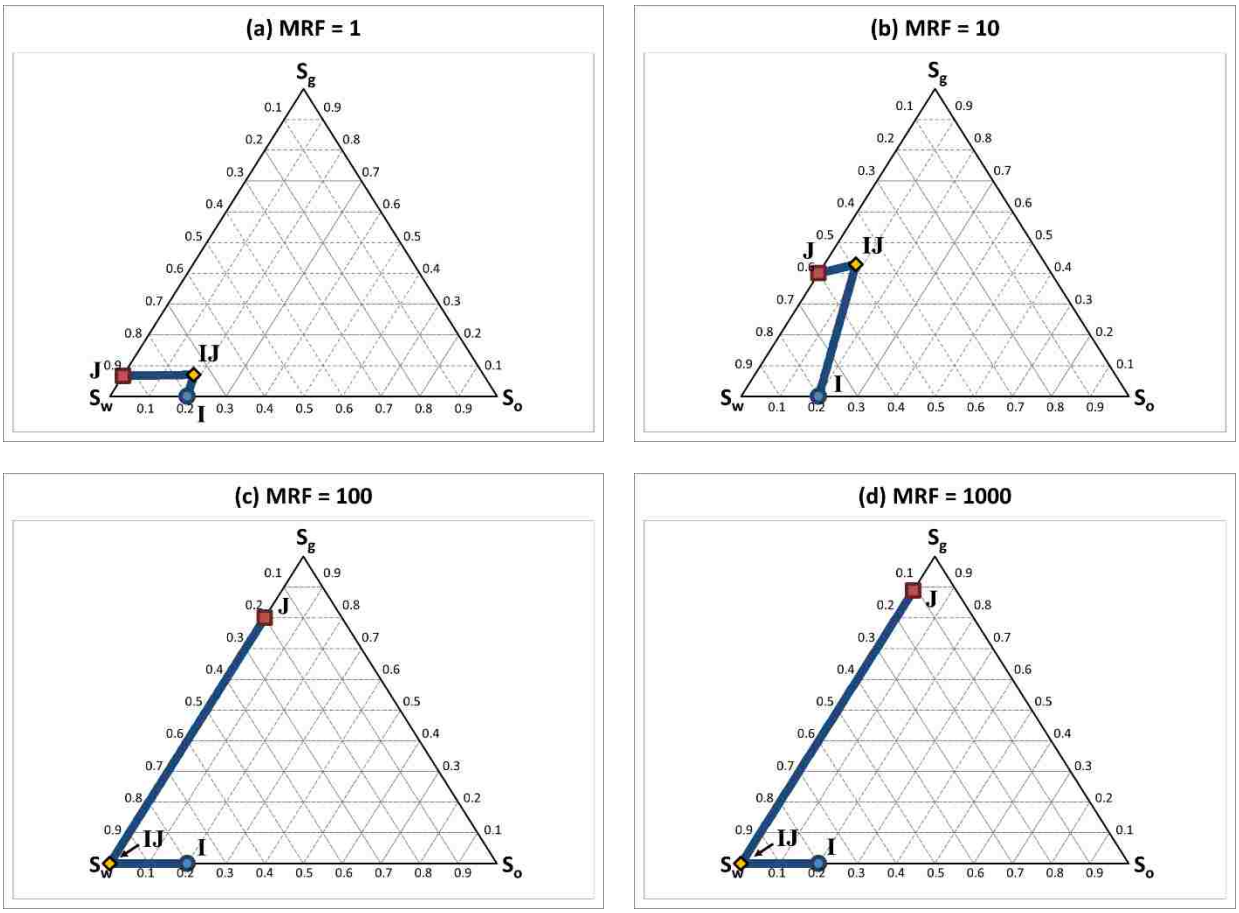

Figure 3.5: Case 3.1: effect of MRF on foam displacement paths with I:(S_w,S_o,S_g) = (0.8,0.2,0) and J:(f_w,f_g) = (0.2, 0.8)

Figure 3.6 shows a comprehensive analysis of the system when MRF = 1 (no foam case) by using fractional flow curves, effluent history, saturation profile, and time-distance diagram all together, with the initial condition of (S_w^I, S_o^I, S_g^I) = (0.8, 0.2, 0.0) and the injection condition of (f_w^J, f_o^J, f_g^J) = (0.2, 0.0, 0.8). Because there is no mobility control in this case, the injection water saturation is relatively high (S_w^J = 0.93), and the entire process is dominated by very fast moving spreading waves, especially those near S_w^I, and by very slow shock wave between S_w^{IJ} and S_w^J. Note that the analysis of saturation velocities would be exactly the same, no matter which phases

are used for velocity interpretation, as described by coherence theory. Because of a dramatic change in wave velocity at IJ (i.e., σ^+ and σ^-), there exists a wide intermediate state.

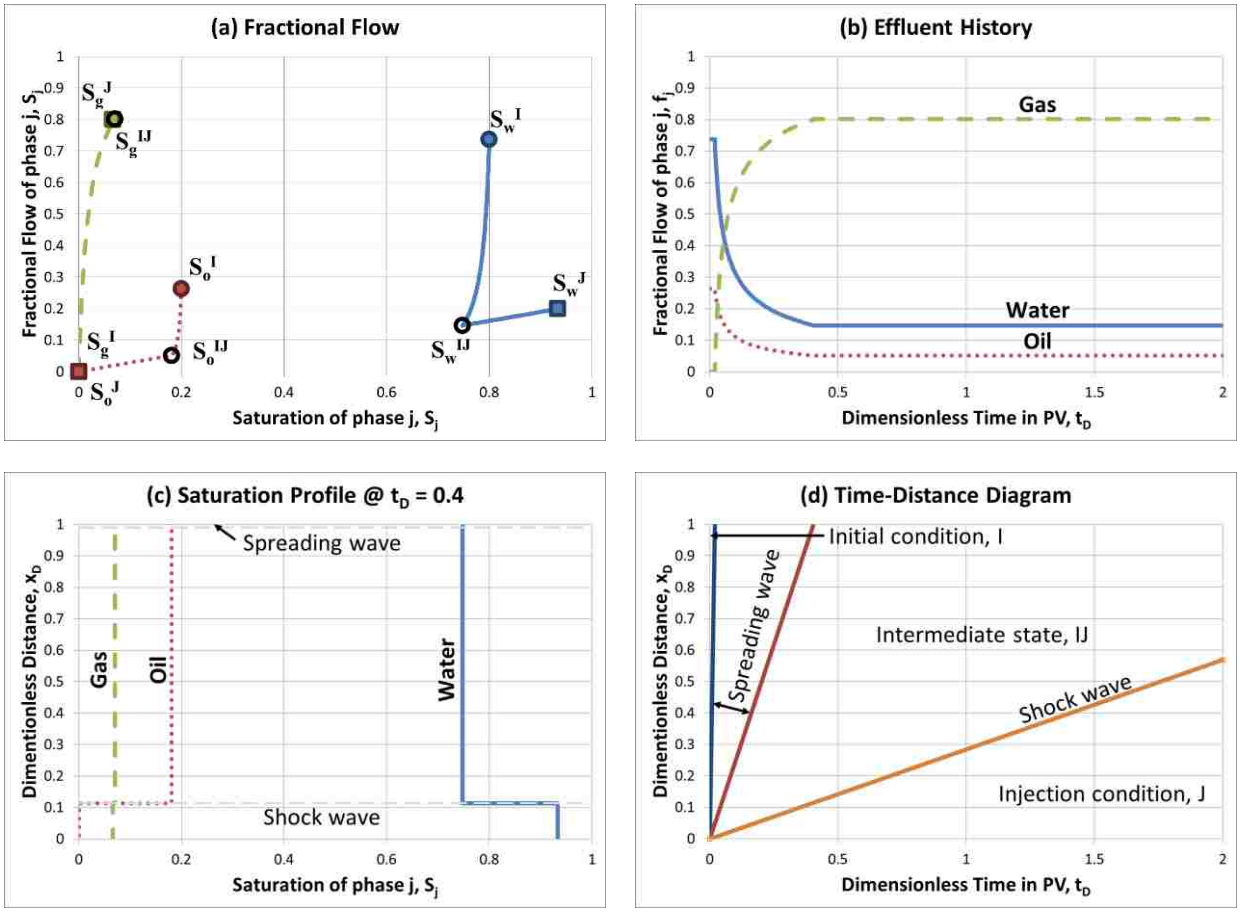

Figure 3.6: Case 3.1: foam displacement at MRF = 1 with I:(S_w,S_o,S_g) = (0.8,0.2,0) and J:(f_w,f_g) = (0.2, 0.8)

Figures 3.7 through 3.9 show the results with MRF = 10, 100, and 1000, respectively. As MRF increases (or, as the effective gas viscosity increases, equivalently), the injection water saturation decreases (S_w^J = 0.60, 0.20 and 0.11 for MRF = 10, 100, and 1000, respectively). Although there are spreading waves between S_w^I and S_w^{IJ} at MRF =10 (Figure 3.7), the velocity of the fastest spreading wave (near S_w^I) is reduced significantly compared to MRF = 1. This implies

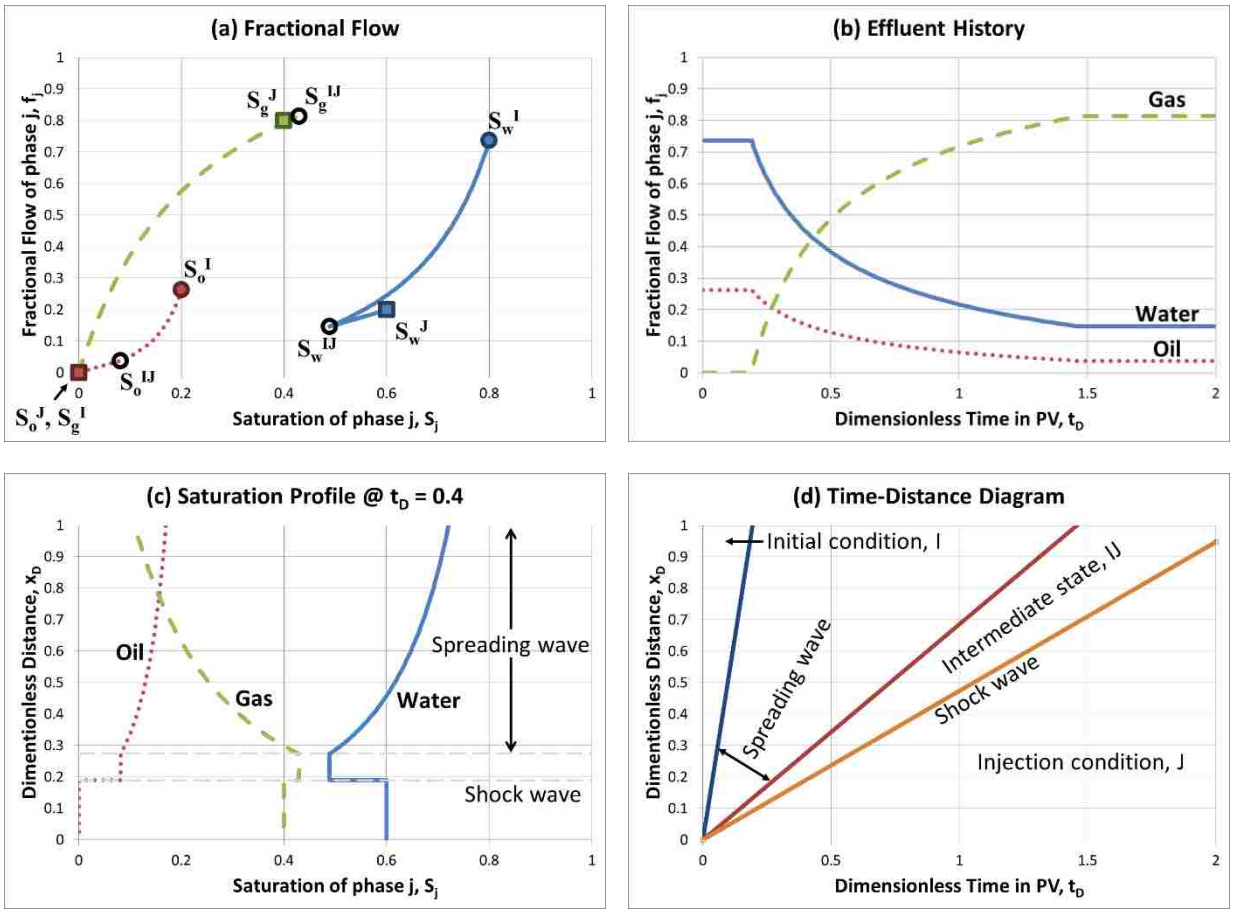

Figure. 3.7: Case 3.1: foam displacement at MRF = 10 with I:(S_w,S_o,S_g) = (0.8,0.2,0) and J:(f_w,f_g) = (0.2, 0.8)

that even with a modest increase in MRF (i.e., from MRF = 1 to MRF = 10), the breakthrough time is improved significantly (almost immediate when MRF = 1 vs. 0.20 PV when MRF = 10). When MRF = 100 and 1000 (Figures 3.8 and 3.9), the position of S_w^{IJ} is located in the other side of fractional flow curve, and the displacement becomes governed by two saturation shocks (a fast moving shock between S_w^I and S_w^{IJ}, followed by a slow moving shock between S_w^{IJ} and S_w^J). This proves why the formation and propagation of strong foams are important for improved sweep efficiency – strong foams with relatively high effective foam viscosity sweep the medium better

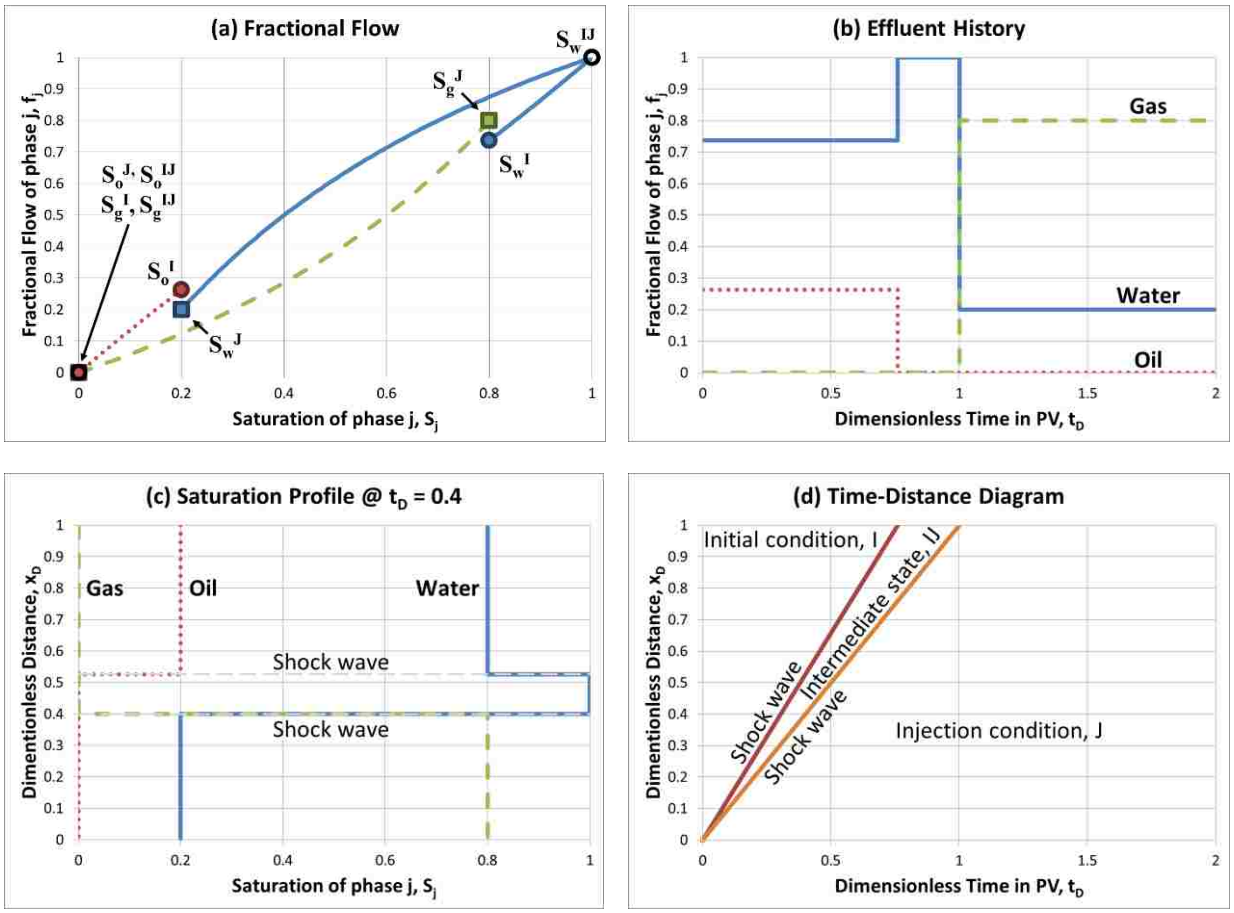

Figure 3.8: Case 3.1: foam displacement at MRF = 100 with I:(S_w,S_o,S_g) = (0.8,0.2,0) and J:(f_w,f_g) = (0.2, 0.8)

by achieving a piston-like displacement. It should be noted that other than a slight difference in S_w^J, there is almost no difference between the two cases of MRF = 100 and MRF = 1000. Although not shown here, the cases with MRF more than 1000 makes almost no difference in terms of displacement compared with MRF = 100.

Figure 3.10 shows pressure profile within the system at t_D = 0.4 and inlet pressure during foam injection, assuming that total injection rate (q_t) = 0.0001 m^3/s, system length (L) = 5 m, cross-sectional area (A) = 0.5 m^2, absolute permeability (k) = 10^{-12} m^2, and outlet pressure (P_{out}) =

101325 Pa (1 atm). As expected, higher pressure gradient is observed at higher MRF, which makes a dramatic difference in terms of inlet pressure. For the cases of MRF = 100 and 1000, there is a huge difference in pressure while their displacement processes are similar.

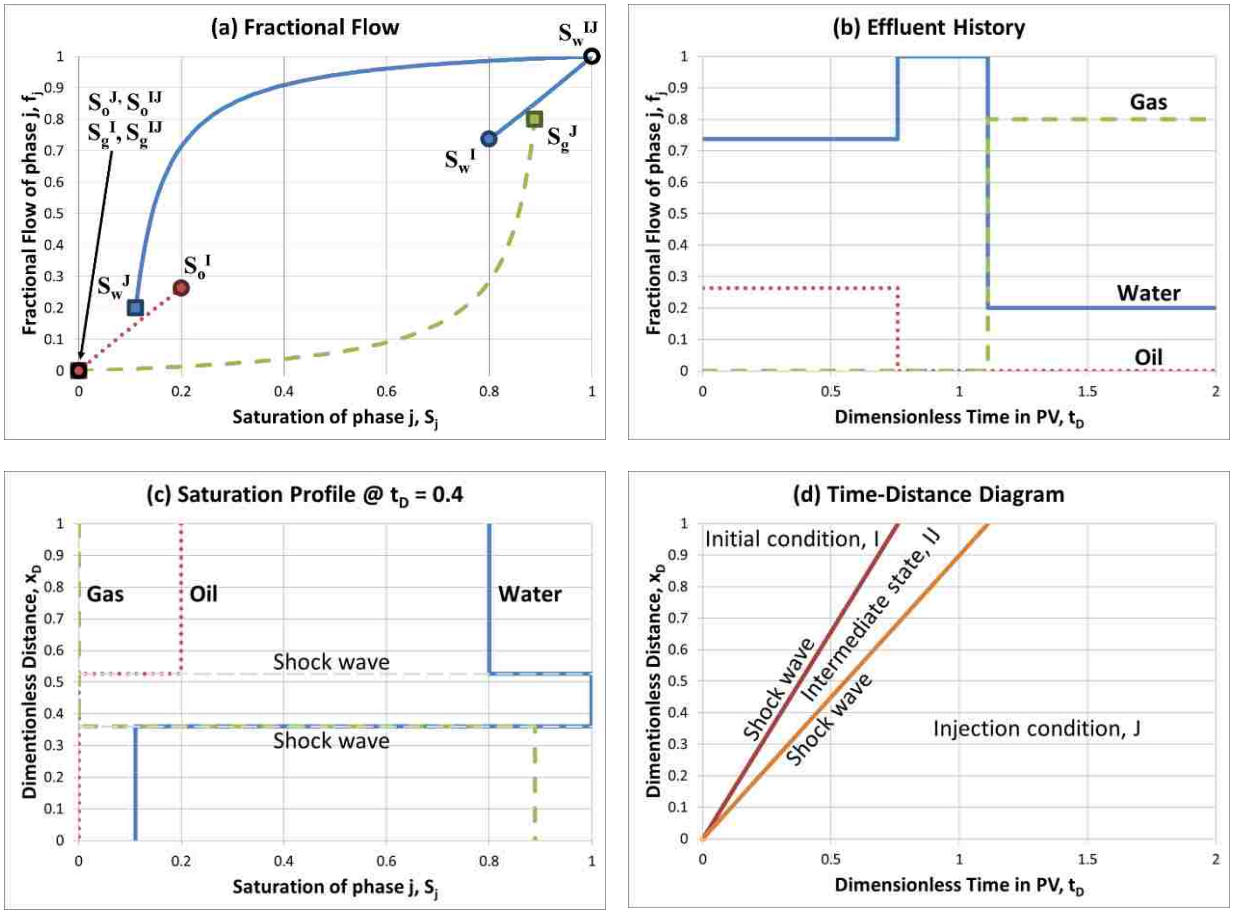

Figure 3.9: Case 3.1: foam displacement at MRF = 1000 with I:(S_w,S_o,S_g) = (0.8,0.2,0) and J:(f_w,f_g) = (0.2, 0.8)

The recovery factor in Figure 3.11 shows that the displacement efficiency is improved significantly with higher MRF values, but there is not much difference between MRF = 100 and 1000. For shallow subsurface remediation, the steady-state inlet pressure buildup observed with

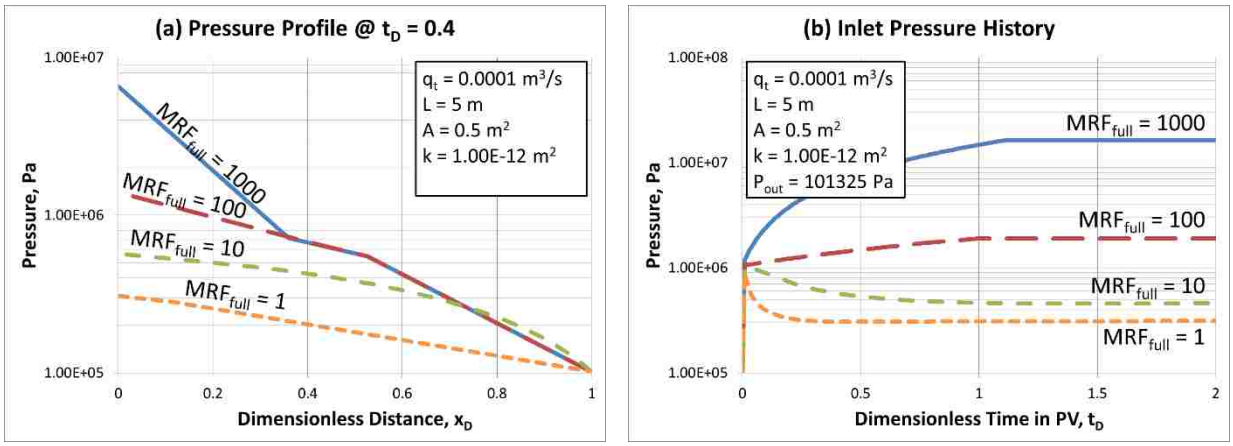

Figure 3.10: Case 3.1: effect of MRF on pressure

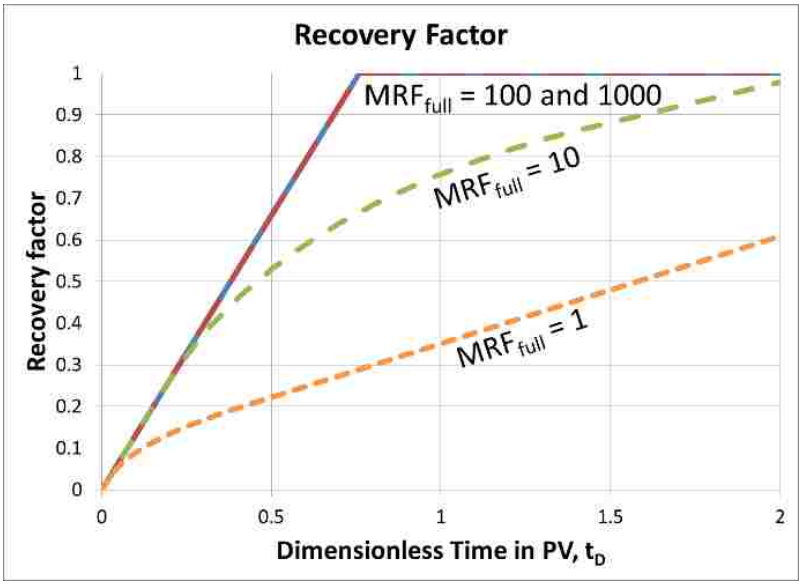

Figure 3.11: Case 3.1: comparison of recovery factor varying MRF

MRF = 100 and 1000 may not be allowed due to the concerns about disturbing the underground system and/or displacing the contaminants out of the area of interest. It is interesting to find, however, that even with MRF = 10, it takes only about 2.1 PV of foam injected to reach near 100

% recovery, which is a significant improvement compared to 3.5 PV required for no foam case (MRF = 1).

3.2.3 Case 3.2: Full strength foams (MRF = MRF_{full}) with water, oil, and gas initially

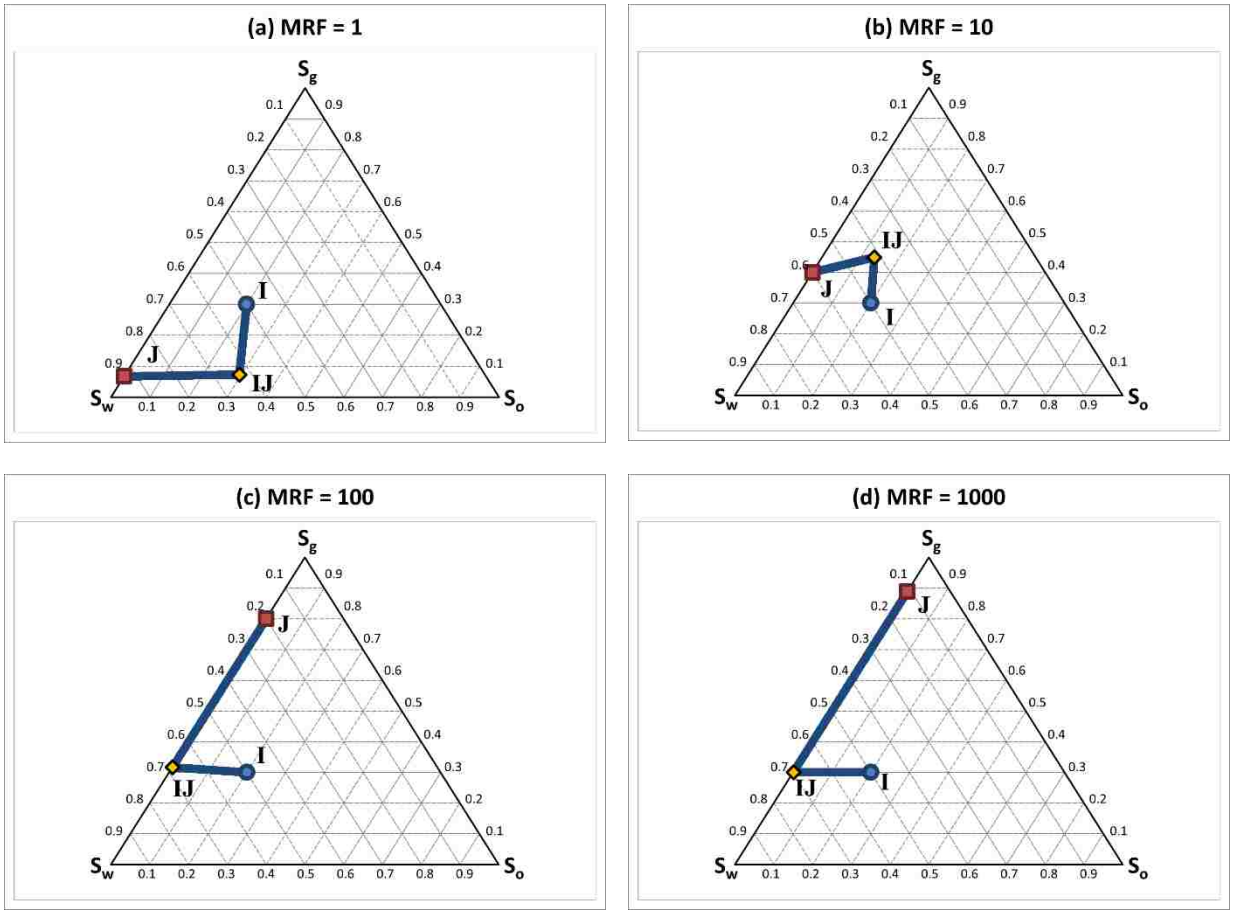

Figure 3.12: Case 3.2: effect of MRF on foam displacement paths with I:(S_w,S_o,S_g) = (0.5,0.2,0.3) and J:(f_w,f_g) = (0.2, 0.8)

Figure 3.12 shows ternary diagrams when 80% quality foams are injected into the medium, initially at (S_w, S_o, S_g) = (0.5, 0.2, 0.3) with various MRF values (MRF = 1, 10, 100 and 1000). Even with some amount of gas phase present to represent LNAPL above water table, the injection water saturations are identical to the ones in Figure 3. 6. At low MRF values (MRF = 1 and 10),

the intermediate state IJ moves up in the ternary diagram as the injection water saturation (S_w^J) decreases (or, injection gas saturation (S_g^J) increases, equivalently). At high MRF values (MRF = 100 and 1000), the IJ point is not within the ternary diagram any longer – rather, the IJ point is positioned at the side of the ternary diagram where only water and gas phases exist, and the general path from I to IJ and from IJ to J does not seem to vary significantly with MRF.

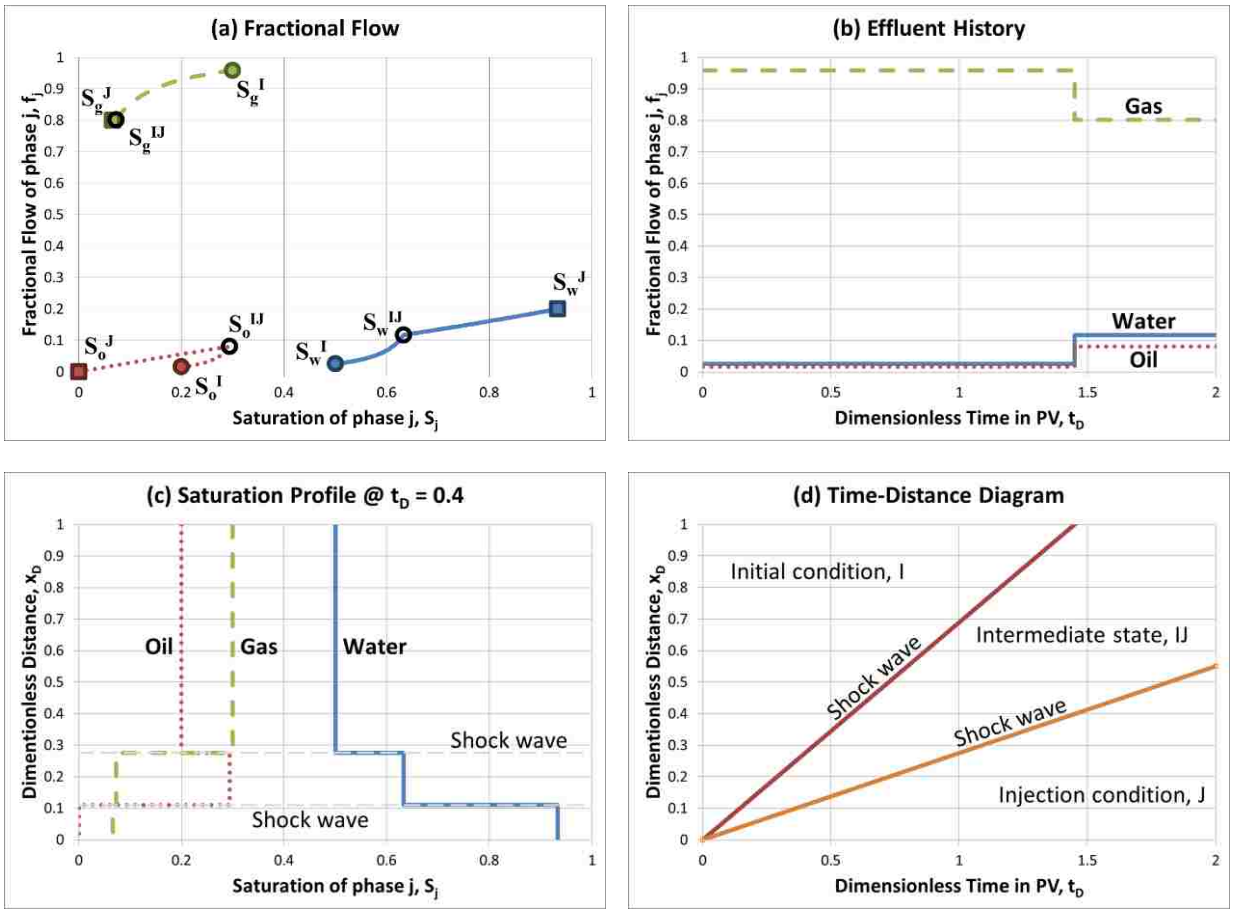

Figure 3.13: Case 3.2: foam displacement at MRF = 1 with I:(S_w,S_o,S_g) = (0.5,0.2,0.3) and J:(f_w,f_g) = (0.2, 0.8)

Figures 3.13 through 3.16 show the results with MRF = 1, 10, 100, and 1000, respectively. In all cases except the case with MRF of 10, two shocks between I and IJ and between IJ and J

govern the entire displacement process. With higher MRF, however, two shock fronts are propagating faster, and the displacement of oil is more efficient. Similar to Case 3.1, there is no significant difference between MRF = 100 and MRF = 1000.

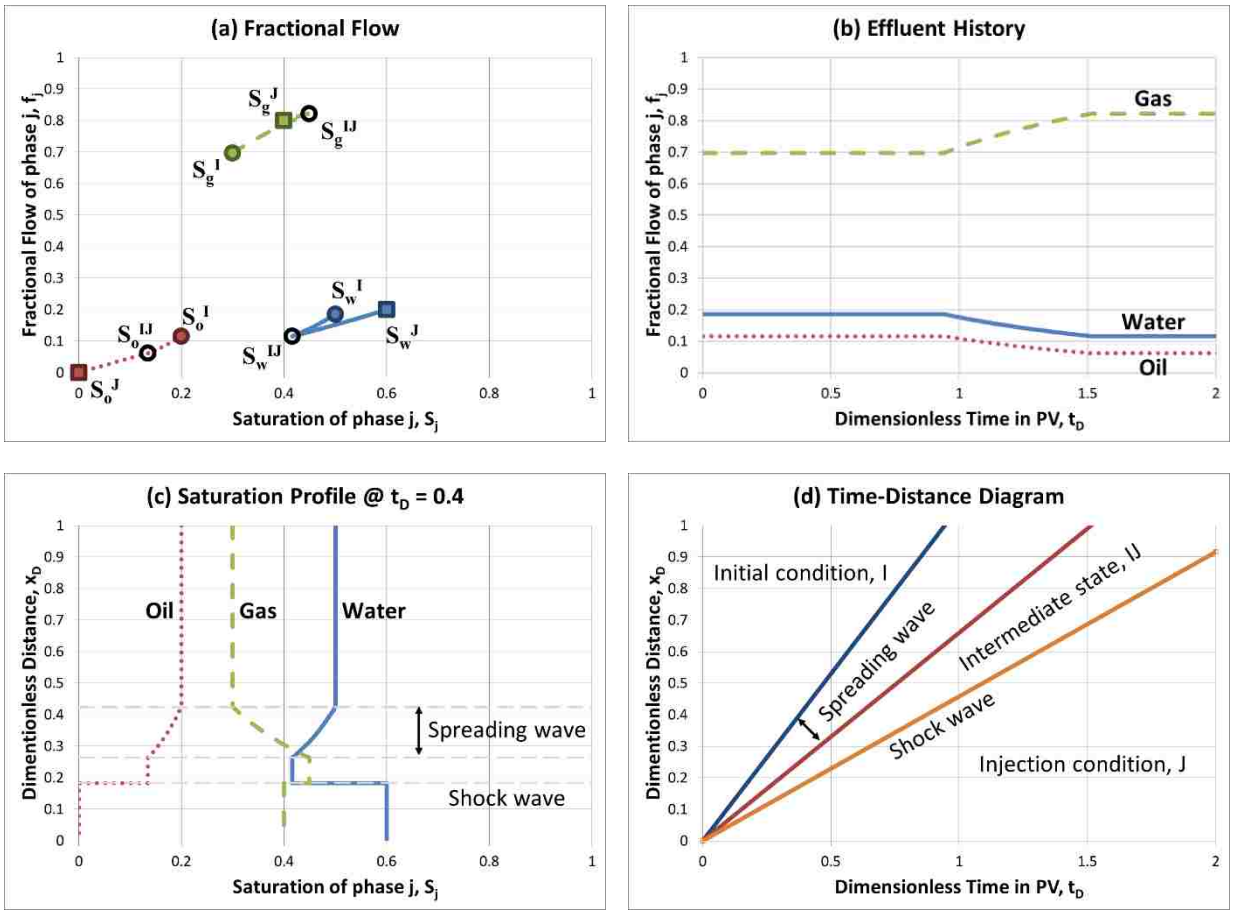

Figure 3.14: Case 3.2: foam displacement at MRF = 10 with I:(S_w,S_o,S_g) = (0.5,0.2,0.3) and J:(f_w,f_g) = (0.2, 0.8)

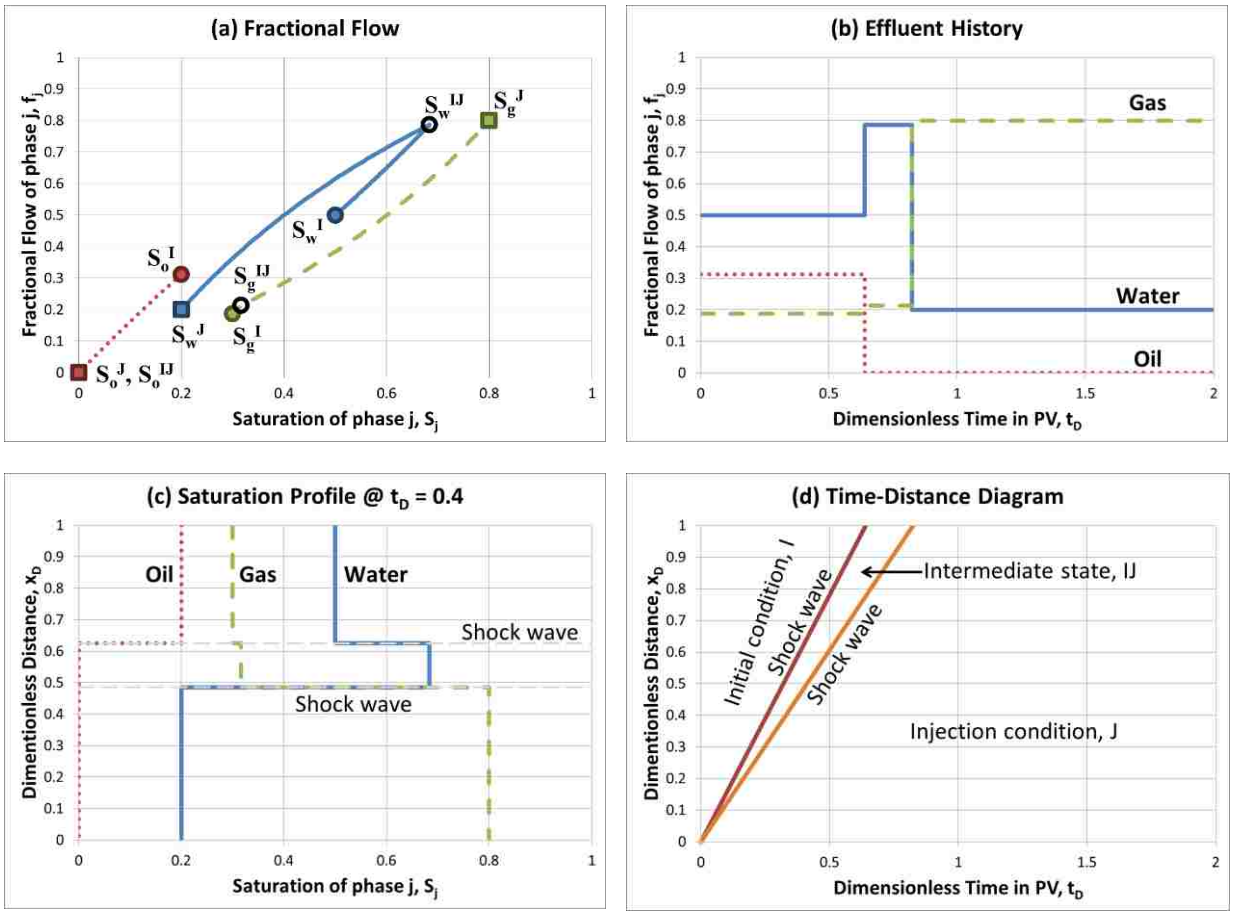

Figure 3.15: Case 3.2: foam displacement at MRF = 100 with I:(S_w,S_o,S_g) = (0.5,0.2,0.3) and J:(f_w,f_g) = (0.2, 0.8)

Figure 3.17 shows corresponding pressure responses in terms of pressure profile at t_D = 0.4 and change in inlet pressure during foam injection. Similar to Case 3.1, the pressure gradient during foam propagation is primarily affected by MRF values as shown by the steep slope of the pressure profile in the first half of the system. Figure 3.18 shows the recovery factor. As expected, the oil recovery is faster and more efficient with higher MRF.

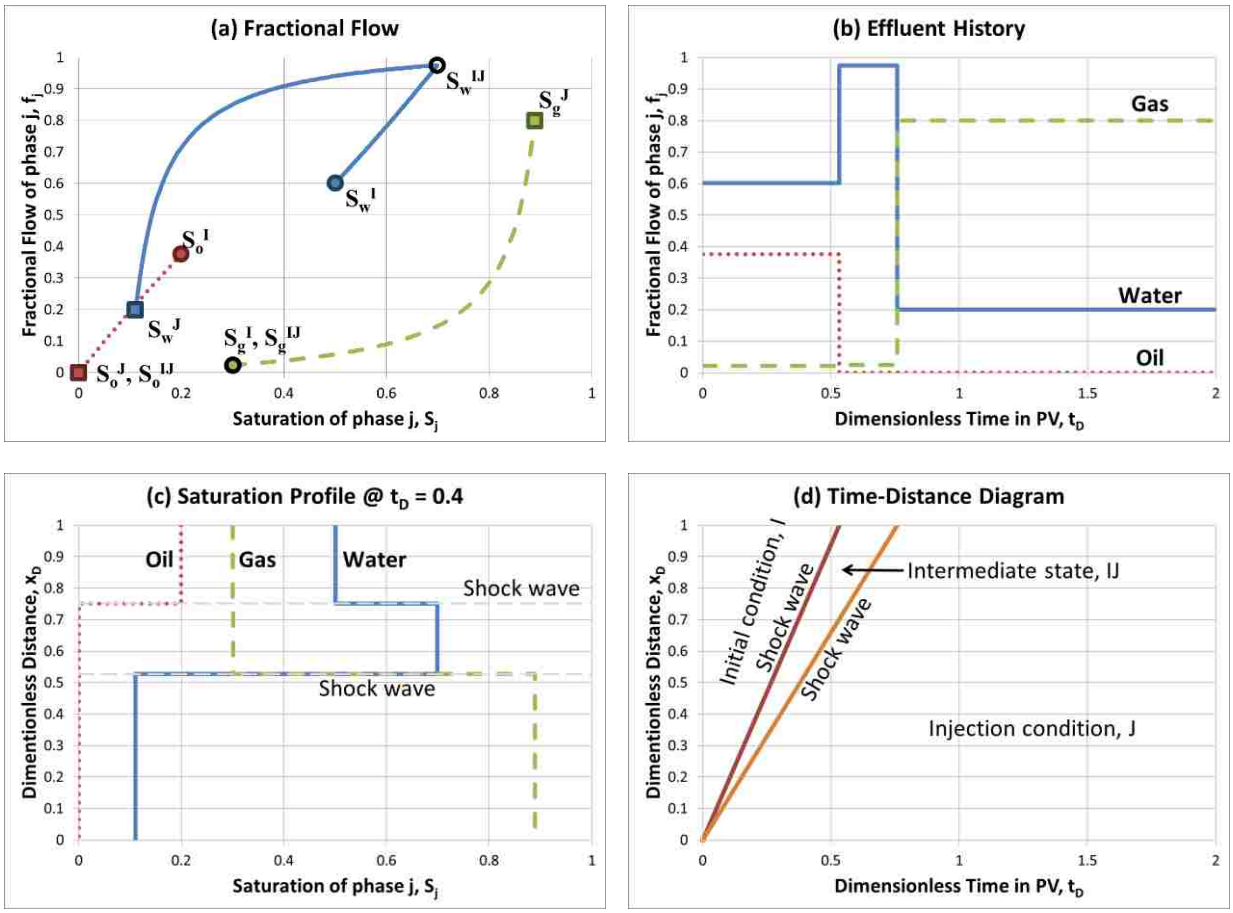

Figure 3.16: Case 3.2: foam displacement at MRF = 1000 with I:(S_w,S_o,S_g) = (0.5,0.2,0.3) and J:(f_w,f_g) = (0.2, 0.8)

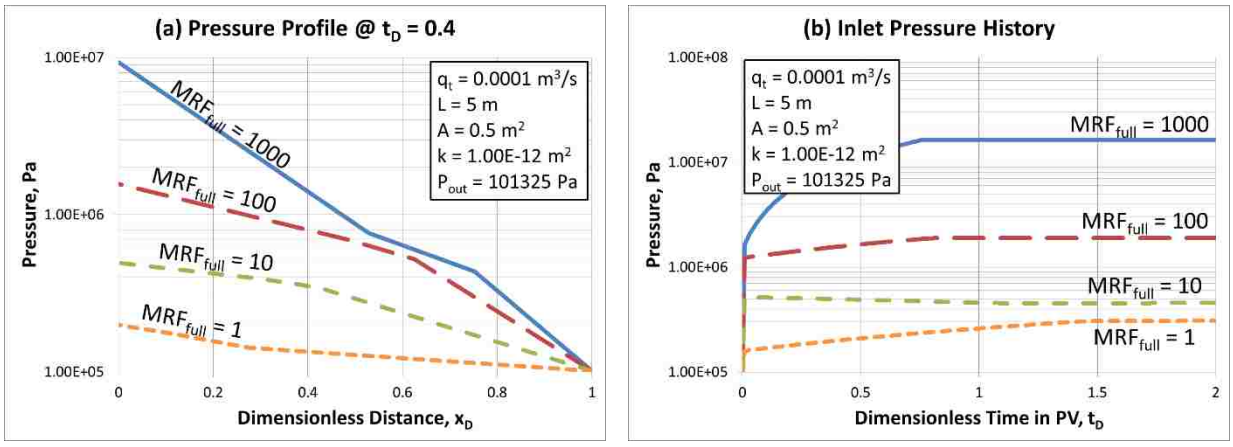

Figure 3.17: Case 3.2: effect of MRF on pressure

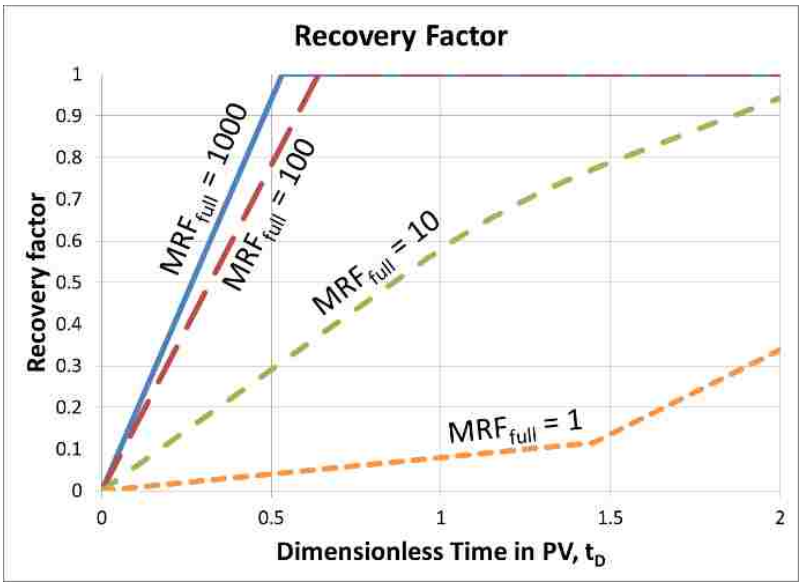

Figure 3.18: Case 3.2: comparison of recovery factor varying MRF

3.2.4 Comparison between fractional flow solutions and simulation results (Case 3.1 and Case 3.2)

In order to confirm the accuracy of foam fractional flow solutions and foam simulation results, two cases of (S_w, S_o, S_g) = (0.8, 0.2, 0.0) with MRF = 10 and (S_w, S_o, S_g) = (0.5, 0.2, 0.3) with MRF = 100 are selected. Figures 3.19 and 3.20 show the comparison in terms of saturation profile and effluent history. The solid lines show the results from fractional flow theory and the dotted lines show the results from 1D numerical simulation with 100 grid blocks. Although a slight numerical dispersion is observed near shock waves, they are in good agreement and the numerical dispersion can be significantly reduced by increasing the number of grid blocks. In fact, the results of all other cases in Case 1 and Case 2 also agree well with simulation, even though not shown here.

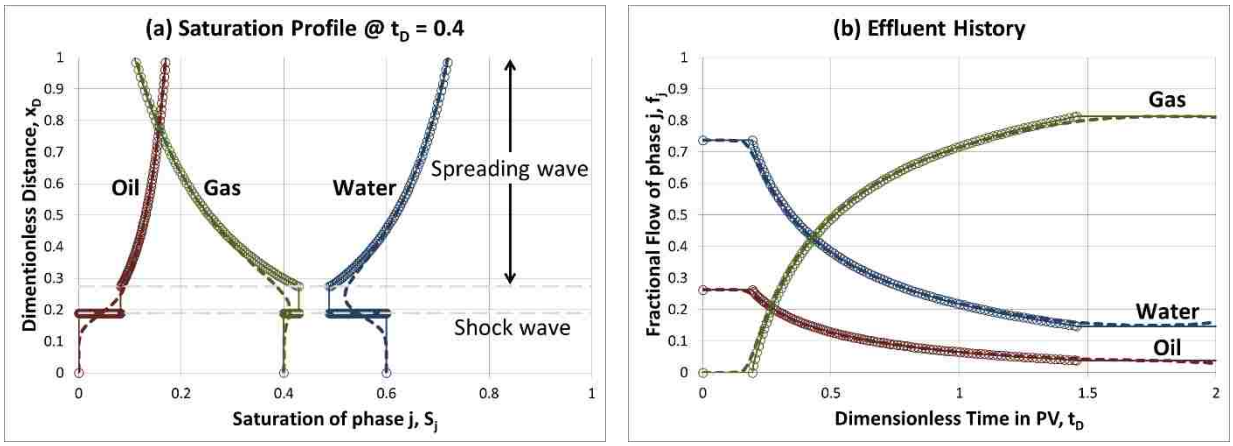

Figure 3.19: Case 3.1: comparison between fractional flow solutions and simulation results in the case of I:(S_w, S_o, S_g) = (0.8, 0.2, 0.0) with MRF = 10

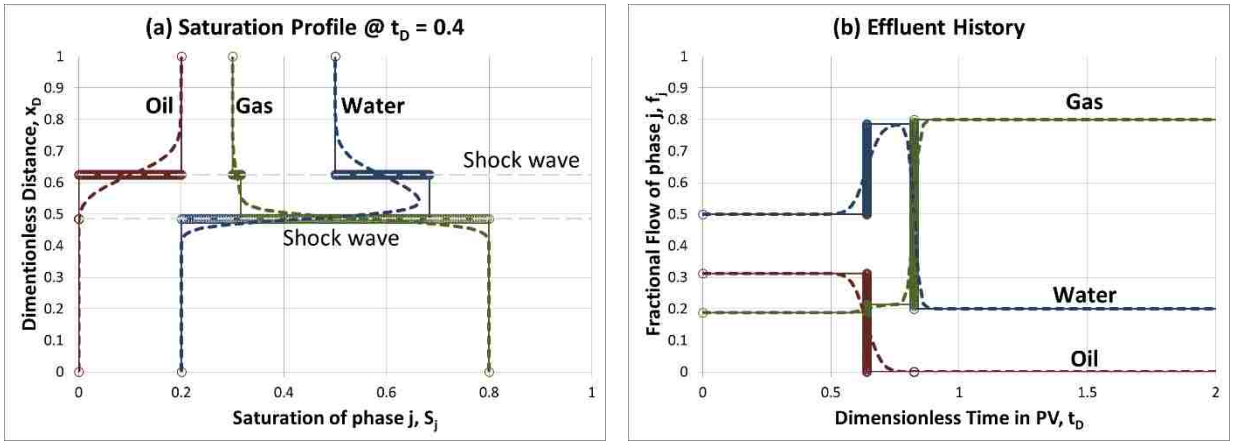

Figure 3.20: Case 3.2: comparison between fractional flow solutions and simulation results in the case of I:(S_w, S_o, S_g) = (0.5, 0.2, 0.3) with MRF = 100

3.2.5 Case 3.3: Foam strength adjusted by limiting water saturation (S_w*)

The effect of limiting water saturation (S_w*) is examined at the S_w* values of 0.4 and 0.6, when the initial condition is (S_w, S_o, S_g) = (0.5, 0.2, 0.3) and MRF_{full} = 100. Although the selection of S_w* is somewhat arbitrary in this modeling study, it is made primarily because S_w* = 0.4

intersects the original path between IJ and J (see IJ and J in Figure 3.12 (c)), and S_w^* = 0.6 intersects original paths between IJ and J and between I and IJ (see I, IJ, and J in Figure 3.12 (c)). The new paths after applying S_w^* values are shown in the ternary diagram of Figure 3.21. In contrast with the original path with no S_w^* effect (Figure 3.12(c)), the MRF values at the injection water saturation (S_w^J) are 28.1 and 11.9 for S_w^*=0.4 and 0.6, respectively (see Figure 3.4(b)), even though MRF_{full} = 100. Since S_w^* value alters the saturations and MRFs at the injection condition, the different values of S_w^* may produce very different displacement paths as shown in Figure 3.21.

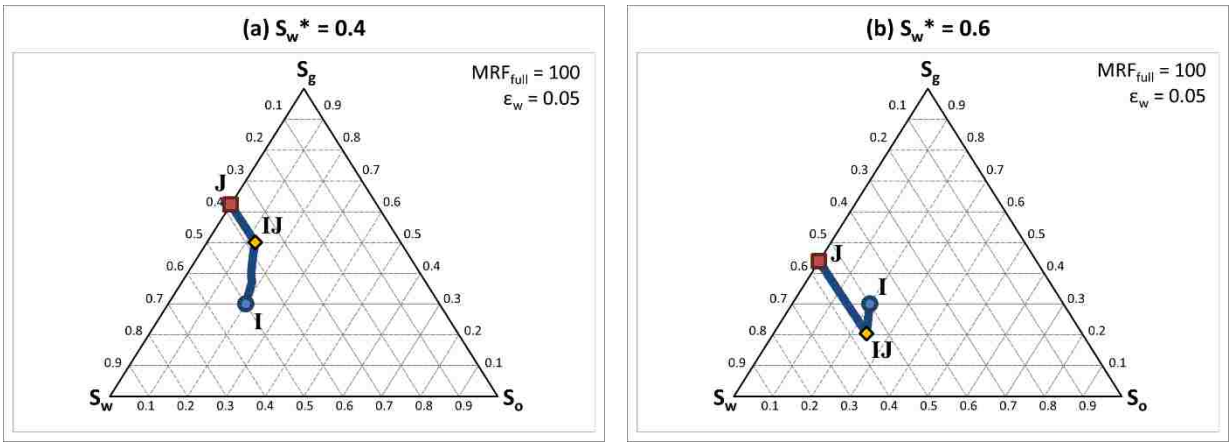

Figure 3.21: Case 3.3: foam displacement at MRF_{full}=100 with I:(S_w,S_o,S_g) = (0.5,0.2,0.3), J:(f_w,f_g) = (0.2, 0.8) and S_w^*

Figure 3.22 shows the detailed results for S_w^* = 0.4. The dotted lines in saturation profile and effluent history are calculated by foam simulation with 1000 grid blocks. As expected, by placing S_w^* between J and IJ, the injection saturation (S_w^J) moves closer to S_w^* and therefore the location of IJ and the velocity of the shock wave are also affected. Because of sharply changing MRF around S_w = S_w^*, a slight discrepancy in saturation profile and effluent history may occur

between fractional flow solutions and foam simulations, which essentially disappears with an increasing number of grid blocks.

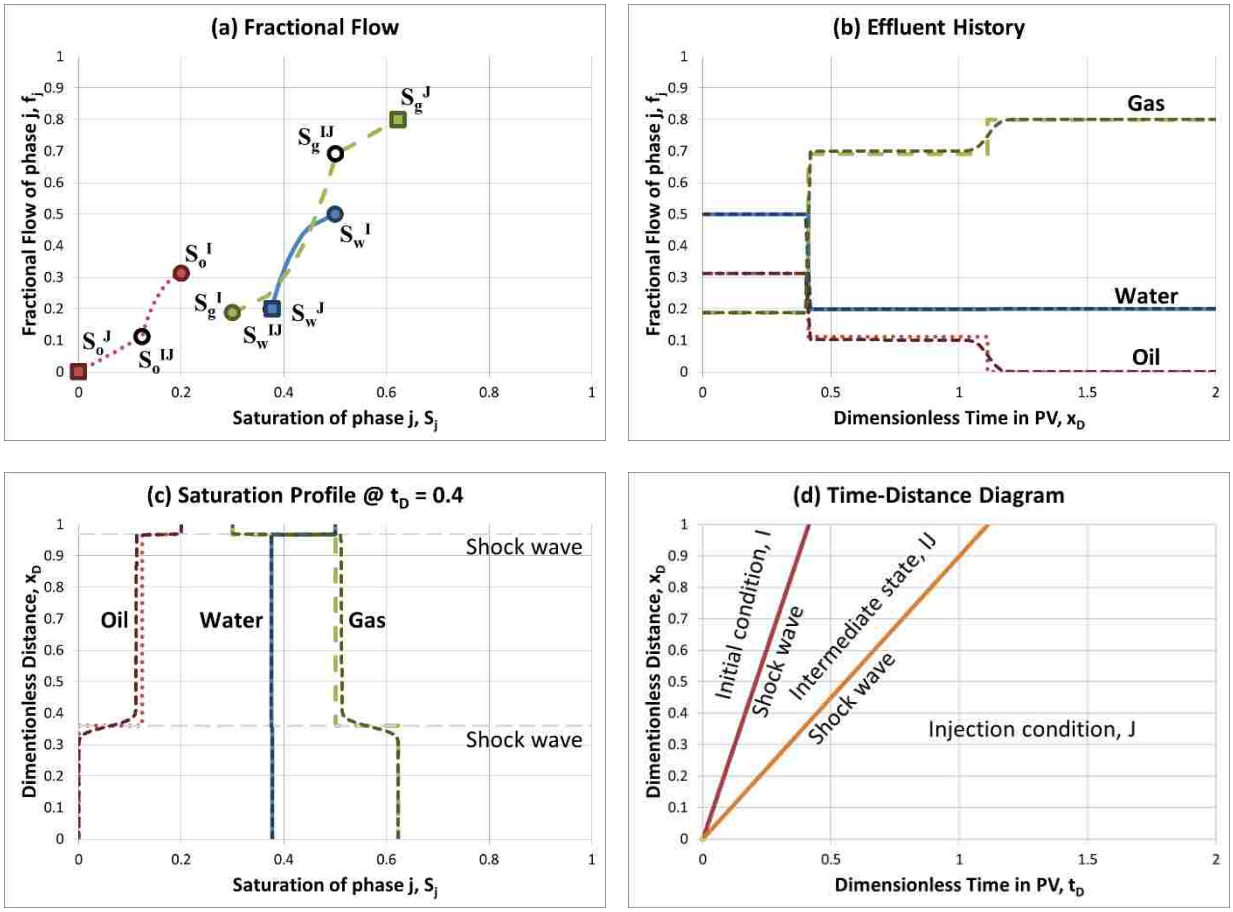

Figure 3.22: Case 3.3: Foam displacement at MRF_{full}=100 with I:(S_w,S_o,S_g) = (0.5,0.2,0.3), J:(f_w,f_g) = (0.2, 0.8), S_w* = 0.4 and S_o* = 1

Figure 3.23 shows similar results for S_w* = 0.6. Because of higher S_w*, MRF values along I, IJ, and J are further reduced compared with those at S_w* = 0.4. This results in a higher gas mobility, which leads to a higher gas fractional flow and a lower gas saturation at the injection condition. Relatively low MRF at S_w* = 0.6 causes the displacement efficiency less favorable

compared with $S_w^* = 0.4$. Both fractional flow solutions and foam simulation results with 1000 grid blocks are in good agreement.

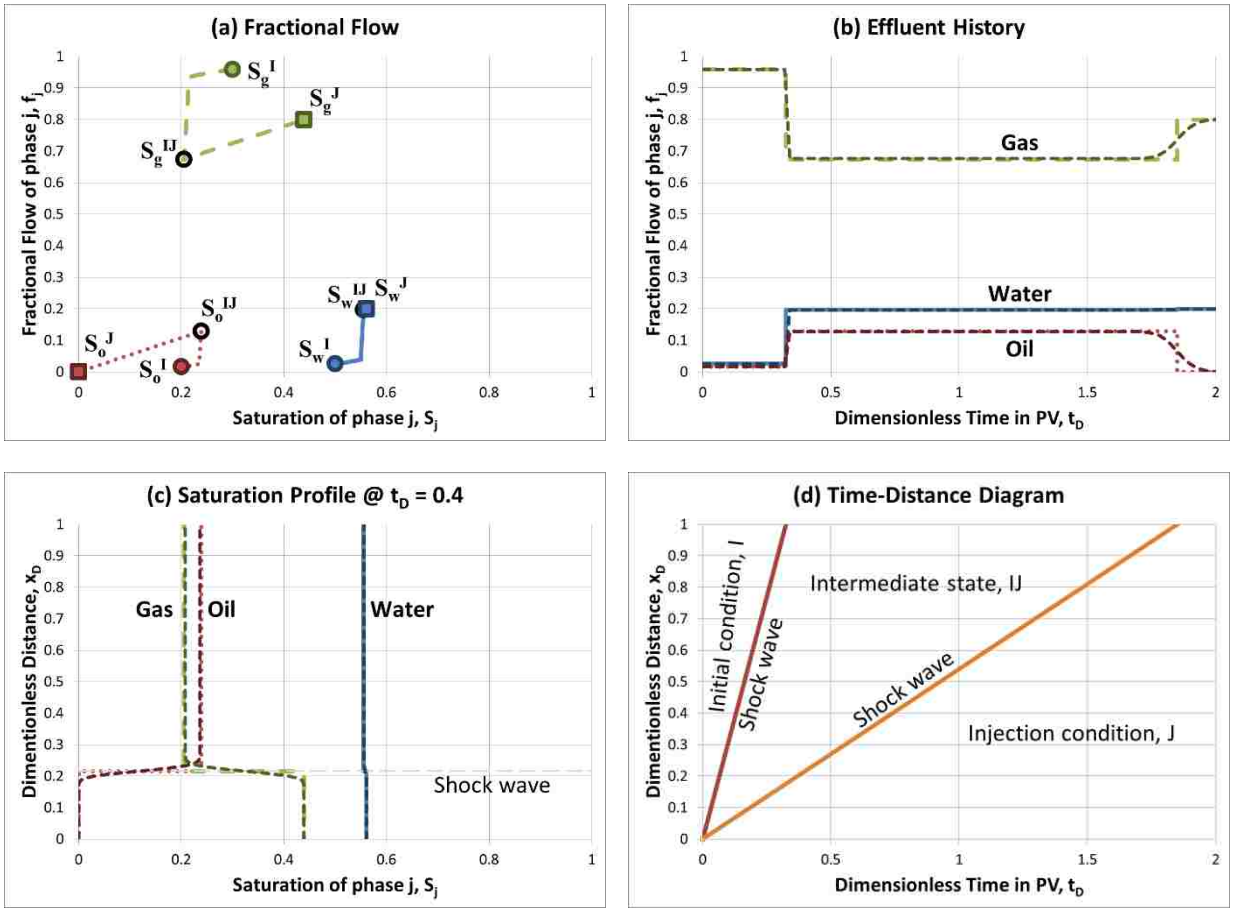

Figure 3.23: Case 3.3: foam displacement at MRF_{full}=100 with I:(S_w,S_o,S_g) = (0.5,0.2,0.3), J:(f_w,f_g) = (0.2, 0.8), $S_w^* = 0.6$ and $S_o^* = 1$

It should be noticed that because of $S_w^* = 0.4$ and 0.6 with $\varepsilon_w = 0.05$, sharp corners are expected in factional flow curves at $S_w = 0.35 - 0.45$ in Fig 23 and at $S_w = 0.55 - 0.65$ in Figure 3.23. Such a sharp corner is shown clearly at $S_w = S_w^* - \varepsilon_w = 0.55$ in water fractional flow curve and at the corresponding points in oil and gas fractional flow curves in Figure 3.23(a).

3.2.6 Case 3.4: Foam strength adjusted by critical oil saturation (S_o*)

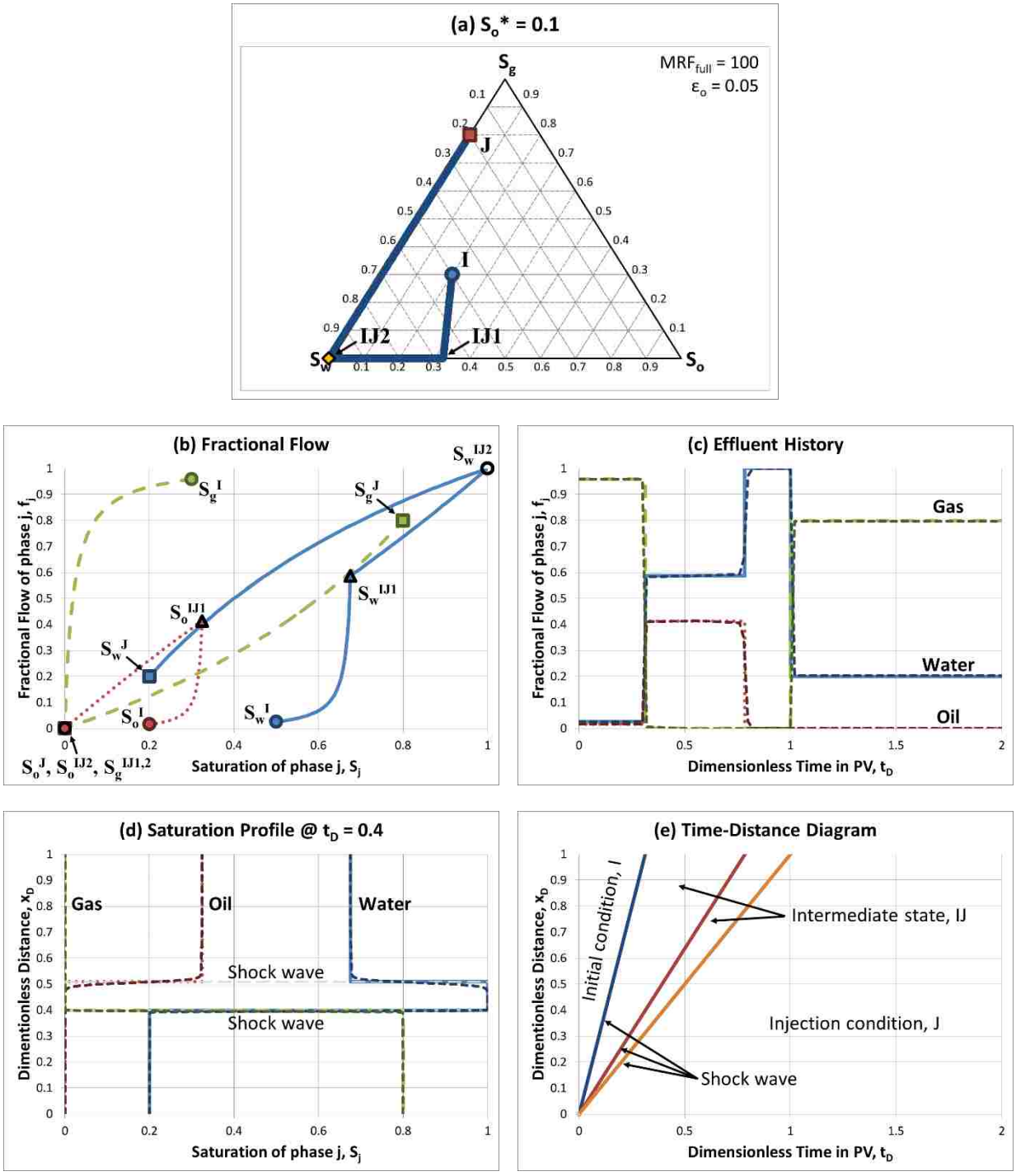

Figure 3.24: Case 3.4: foam displacement at MRF_{full} = 100 with I:(S_w,S_o,S_g) = (0.5,0.2,0.3), J:(f_w,f_g) = (0.2, 0.8), S_w* = 0 and S_o* = 0.1

The effect of critical oil saturation (S_o*) is examined at the S_o* value of 0.1, when the initial condition is (S_w, S_o, S_g) = (0.5, 0.2, 0.3) and MRF_{full} = 100. As presented by the ternary diagram with no S_o* accounted for, this value of S_o* intersects the original path between I and IJ (Figure 3.12(c)). Because the initial condition has oil saturation (S_o^I = 0.2)) higher than S_o* + ε_o (S_o = S_o* + ε_o = 0.15) and the injection condition has oil saturation (S_o^J = S_{or} = 0.0)) lower than S_o* - ε_o (S_o = S_o* - ε_o = 0.05), MRF values change from MRF = MRF_{full} = 100 to MRF = 1 from J to I due to the imposed S_o*. Figure 3.24 shows detailed results for S_o* = 0.1. The displacement path from fractional flow theory is described in the ternary diagram. As shown in the fractional flow curve, there are three different shock waves; in this case, forming two different constant states (IJ_2 is the constant state between σ^+ and σ^- while IJ_1 is a new constant state created by S_o* = 0.1). The fractional flow solutions and foam simulation results with 1000 grid blocks match well when the effluent history and the saturation profile are contrasted.

3.2.7 Case 3.5: Foam strength adjusted by limiting water saturation (S_w*) and critical oil saturation (S_o*)

If both S_w* and S_o* are applied, the calculation becomes more complicated because a larger portion of the ternary diagram falls within S_w* - ε_w < S_w < S_w* + ε_w and S_o* - ε_o < S_o < S_o* + ε_o, where MRF changes from its full value (MRF = MRF_{full}) to the unity (MRF = 1). Dealing with these two discontinuities implies two things within the context of this study: (i) due to the presence of multiple sharp corners in the fractional flow curves as explained in Figures 3.23 and 3.24 which result in a wide range of possible solution paths, one cannot solve foam fractional flow curves easily; and (ii) because of this difficulty, it is convenient to rely on foam simulations at first in order to identify the paths ahead of fractional flow calculations - a good combination of time step

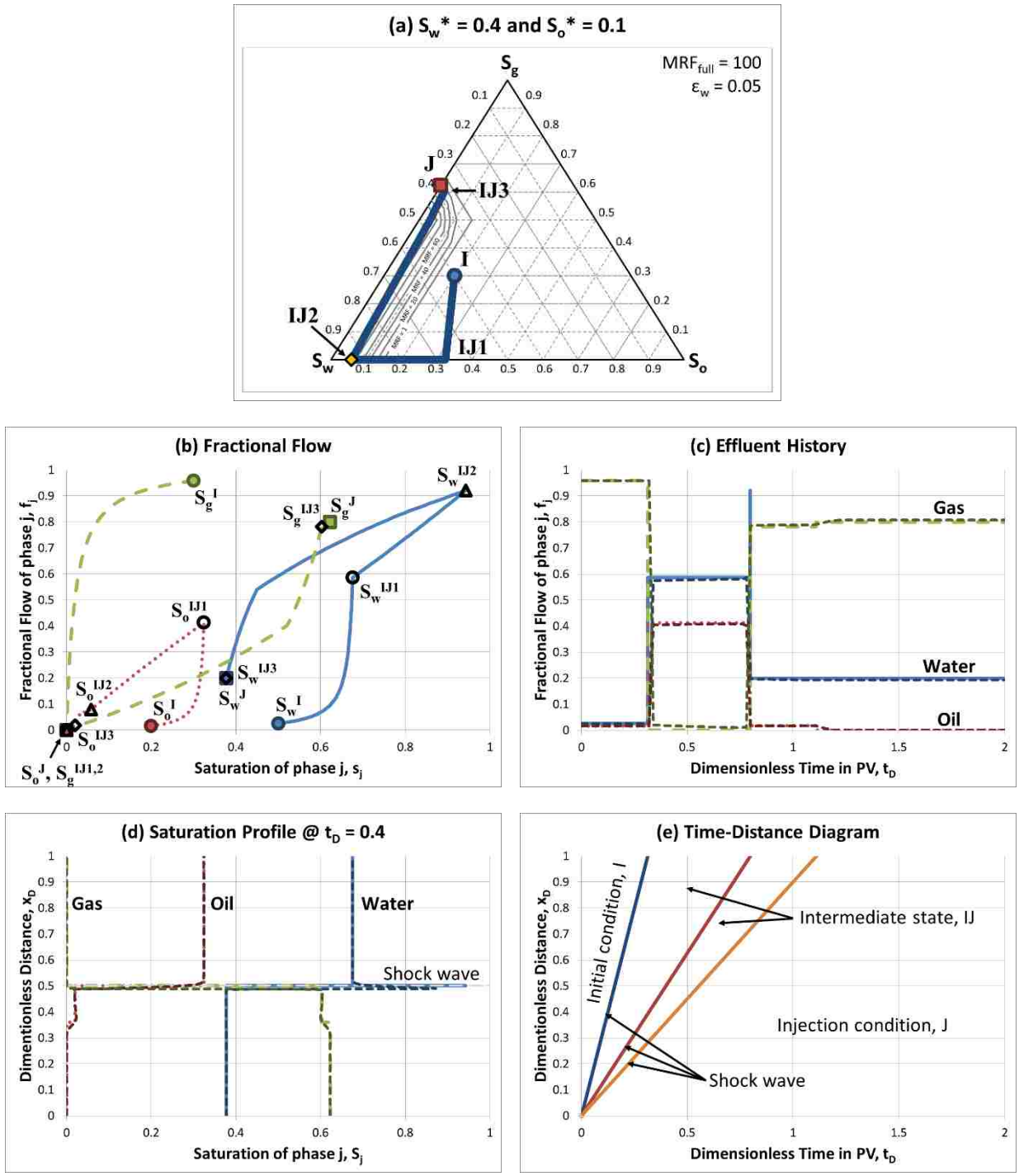

Figure 3.25: Case 3.5: Expected foam displacement at MRF_{full} = 100 with I:(S_w,S_o,S_g) = (0.5,0.2,0.3), J:(f_w,f_g) = (0.2, 0.8), S_w* = 0.4 and S_o* = 0.1

size and grid block size is required, however, to make the simulation stable and convergent.

One example of such a case is shown in Figure 3.25 where $S_w^* = 0.4$ and $S_o^* = 0.1$ are imposed together and finding the saturation paths satisfying coherence theory is thus complicated. The task can still be done, even though it is slow, time-consuming, and labor-intensive (see numerous possible paths between J and IJ_2 in Figure 3.25(a) for example). There exist three constant states - IJ_2 between σ^+ and σ^-, IJ_1 due to $S_o^* = 0.1$ and IJ_3 due to $S_w^* = 0.4$. Again, the fractional flow solutions and foam simulation results with 1000 grid blocks show good agreements.

3.2.8 Case 3.6: Non-uniform initial condition with S_w^* and S_o^*

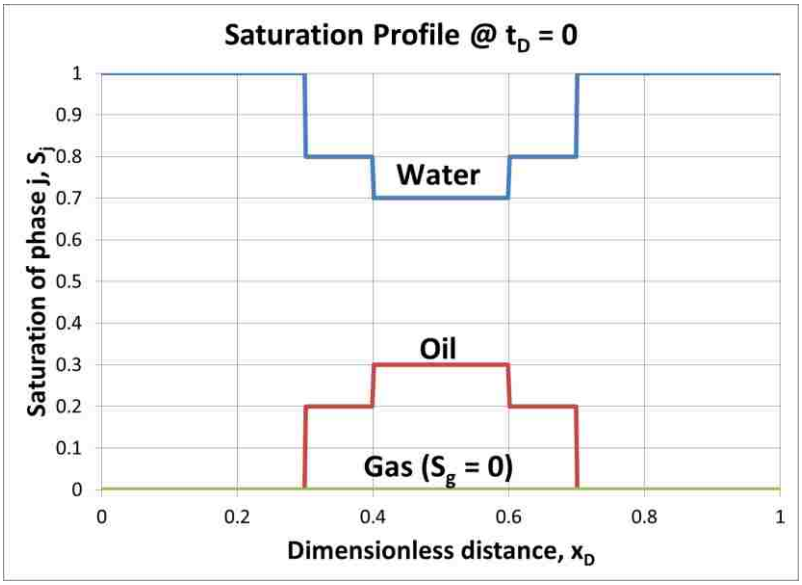

Figure 3.26: Case 3.6: Initial condition of $MRF_{full} = 100$ with non-uniform initial condition, J:$(f_w,f_g) = (0.2, 0.8)$, $S_w^* = 0.4$ and $S_o^* = 0.1$

The uniform initial conditions applied in all previous cases are not necessarily valid in actual field conditions. In fact, the typical distribution of contaminants is likely that the concentration is the highest near the center of the plume and decreases away from the center

gradually. Unfortunately such a non-uniform initial condition has been beyond the interest of fractional flow analysis because of complexity caused by the collision of numerous saturation waves. For those complex problems, foam simulation validated and guided by foam fractional flow analysis can be used. Figure 3.26 shows an example of non-uniform initial condition where the center of the plume has oil saturation as high as 0.3, and decreasing down to 0.2 and zero step by step, with no gas present.

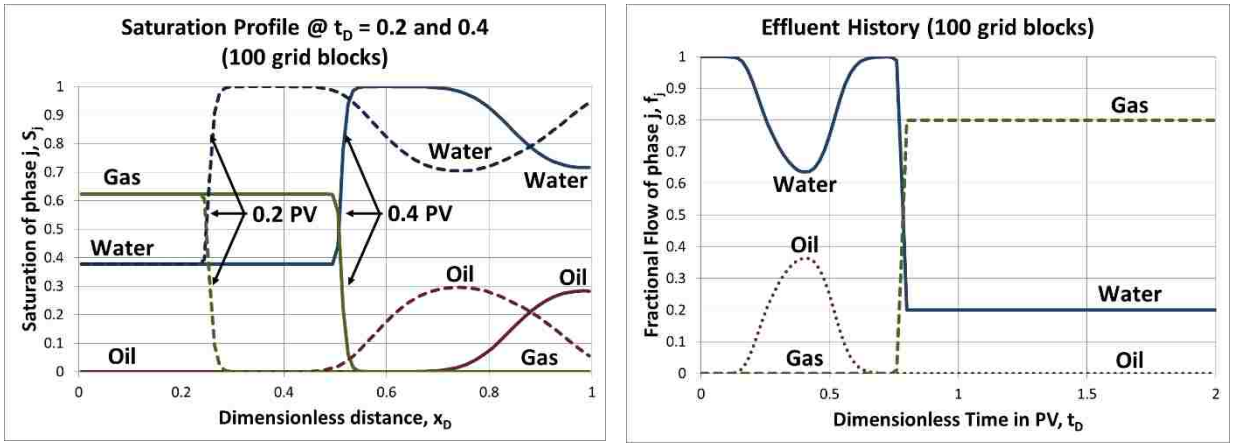

Figure 3.27: Case 3.6: Saturation profile and effluent history at MRF_{full} = 100 with non-uniform initial condition, J:(f_w,f_g) = (0.2, 0.8), S_w* = 0.4 and S_o* = 0.1 (100 grid blocks)

Figures 3.27 and 3.28 show the saturation profile and effluent history constructed by foam simulation (not by the fractional flow analysis) at two different dimensionless times of 0.2 PV and 0.4 PV with 100 and 500 grid blocks, respectively, where MRF_{full} = 100, S_w* = 0.4, and S_o* = 0.1. The results show that the stable foam injected at the inlet displaces oil plume efficiently. Enough resolution is needed, however, in order to see the change in saturations accurately – a numerical dispersion may significantly smear out the initial distribution of oil when 100 grid blocks are used, while such a symptom is improved somewhat at 500 grid blocks. Figures 3.27 and 3.28

demonstrate the strength of foam numerical simulation, which is ready to solve foam displacement in practical field applications once finely validated and tuned with analytical solutions from the MoC-based fractional flow solutions.

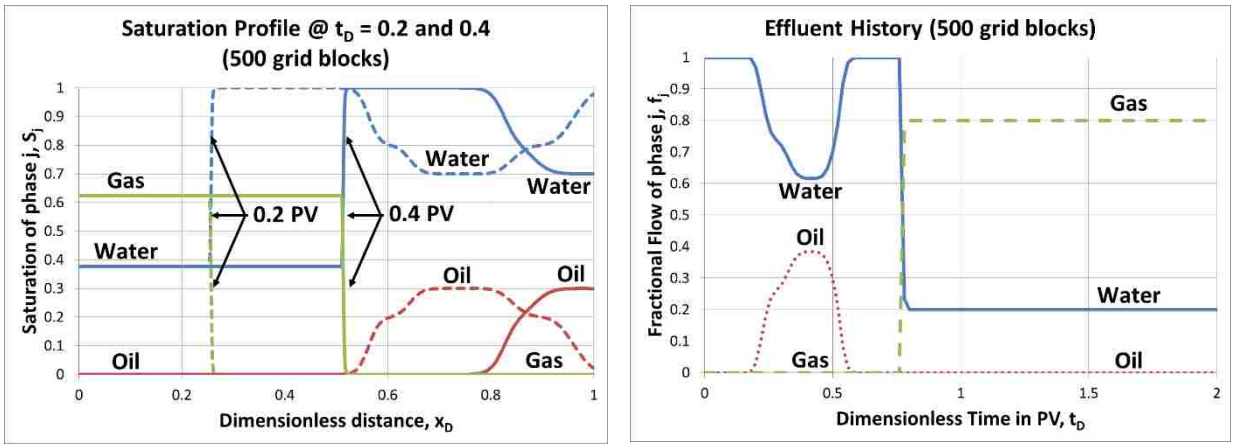

Figure 3.28. Case 6: Saturation profile and effluent history at MRF_{full} = 100 with non-uniform initial condition, J:(f_w,f_g) = (0.2, 0.8), S_w* = 0.4 and S_o* = 0.1 (500 grid blocks)

In contrast with Figure 3.28, one more case (Fig 3.29) is simulated when the non-uniform initial saturation profile is positioned at the inlet rather than at the center of the medium (cf. Fig 3.26). The results in Figures 3.30 and 3.31 show that the solution in this case can be much more complicated because the injected foams interact with the oil initially present. Therefore, the effect of oil saturation on foam stability is inevitable. Except the position of oil bank, other conditions are the same as the case of Figures 3.26 through 3.28. Figures 3.30 and 3.31 show the saturation profile and effluent history at 0.2 PV and 0.4 PV with 100 and 500 grid blocks. Although some of injected gas passes through the oil bank because of the effect of oil, it propagates as a small foam bank just ahead of the oil bank with almost same velocity of injected foam. Since surfactant pre-flush is assumed prior to foam injection, the bypassed gas makes a strong foam again after passing

through the oil bank. Not only analytical methods but also simulations should be used together to have a good insight in such complicated cases.

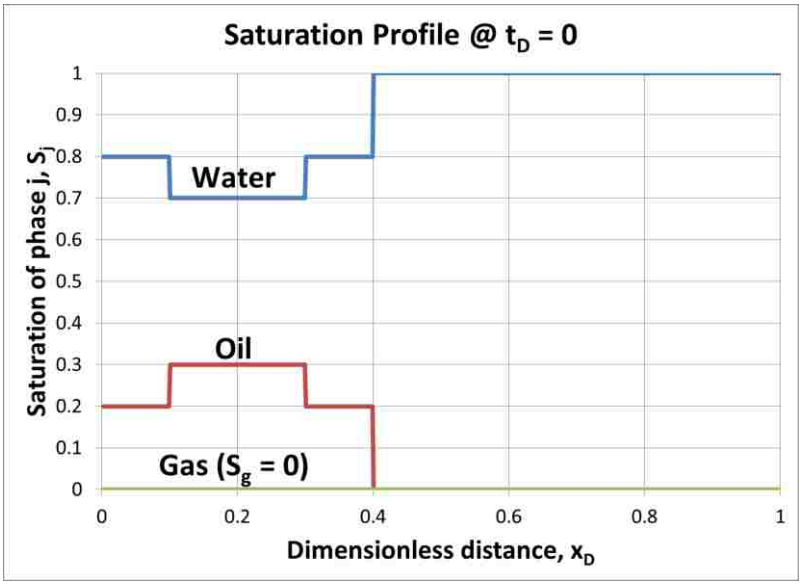

Figure 3.29: Case 3.6: Initial condition of MRF_{full} = 100 with non-uniform initial condition, J:(f_w,f_g) = (0.2, 0.8), S_w* = 0.4, S_o* = 0.1 and $\varepsilon_w = \varepsilon_o$ = 0.05

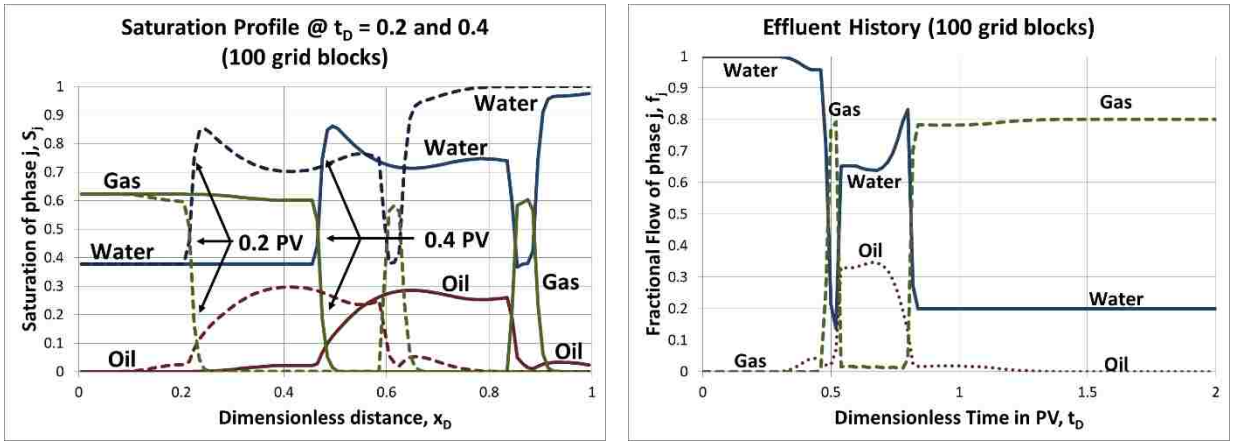

Figure 3.30: Case 3.6: Saturation profile and effluent history at MRF_{full} = 100 with non-uniform initial condition, J:(f_w,f_g) = (0.2, 0.8), S_w* = 0.4, S_o* = 0.1 and $\varepsilon_w = \varepsilon_o$ = 0.05 (100 grid blocks)

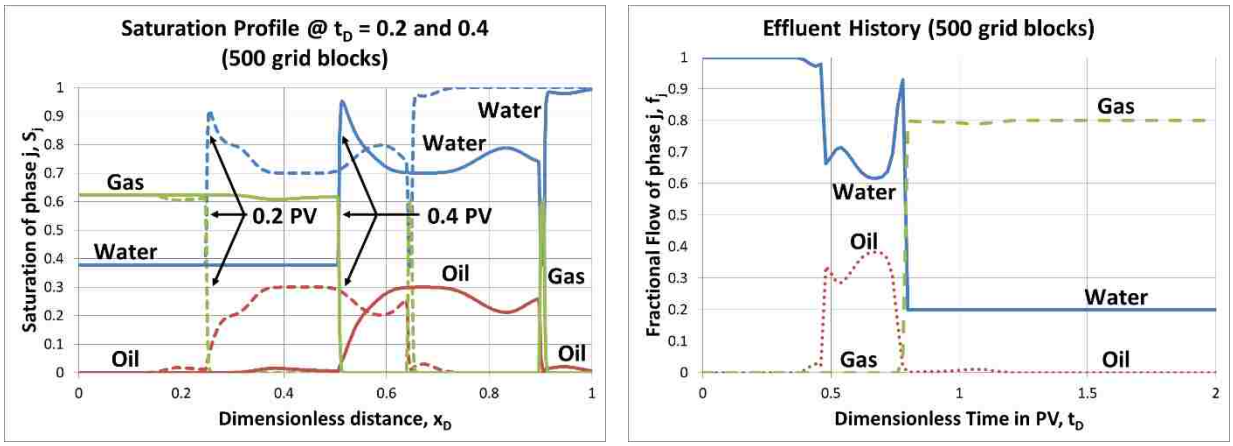

Figure 3.31: Case 6: Saturation profile and effluent history at MRF_{full} = 100 with non-uniform initial condition, J:(f_w,f_g) = (0.2, 0.8), S_w* = 0.4 and S_o* = 0.1 (500 grid blocks)

CHAPTER 4
EXTENSION OF THE MODEL FOR MULTI-LAYER SYSTEMS WITH SUBSURFACE HETEROGENEITY

This chapter investigates how the foam model developed in the previous chapter can be extended and utilized for a complex subsurface system – multiple horizontal layers with differing properties in the absence of vertical communications. Results are analyzed in terms of displacement efficiency in individual layers as well as fluid injectivity into each layer. This is a step necessary to match laboratory experimental data to understand foam diversion process, which can then be followed by full field-scale foam applications in the presence of vertical communications.

4.1 Methodology

For the extension of the model developed in Chapter 3 into multi-layer systems, additional features should be added.

First, the process of surfactant injection prior to foam injection (so-called surfactant pre-flush) needs to be included in the calculation. This requires surfactant adsorption during surfactant pre-flush be considered in the model. (This can be carried out by using a surfactant adsorption parameter, D_{sf},; see more in the following Methodology section.) In fractional flow theory, no dispersion and diffusion of components, uniform adsorption of polymer on rock, continuous injection of polymer at fixed concentration, no chemical reactions, surfactant only in aqueous phase (does not partition to oil) and local equilibrium adsorption of polymer on rock are assumed.

Second, by taking surfactant pre-flush into account, the process of surfactant and foam injection now deals with three phases with four different components. In other words, the gas and

oil phases consist of only one component while the aqueous phase may consist of either surfactant-free water or surfactant solution. In conjunction with surfactant adsorption, this implies that the fractional flow solution should incorporate not only saturations waves but also chemical waves too. How to deal with chemical shock in such a case can be found in other studies (Roostapour and Kam, 2012 and 2013).

4.1.1 Extension of the Model with Surfactant Component

In order to incorporate surfactant preflush into foam modeling, the Method of Characteristics (MoC) based model should be extended with surfactant component. With similar assumptions for the MoC analysis described in the previous chapter, the surfactant component in the aqueous phase can be expressed as

$$\phi \frac{\partial \left(S_w C_{sf,w}\right)}{\partial t} + \phi \frac{\partial \hat{C}_{sf}}{\partial t} + u_t f_w \frac{\partial C_{sf,w}}{\partial x} = 0 \tag{4.1}$$

by using material balance where, ϕ is porosity, S_w is water saturation, $C_{sf,w}$ is surfactant concentration in the aqueous phase, $\hat{C}_{sf}$ is surfactant concentration in the solid phase per unit pore volume of rock, u_t is total velocity, and f_w is water fractional flow. In equation (4.1), the surfactant adsorption term, $\hat{C}_{sf}$, is defined as

$$\hat{C}_{sf} = \frac{(1-\phi)\rho_s A_{sf}}{\phi} \tag{4.2}$$

where ρ_s is the grain density of rock (or matrix) and A_{sf} is adsorption of surfactant per unit mass of rock. Because surfactant molecules exist only within bulk aqueous phase or onto rock surface, this equation could be written as

$$\phi \frac{\partial C_{sf,w}}{\partial t}\left(S_w + \frac{\partial \hat{C}_{sf}}{\partial C_{sf,w}}\right) + u_t f_w \frac{\partial C_{sf,w}}{\partial x} = 0 \tag{4.3}$$

If the adsorption coefficient for surfactant molecules, D_{sf}, is defined as

$$D_{sf} = \frac{\partial \hat{C}_{sf}}{\partial C_{sf,w}} \tag{4.4}$$

and if the definitions of dimensionless distance, x_D, and time, t_D, are applied, equation (4.3) becomes

$$\frac{\partial C_{sf,w}}{\partial t_D}\left(S_w + D_{sf}\right) + f_w \frac{\partial C_{sf,w}}{\partial x_D} = 0 \tag{4.5}$$

As a result, the characteristic velocity of surfactant component in aqueous phase in dimensionless form (or, dimensionless velocity of surfactant chemical shock) becomes

$$\frac{dx_D}{dt_D} = \left(\frac{f_w}{S_w + D_{sf}}\right)^J \tag{4.6}$$

See Pope (1980) and Lake (1989) for more details about derivation procedures.

4.1.2 Surfactant/Foam Displacement in Multi-layer Systems

The solution scheme required for a single-layer system (i.e., identifying saturation paths, constructing saturation velocities in a manner consistent with velocity constraints, and determining saturation profile, effluent history, time-distance diagram, and pressure profile and history) is extended to a system with non-communicating multiple layers in this study in order to investigate how surfactant and foam propagate in such a composite system.

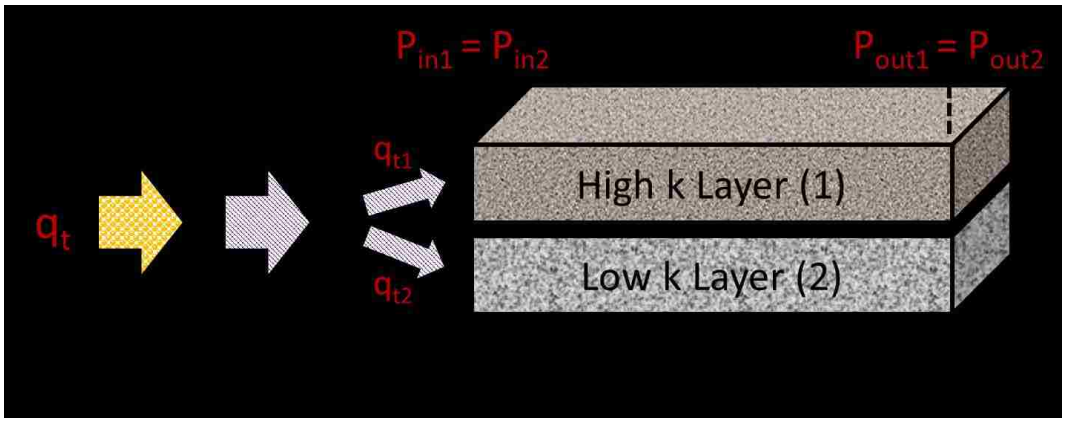

Figure 4.1: A schematic for two-layer system sharing the same inlet and outlet pressures ($P_{in1} = P_{in2}$ and $P_{out1} = P_{out2}$) and material balance ($q_t = q_{t1} + q_{t2}$)

Figure 4.1 defines a system used in this study: each layer is specified with its own petrophysical and fluid properties such as porosity, permeability, relative permeability, residual saturations, initial conditions, foam properties (mobility reduction factor (MRF), limiting water saturation (S_w*), and critical oil saturation (S_o*)), and so on. Surfactant solution or foam is injected at the fixed flow rate of q_t, at the injection foam quality of 80%, but the fraction of flow into each layer (q_{t1}, q_{t2}) changes with time depending on the resistance of each layer. During fluid injection, the inlet pressure for each layer is identical but changes with time, while the outlet pressure for each layer is fixed at a constant value (i.e., not changing with time) as a backpressure. It is further assumed that the layers do not communicate in the vertical direction, meaning that there is no cross flow between the layers. (A vertical communication between the layers can be important in field cases, but this assumption allows the model to investigate how foam works in more idealized system, as a first step, without dealing with complicated nature of flow in multi-dimensional space.)

4.2 Results

This study first presents the results of a series of surfactant and foam injection into a single-layer system (Case 4.1), and then moves into a two-layer system with MRF values invariant (Case 4.2); MRF values as a function of absolute permeability (k) (Case 4.3), as a function of S_w (or, S_w* effect, Case 4.4), as a function of initial condition (three phases, Case 4.5), and as a function of S_o (or, S_o* effect, Case 4.6); and lastly, a three-layer system with all those complexities combined (Case 4.7).

Table 4.1: Model parameters for construction of fractional flow curves

End-point relative permeability: $k^0_{rw} = k^0_{ro} = k^0_{rg} = 1$		
Relative permeability exponents: n_w,= $n_o = n_g = 1$		
Residual saturation: water (S_{wr}) = 0.1, oil (S_{or}) = 0, gas (S_{gr}) = 0		
Surfactant adsorption parameter (D_{sf}) = 0.2		
Water viscosity (μ_w) = 1 cp	Oil viscosity (μ_o) = 0.89 cp (5 cp for Case 6 and 7)	Gas viscosity (μ_g) = 0.02 cp

Table 4.2. Model parameters for pressure and injectivity calculations

Total injection rate (q_t) = 6000 ml/min	Cross-sectional area of each layer (A) = 0.5 m^2
Outlet pressure = 101,425 Pa (1 atm)	Length of each layer (L) = 5 m

Table 4.1 shows the parameters for petrophysical properties used in the calculations, and Table 4.2 shows dimensional parameters for the calculation of pressures and injectivity into each layer as a function of time. In addition, Table 4.3 and Table 4.4 show related input parameters for

Case 4.2 through Case 4.6 and Case 4.7, respectively, associated with initial conditions, injection conditions, and foam properties.

Table 4.3. Initial and injection conditions for a two-layer system (Case 4.2 through 4.6)

	High-permeability layer (1 darcy)	Low-permeability layer (0.5 darcy)
I:(S_w, S_o, S_g)	I:(0.7, 0.3, 0) (I:(0.5, 0.3, 0.2) for Case 4.5)	I:(0.3, 0.7, 0) (I:(0.2, 0.5, 0.3) for Case 4.5)
J_1:(f_w)	J_1:(1)	
J_2:(f_w, f_g)	J_2:(0.2, 0.8)	

Table 4.4. Initial and injection conditions for a three-layer system (Case 4.7)

	High-permeability layer (2 darcy)	Intermediate-permeability layer (1 darcy)	Low-permeability layer (0.5 darcy)
I:(S_w, S_o, S_g)	I:(0.7, 0.2, 0.1)	I:(0.4, 0.4, 0.2)	I:(0.2, 0.6, 0.2)
J_1: (f_w, f_g)		J_1:(1.0, 0.0)	
J_2:(f_w, f_g)		J_2:(0.2, 0.8)	
MRF_{full}	400	200	100
S_w*	0.2	0.3	0.8
S_o*	0.2	0.2	0.2

4.2.1 Case 4.1: displacement in a single-layer system with surfactant adsorption

Figure 4.2 shows the process where surfactant preflush and foams are injected into a medium initially with 70 % water saturation and 30 % oil saturation (i.e., I: (S_w, S_o, S_g) = (0.7, 0.3, 0.0)). The injection of surfactant solution is denoted by J_1 where only the aqueous phase is injected (i.e., J_1: (f_w, f_o, f_g) = (1.0, 0.0, 0.0)) and the subsequent foam injection is denoted by J_2 where 80 %

quality foams are injected (i.e., J_2: (f_w, f_o, f_g) = (0.2, 0.0, 0.8)). Therefore, the solution to the entire process is a combination of "injection condition of J_1 into a medium with initial condition I" and "injection condition of J_2 into a medium with initial condition (I) and the first injection condition (J_1)". In this case, 0.3 PV of surfactant solution is considered prior to foam injection for demonstration purpose, and furthermore all mobile oils are assumed to be displaced by surfactant injection (i.e., residual oil saturation (S_{or}) after surfactant flooding = 0.0), for simplicity, so that the injected foams do not interact with oils. More complicated situations where the injected foams interact with oil follow in the later cases.

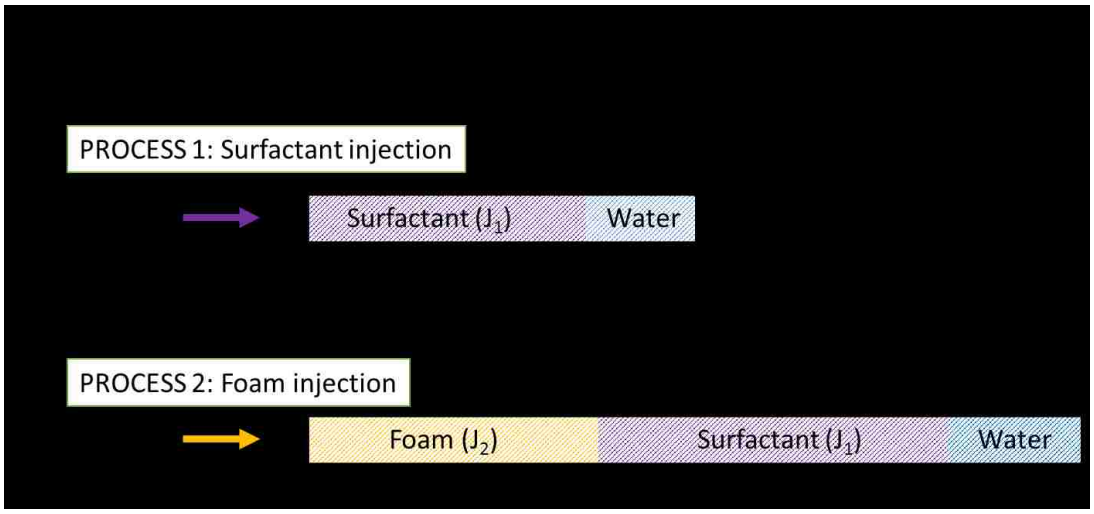

Figure 4.2: A schematic of Case 4.1: surfactant injection (process 1) followed by foam injection (process 2)

Figures. 4.3(a) through 4.3(d) show the displacement process during surfactant preflush and foam injection, consisting of fractional flow curves, effluent history, saturation profile, and time-distance diagram (a set of these four plots is sometimes referred to as Walsh diagram). As

shown in Fig. 4.3(a), the initial condition is given by I: (S_w, S_o) = (0.7, 0.3) on the water-oil fractional flow curve, and the injection conditions for surfactant preflush and foam injection are given by J_1: (f_w, f_g) = (1.0, 0.0) on the surfactant-oil fractional flow curve and J_2: (f_w, f_g) = (0.2, 0.8) on the surfactant-gas fractional flow curve, respectively. Note that the water-oil and surfactant-oil fractional flow curves are placed on the top of each other because viscosity and density of surfactant solution are assumed to be the same as surfactant-free water, for simplicity. The level of surfactant adsorption is shown by D_{sf}: (-0.2, 0.0). The MRF value of foams is set to be 100.

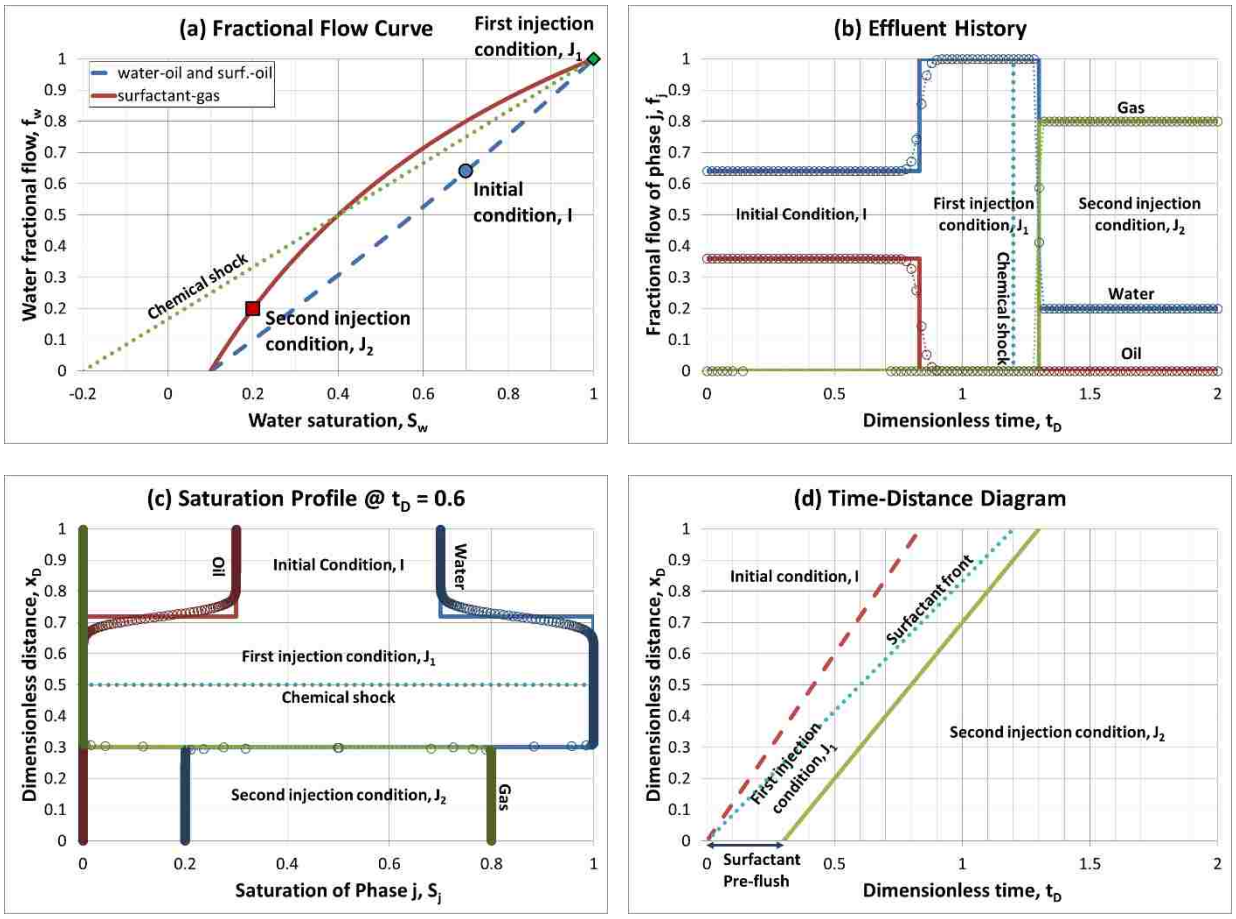

Figure 4.3: Case 4.1: displacement in a single layer system at MRF = 100 with I:(S_w, S_o, S_g) = (0.7, 0.3, 0), J_1: (f_w,f_g) = (1.0, 0.0) and J_2:(f_w, f_g) = (0.2, 0.8)

Following the velocity constraint (in this case, saturation velocity must increase from J_1 to I and J_2 to J_1), two shock waves govern the entire displacement process – the first traveling at the dimensionless velocity equivalent to the slope of the line I and J_1 ($v_D = df_w/dS_w = 1.2$); and the second at the dimensionless velocity equivalent to the slope of the line J_1 and J_2 ($v_D = df_w/dS_w = 1.0$). The velocity of chemical shock can be determined by connecting D_{sf} and J_1, i.e., $v_s = 0.83$, which is somewhat slower than other saturation shocks.

Figures. 4.3(b) and 4.3(c) show effluent history (i.e., fractional flow at the outlet as a function of dimensionless time t_D in PV) and saturation profile (i.e., saturations as a function of dimensionless distance, $x_D = x/L$) at $t_D = 0.6$. In both plots, the presence of three constant states (I, J_1, and J_2) and saturation velocities are well captured, and the analytical solutions in solid lines are in good agreement with simulation results in dotted lines with symbols. Note that the surfactant chemical front, represented by dashed lines, show a delay in surfactant propagation because of surfactant adsorption.

Figure 4.3(d) shows time-distance diagram to present wave propagation. The plot shows consistency with Figures 4.3(a) through 4.3(c) in that there exist a fast shock between I and J_1, a slow shock between J_1 and J_2, and a surfactant chemical shock lagging behind the fast shock. Because of 0.3 PV of surfactant pre-flush, the presence of surfactant is always guaranteed during foam injection. During t_D from 0.3 PV to 0.834 PV, all three conditions (I, J_1, and J_2) are present in the medium, but foams do not interact directly with the initial condition. The results show that injection of surfactant pre-flush less than 0.2 PV causes foam front to catch up and interact with the initial condition, which may reduce sweep efficiency significantly. Such a complicated situation is discussed later.

4.2.2 Case 4.2: displacement in a two-layer system with permeability contrast

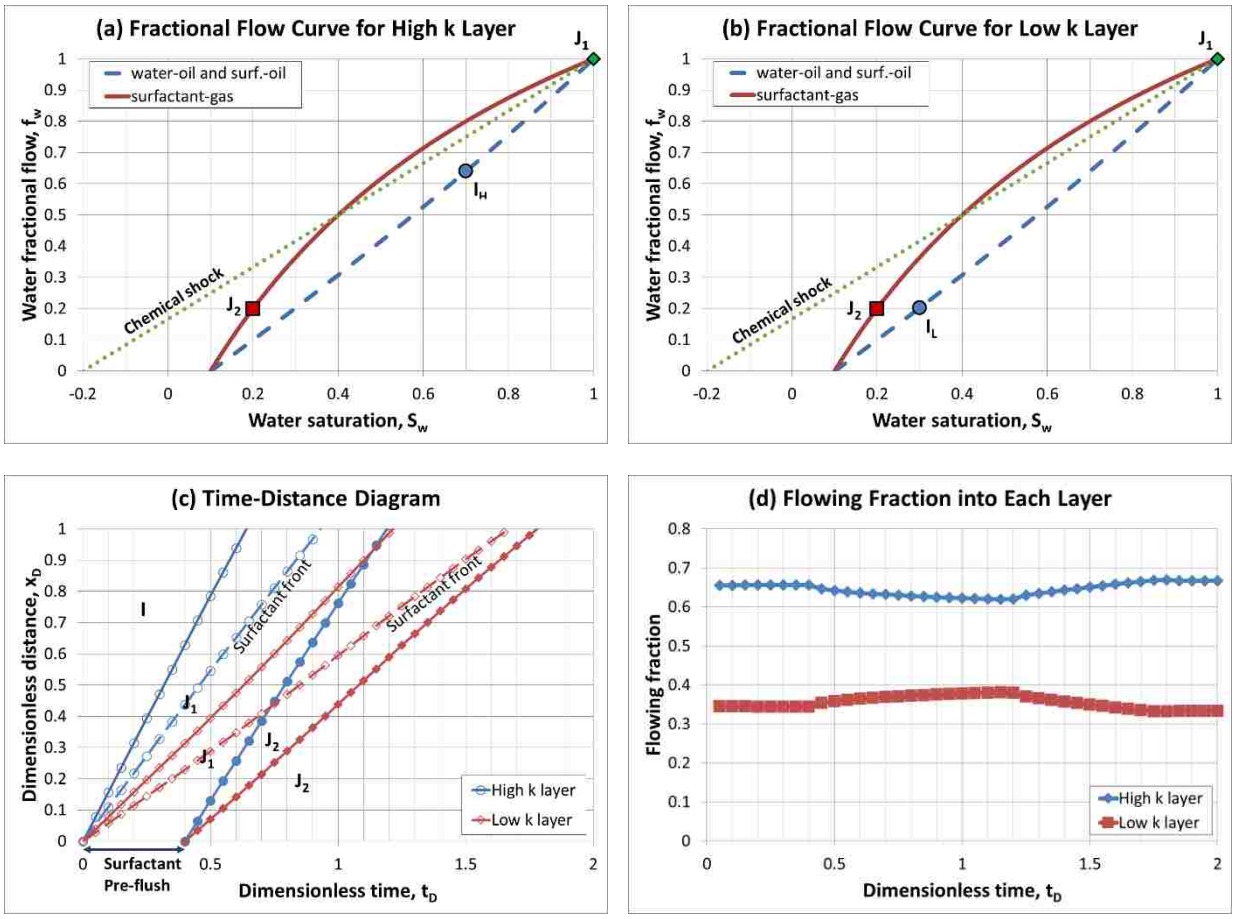

Figure 4.4: Case 4.2: displacement in a two-layer system with permeability contrast of 2 (k_H:k_L = 1 darcy:0.5 darcy) and the same MRF of 100 for both layers

Figures 4.4(a) and 4.4(b) show fractional flow curves for a two-layer system with different permeabilities - 1 darcy to represent high-permeability layer and 0.5 darcy for low-permeability layer, respectively, keeping other properties the same. This example assumes higher oil saturation in the high-permeability layer (I_H: (S_w, S_o) = (0.7, 0.3)) than the low-permeability layer (I_L: (S_w, S_o) = (0.3, 0.7)), as is often the case in the field. The injection conditions are the same as Case 4.1, which is surfactant preflush (J_1: (f_w, f_g) = (1.0, 0.0)) followed by foam injection (J_2: (f_w, f_g) = (0.2,

0.8)) with MRF = 100 in both layers. The level of surfactant adsorption is also given by D_{sf}: (-0.2, 0.0). Irrespective of the difference in terms of initial conditions, the nature of displacement in both layers is almost identical – two saturation shocks and one chemical shock, similar to Case 4.1. In addition, the velocity from I_H to J_1 and the velocity from I_L to J_1 are the almost same.

How the injected surfactant solution and foam propagate into each layer is shown in Figure 4.4(c), with foam injection starting with 0.4 PV delay (Note that this PV is the pore volume of the entire system). As expected, both surfactant and foam fronts in the high-permeability layer propagate faster primarily because of permeability difference. Figure 4.4(d) shows the fraction of injected flow into each layer with time. Overall, about two-thirds of fluids are injected into the high-permeability layer (or, one-third into the low-permeability layer, equivalently) during both surfactant and foam injections. This is expected because the permeability contrast between two layers is two (i.e., $k_H/k_L = 2.0$) and the MRF values are identical, meaning that foam does not play a role to modify injectivity into each layer.

4.2.3 Case 4.3: displacement in a two-layer system with MRF effect

Case 4.3 investigates the case with different MRF values – higher MRF at lower capillary pressure environment (or more stable foams at higher permeability) and lower MRF at higher capillary pressure environment (or less stable foams at lower permeability). More specifically, the MRF values for high-permeability and low-permeability layers are set to be 200 and 100, respectively, keeping all other conditions the same as Case 4.2. Note that the MRF ratio between the two layers is 2 (i.e., $MRF_H/MRF_L = 2.0$) which is identical to be the permeability contrast of 2 (i.e., $k_H/k_L = 2.0$).

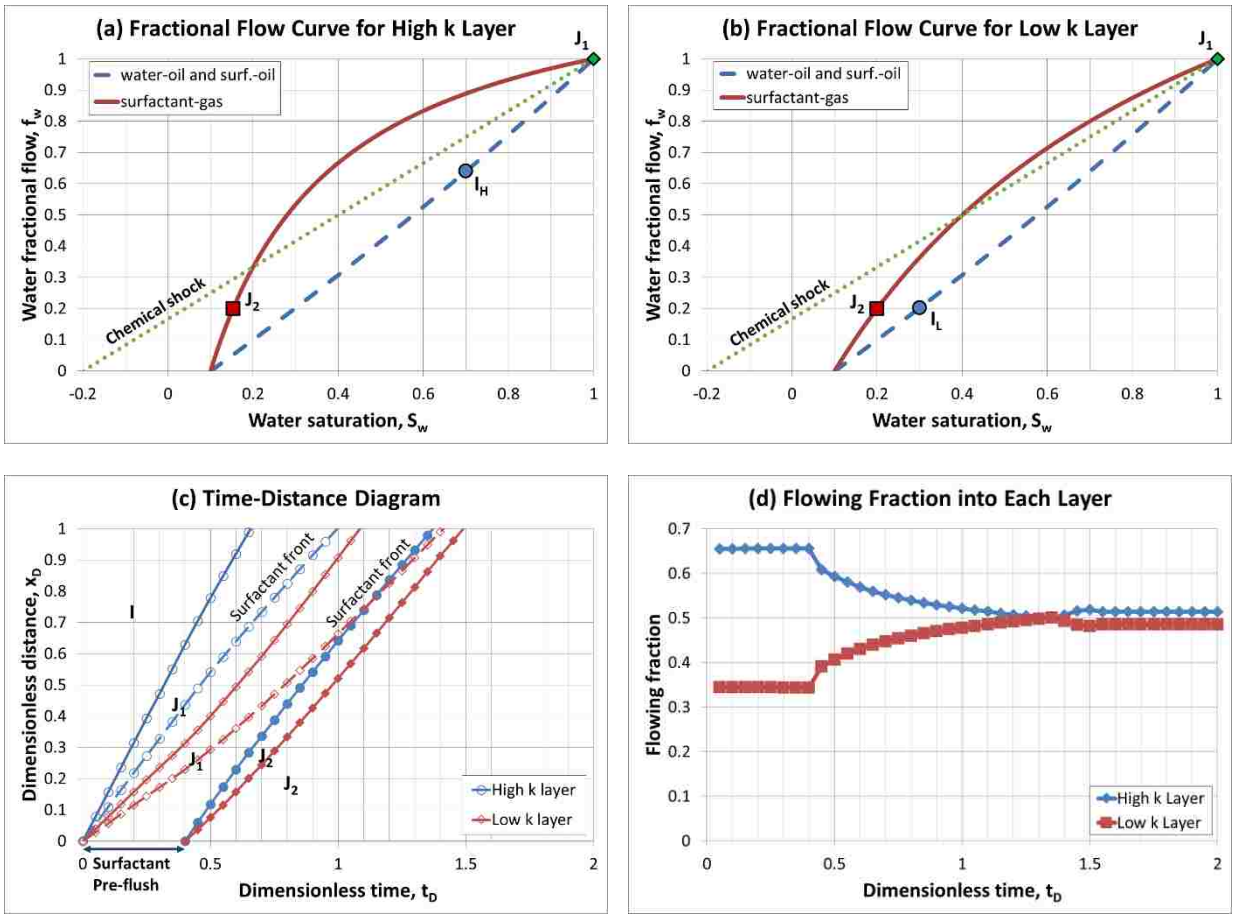

Figure 4.5: Case 4.3: displacement in a two-layer system with MRF compensating heterogeneity (MRF_H:MRF_L = 200:100 ; k_H:k_L = 1 darcy:0.5 darcy)

Figures 4.5(a) and 4.5(b) show the fractional flow curves for the high-permeability layer (k_H = 1 darcy, MRF_H = 200) and low-permeability layer (k_L = 0.5 darcy and MRF_L = 100), respectively. Note that the foam fractional flow curve in Figure 4.5(a) is curved more due to higher MRF (200 rather than 100), but all others remain the same compared to Case 4.2 (Figures 4.4(a) and 4.4(b)). When the time-distance diagram in Figure 4.5(c) is compared, the response prior to foam injection (i.e., t_D < 0.4 PV) is in fact identical to that in Figure 4.4(c) due to the same inputs, while as foam is injected (i.e., t_D > 0.4 PV), the surfactant and foam fronts slightly curve down in

the high-permeability layer and curve up in the low-permeability layer. This is because as foam moves into the system, the high MRF in the high-permeability tends to block the layer and divert the following foams into the low-permeability more and more with time. Figure 4.5(d) confirms this process more in detail. During surfactant pre-flush, about two-thirds and one-third of surfactant solution are admitted into the high-permeability and low-permeability layers, respectively, following the permeability ratio (similar to Case 4.2). As foams move into the system, however, the MRF ratio (MRF_H:MRF_L = 200:100) cancels out the permeability ratio (k_H:k_L = 1 darcy:0.5 darcy) and thus almost the same amount of injected foam is distributed into the two layers.

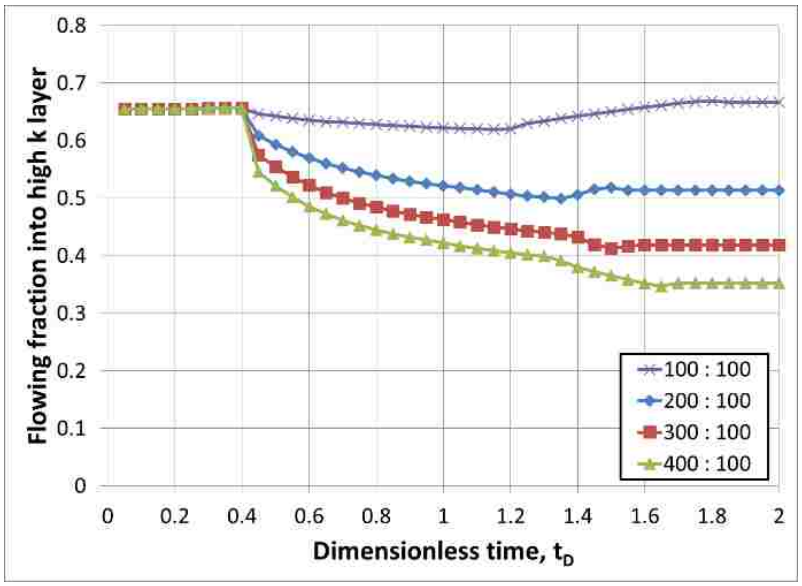

Figure 4.6: Effect of different MRF ratios (Case 4.3) for flowing fractions in a two-layer system (MRF_H:MRF_L is shown)

Figure 4.6 shows how the flowing fraction (or, injectivity) into the high-permeability layer changes with time in different scenarios of MRF ratios (MRF_H:MRF_L) ranging from 100:100 to 400:100. Note that when MRF_H:MRF_L = 100:100 (Figure 4.4 in Case 4.2), foam does not distort

the injectivity significantly from the permeability ratio as discussed earlier. On the other hand, when MRF_H:MRF_L = 200:100 (Figure 4.5 in Case 4.3), foam cancels out the permeability ratio. For the ratio of MRF_H:MRF_L = 300:100 and 400:100, the flowing fraction of following foam is in fact higher into the lower-permeability layer, which may significantly improve sweep efficiency. This example shows quantitatively how important foam stability is at different capillary pressure environment.

4.2.4 Case 4.4: displacement in a two-layer system with S_w* effect

Figures. 4.7 and 4.8 show the effect of S_w* on foam displacement, more specifically Figure 4.7 with S_{wH}*:S_{wL}* = 0.2:0.8 to examine the role of S_w*, and Figure 4.8 with S_{wH}*:S_{wL}* = 0.6:0.8 to investigate the sensitivity of the ratio to the results. Figures 4.7(a) and 4.7(b) show fractional flow curves for the high-permeability and low-permeability layers, respectively. Note that higher S_{wL}* in the low-permeability layer means foams are less stable in that layer, and as a result a large portion of the foam fractional flow curve in Figure 4.7(b) (i.e., $S_w < S_w^* - \varepsilon_w$) is near the x axis due to the low effective gas viscosity. Although MRF_{full} values for both layers are set to be 100, the MRF values at the injection conditions are MRF_H = 76.56 and MRF_L = 4.71 due to the effect of S_w*. As shown in Figure 4.7(c), as foam is injected after 1.4 PV of surfactant pre-flush, it is interesting to find that foams are diverted more into the lower-permeability layer. Such a symptom is also well demonstrated in Figure 4.7(d) where the flowing fractions, proportional to the permeability ratio initially, cross over each other during foam injection so that the low-permeability layer has more fluid intake essentially. This result shows how significantly S_w* affect the overall sweep efficiency.

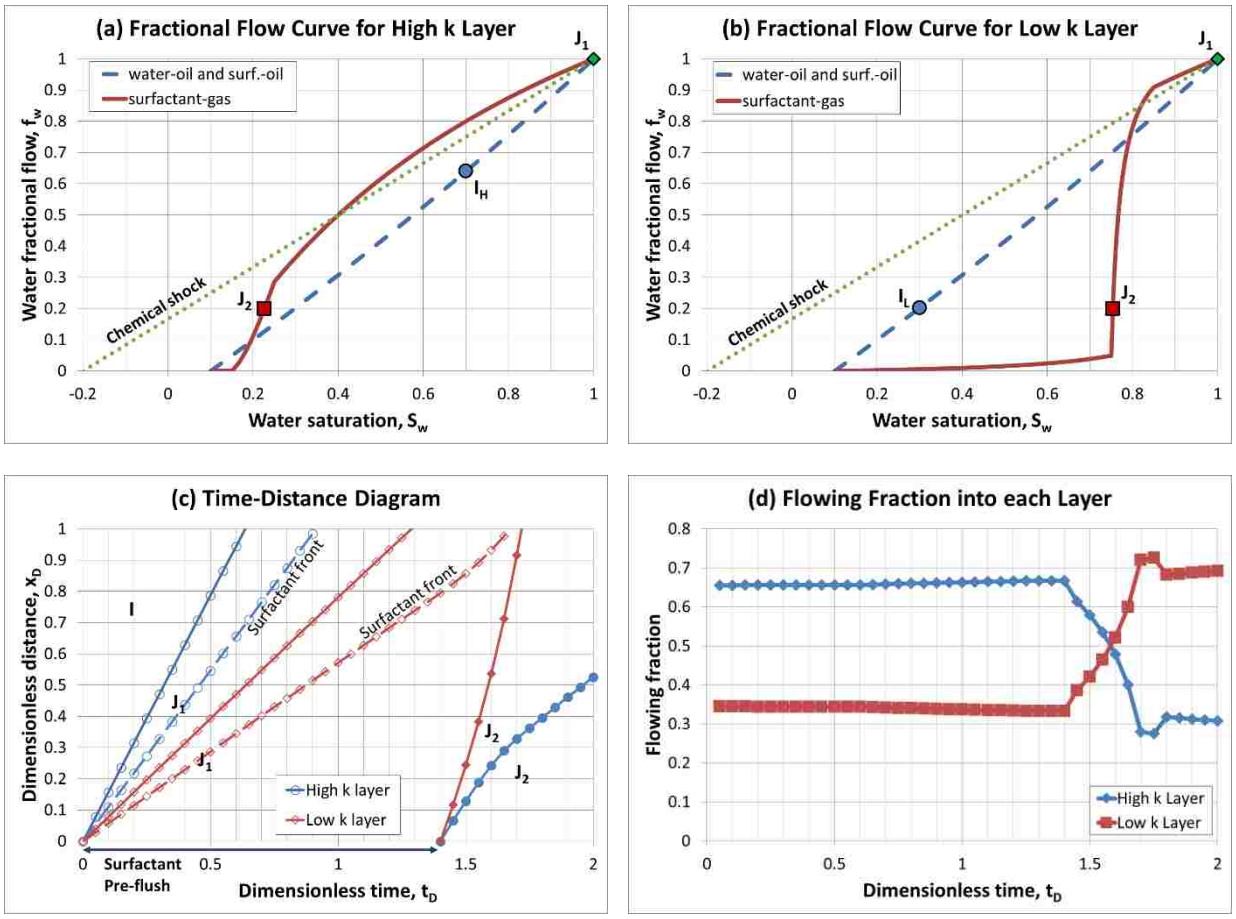

Figure 4.7: Case 4.4 (a): displacement in a two-layer system with S_w* effect (S_{wH}* = 0.2 and S_{wL}* = 0.8)

Figure 4.8 shows the results when S_{wH}* = 0.6 while keeping all other parameters the same as those in Figure 4.7. The MRF values at the injection conditions are MRF_H = 11.9 and MRF_L = 4.71, respectively. Overall, the injectivity improves somewhat, but the high-permeability layer still receives more than the low-permeability layer (about 0.59 and 0.41 as shown in Figure 4.8(d). As a result, foam propagates in both layers at the comparable velocities.

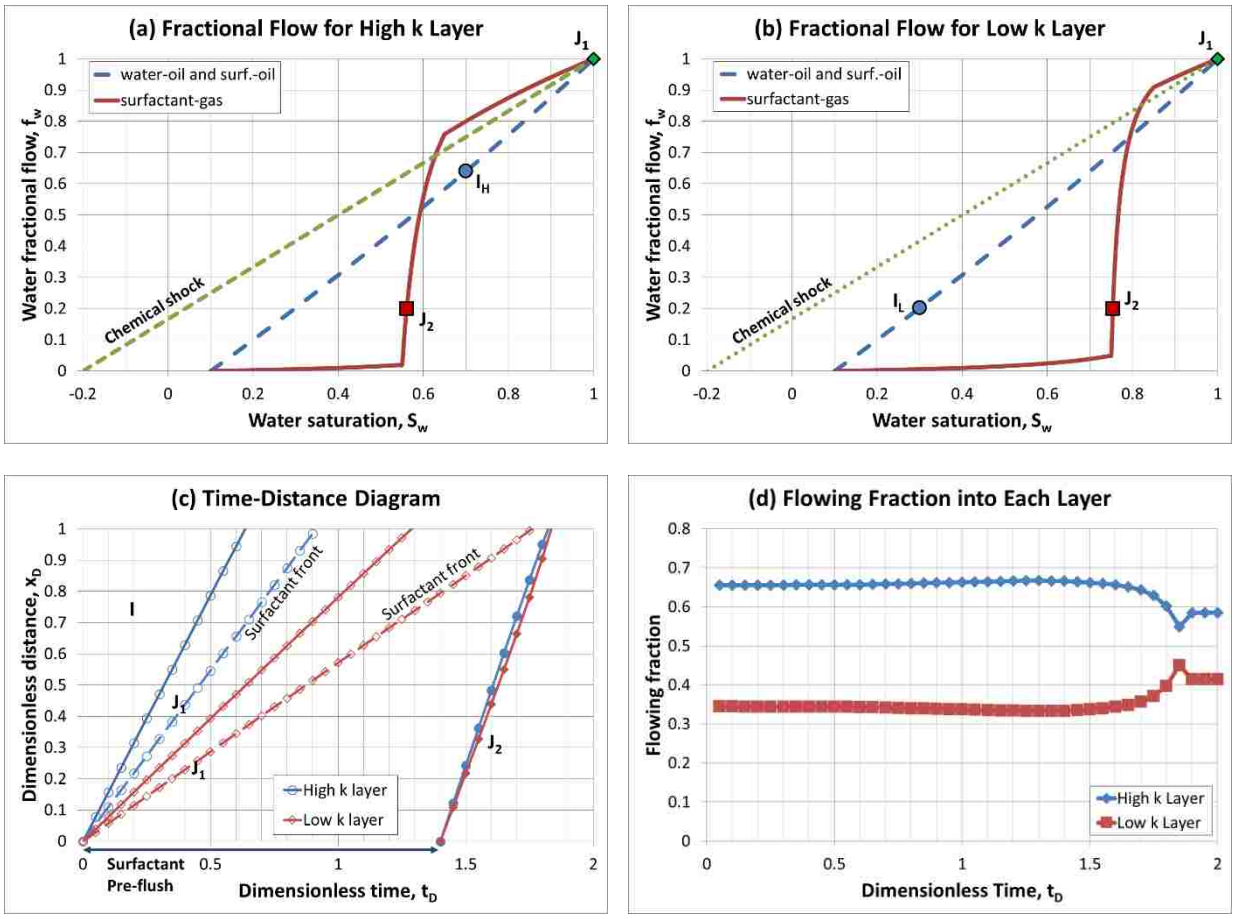

Figure 4.8: Case 4.4(b): displacement in a two-layer system with S_w* effect (S_{wH}* = 0.6 and S_{wL}* = 0.8)

Figure 4.9 shows the effect of S_w* ratio in this system, such as S_{wH}*:S_{wL}* = 0.2:0.8 (Figure 4.7), 0.4:0.8, 0.6:0.8 (Figure 4.8), and 0.8:0.8. By setting S_{wL}* = 0.8, foams in the low-permeability layer is assumed to be unstable. As foam becomes more stable in the high-permeability layer (i.e., S_{wH}* moves from 0.8 to 0.2), more and more foams are introduced into the low-permeability layer as expected. When S_{wH}* = S_{wL}* = 0.8, the injectivity into each layer is similar to the permeability ratio. The fluctuation between t_D = 1.2 and 1.9 occurs as injected foams displace I and J_1, before it reaches a steady state. The MRF_H values are 4.71 and 76.56 at S_{wH}* = 0.8 and 0.2, respectively.

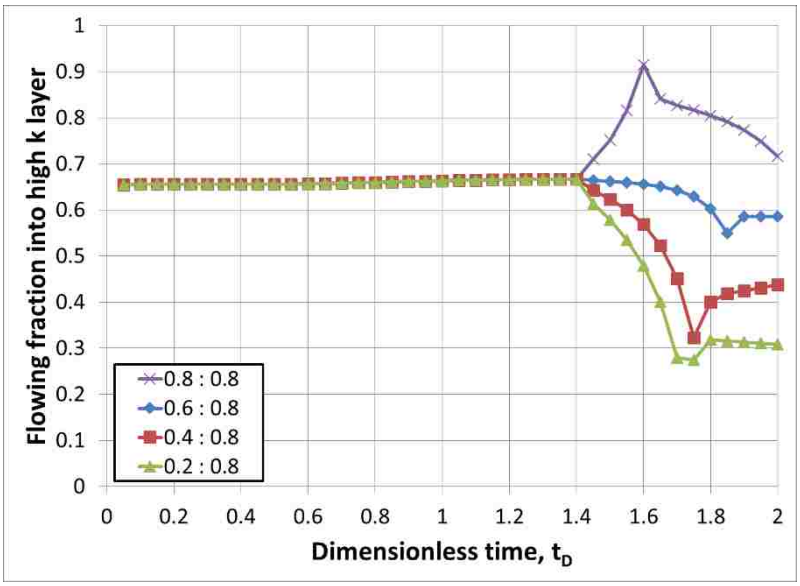

Figure 4.9: Effect of different S_w* values (Case 4) on flowing fractions in a two-layer system (S_{wH}*:S_{wL}* is shown)

4.2.5 Case 4.5: displacement in a two-layer system with three phases present initially

Once three phases interact during the flow, the analysis for the displacement becomes more complicated and the use of ternary diagram is very helpful. Figure 4.10 shows the initial conditions for both high-permeability and low-permeability layers - more specifically, I_H:(S_w, S_o, S_g) = (0.5, 0.3, 0.2) and I_L:(S_w, S_o, S_g) = (0.2, 0.5, 0.3). Except the initial condition, other parameters are the same as Case 4.2 (MRF = 100 for both layer). Note that in general there are paths from I to J_1 and then to J_2, and in addition there is one more constant state IJ because the paths suddenly change the direction by reaching the base of the diagram. The same paths can be represented by fractional flow curves as shown in Figure 4.10 where not only the positions of constant state (I, IJ, J_1, and J_2) but also the saturation velocities are specified. Following the velocity constraint, there are three saturation shocks governing the displacement in both high-permeability and low-permeability layers – I to IJ, IJ to J_1 and J_1 to J_2 in Figures 4.10(a) through 4.10(d).

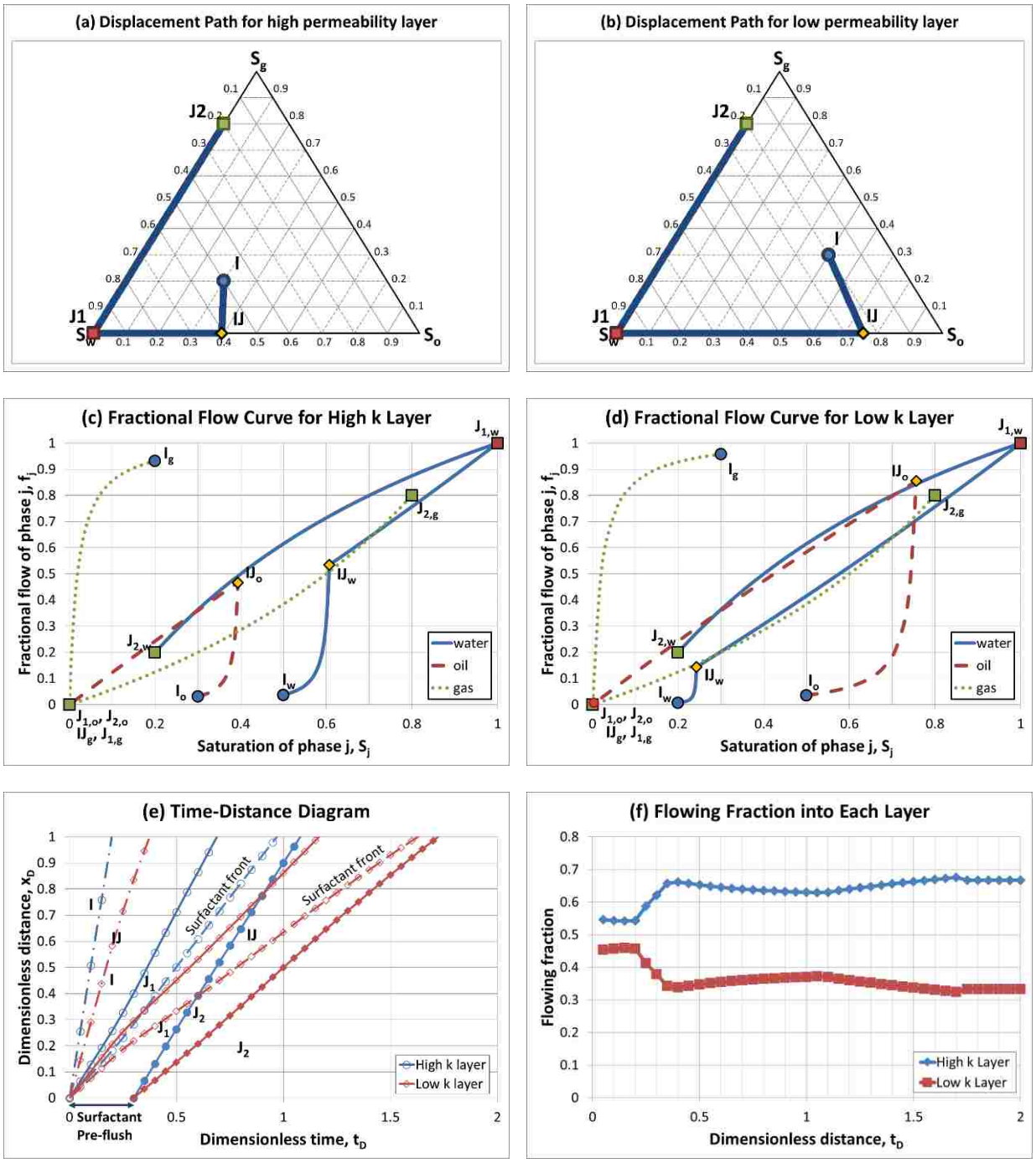

Figure 4.10: Case 4.5: displacement in a two-layer system with I_H:(S_w, S_o, S_g) = (0.5, 0.3, 0.2) and I_L:(S_w, S_o, S_g) = (0.2, 0.5, 0.3)

Time-distance diagram and flowing fractions are shown in Figures 4.10(e) and 4.10(f). After surfactant pre-flush of 0.3 PV is applied, foam starts to invade the high-permeability layer faster making the front in the high-permeability layer curves upward slightly (Figure 4.10(e)). The flowing fraction shows similar responses (Figure 4.10(f)). Note that during surfactant injection, the flowing fraction is not proportional to permeability contrast in this case because the initial conditions are not the same and the pressure drop during three-phase flow is path-dependent.

4.2.6 Case 4.6: displacement in a two-layer system with S_o* effect

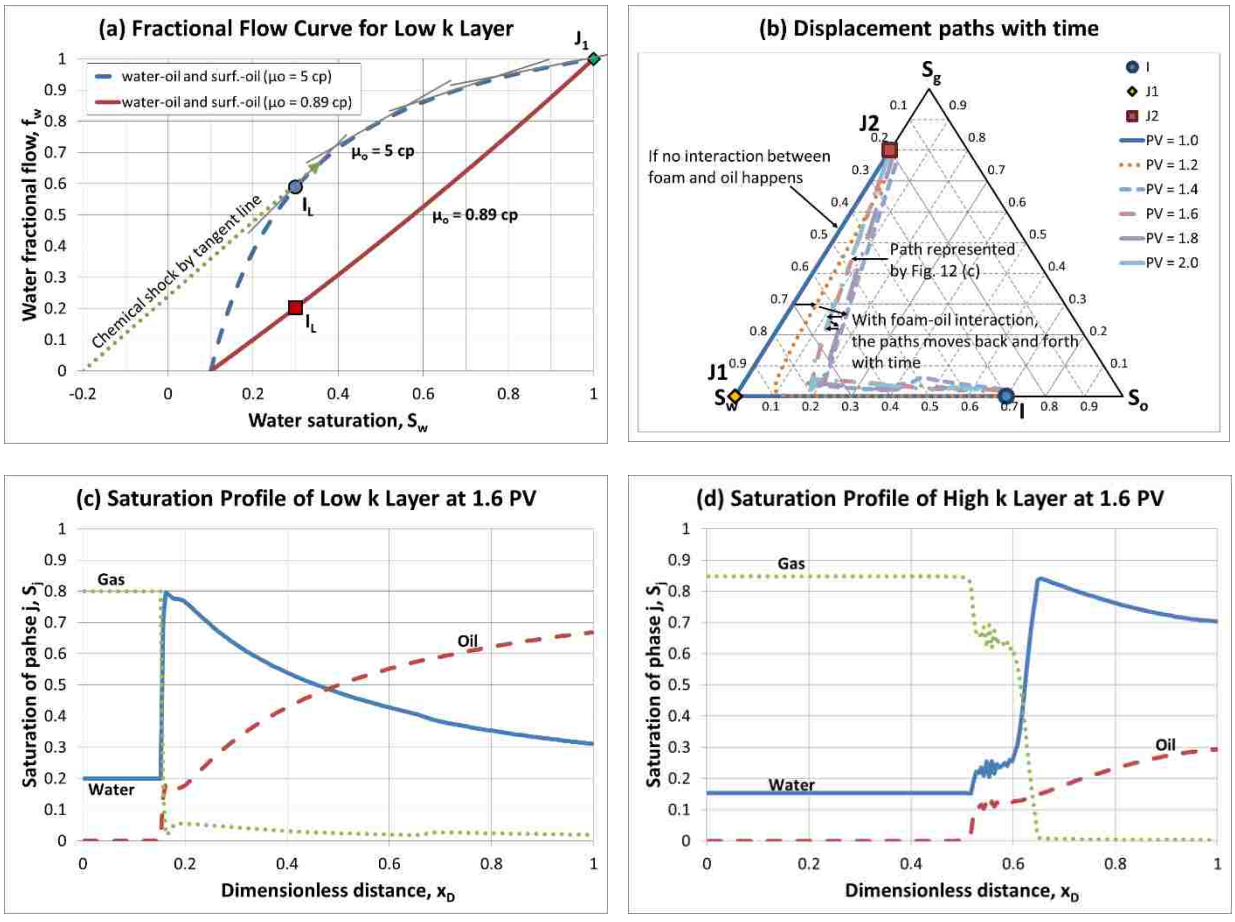

Figure 4.11: Case 4.6 (a): displacement in a two-layer system with S_o* of 0.1 for both layer

An example to see the effect of S_o^* is somewhat tricky because in all previous cases, post-surfactant residual oil saturation is assumed to be zero. In order to make this investigation meaningful, oil viscosity is assumed to be 5 cp – this high oil viscosity makes oil displacement by surfactant less efficient with slow spreading waves, and thus the injected foam has a chance to interact with oil during foam injection. The two layers of interest have $MRF_{full,H} = 200$ and $S_o^* = 0.1$ for the high-permeability layer and $MRF_{full,L} = 100$ and $S_o^* = 0.1$ for the low-permeability layer. The initial and injection conditions (injection of surfactant pre-flush and following foam) are the same as Case 2, that is, I_H: $(S_w, S_o, S_g) = (0.7, 0.3, 0)$ for the high-permeability layer, I_L: $(S_w, S_o, S_g) = (0.3, 0.7, 0)$ for the low- permeability layer, J_{1L}: $(f_w, f_g) = (1.0, 0.0)$for surfactant pre-flush, and J_{2L}: $(f_w, f_g) = (0.2, 0.8)$ for foam injection.

Figures 4.11(a) and 4.11(b) show the case of low-permeability layer where J_1 and J_2 are applied as injection conditions consecutively and $S_o^* = 0.1$ and $\varepsilon o = 0.05$ are chosen. The two-phase fractional flow curve in Figure 4.11(a) represents the initial phase of surfactant injection where the process is governed by spreading waves between I and J_1 when $\mu_o = 5$ cp (such spreading waves do not exist when $\mu_o = 0.89$ cp as shown). Note that the saturation velocity at low oil saturation (or, at high water saturation) can be significantly lower, which dramatically increases the possibility of wave collision with following foam front. These numerous spreading waves serve as new initial conditions for foam injection. Because the initial condition for foam injection is not a constant state, a series of possible initial conditions can be mapped out in the ternary diagram with time as shown in Figure 4.11(b) from numerical calculations. Note that (i) if there are no interactions between oil and foam, the path goes all the way to the left-hand-side corner of the ternary diagram and (ii) if there are interactions between oil and foam, the path moves inside the ternary diagram – this happens because the foam front is in touch with oil bank ahead, and exactly

which path to follow in the ternary diagram depends on oil saturation ahead of foam front and the size of oil bank.

Solving such a case analytically is very complicated, but the simulation can provide reliable results as shown by saturation profiles for the low-permeability and high-permeability layers in Figures 4.11(c) and 4.11(d), respectively, when 1 PV of surfactant solution is injected followed by 0.6 PV of foam injection. As expected, where the front of injected foam is in contact with oil phase with $S_o > S_o^* + \varepsilon_o$ (or, $S_o > 0.15$), foam quickly collapses and therefore gas saturation is reduced significantly (i.e., no foam) as shown in Figure 4.11(c). In the meantime, where the front of injected foam is in contact with oil phase with $S_o^* - \varepsilon_o < S_o < S_o^* + \varepsilon_o$ (or, $0.05 < S_o < 0.15$), foam experiences a transition in which foam becomes weakening before collapsing completely as shown by the reduced gas saturation zone (x_D = 0.52 to 0.6 PV) in Figure 4.11(d).

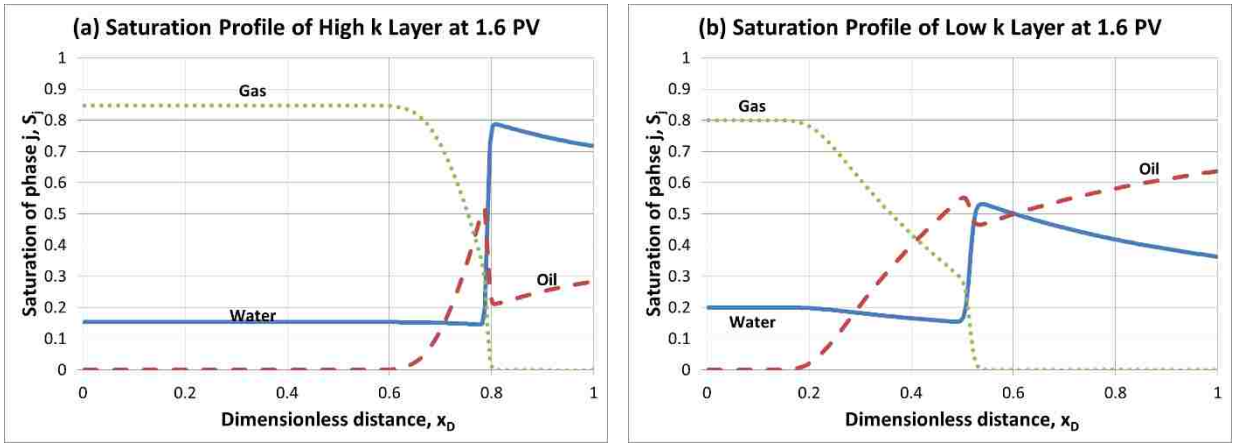

Figure 4.12: Case 4.6(b): displacement in a two-layer system with S_o^* of 1.0 for both layer

Figures 4.12(a) and 4.12(b) repeat the same case as shown in Figure 4.11 but with S_o^* = 1.0 (i.e., foam always stable even with oils). Because stable foam displaces high-viscosity oil in this case, gas and oil saturations change progressively at the foam front (x_D = 0.63 to 0.80 in Figure

4.12(a) and x_D = 0.19 to 0.50 in Figure 4.12(b)). This is obviously different from Figure 4.11 where there are sharp and drastic changes at the foam front due to collapsing foams. The results therefore clearly demonstrate that how foam's sensitivity to oil affects the displacement and sweep efficiency.

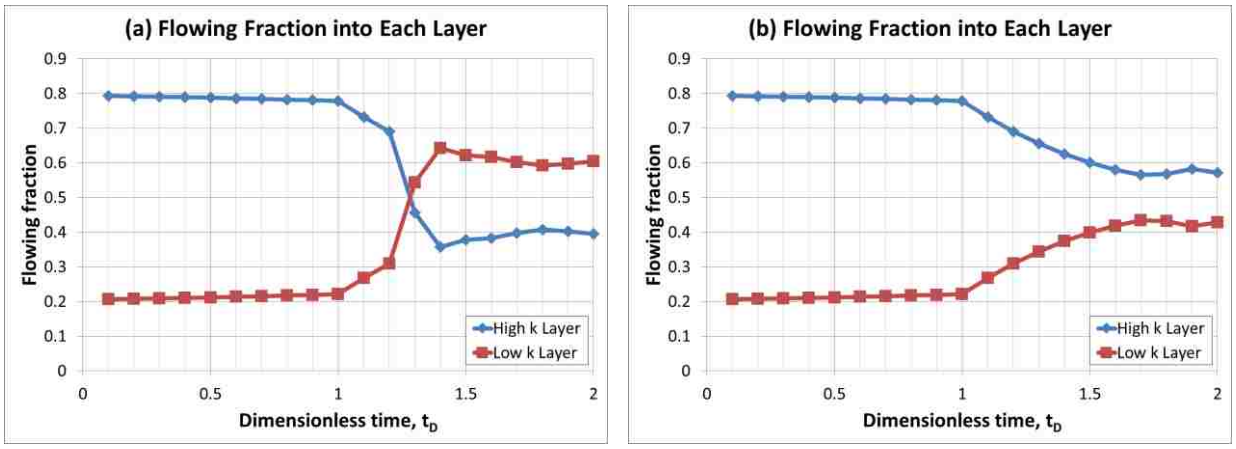

Figure 4.13: Case 4.6: Comparison of flowing fraction vs time with varying S_o*: (a) S_o* = 0.1 and (b) S_o* = 1.0

Figure 4.13 compares flowing fraction into each layer with time to compare these two cases. The results show that if foam is sensitive to oil (Figure 4.13(a); cf. Figure 4.11), more foams can be introduced into the low-permeability layer where the high oil saturation destabilizes foam more.

4.2.7 Case 4.7: displacement in a three-layer system with all effects (MRF, S_w* and S_o*) combined

This is the most complicated case in presence of multiple layers. The number of layers can be any, but is selected to be three arbitrarily for demonstration purpose. Each layer is allowed to have its own rock and fluid properties as well as foam properties, for example, $MRF_{full,H}$ = 400, $S_{w,H}$* = 0.2, and k_H = 2 darcy for the high-permeability layer; $MRF_{full,I}$ = 200, $S_{w,I}$* = 0.3, and k_I =

1 darcy for the intermediate-permeability layer; and $MRF_{full,L}$ = 100, $S_{w,L}$* = 0.8, and k_L = 0.5 darcy for the low-permeability layer. S_o* is fixed as 0.1 for all layers. The initial conditions are slightly different for each layer (I_H:(S_w,S_o,S_g) = (0.7,0.2,0.1) for the high-permeability layer; I_I:(S_w,S_o,S_g) = (0.4,0.4,0.2) for the intermediate-permeability layer; and I_L:(S_w,S_o,S_g) = (0.2,0.6,0.2) for the low-permeability layer; see Table 4.4 for more details), while the same injection condition (surfactant pre-flush followed by foam) is applied. Note that the mobility reduction factor corresponding to the injection conditions are MRF_H = 125.88, MRF_I = 51.63, and MRF_L = 4.71 for the high-permeability, intermediate-permeability, and low-permeability layers.

Figure 4.14 shows saturation profile in each layer at two different dimensionless times such as 1.2 PV (Figure 4.14(a)) and 1.6 PV (Fig. 4.14(b)) of fluid injections (both including 1.0 PV of surfactant pre-flush). The results show that the injected foams break down in the low-permeability layer because foam collapses as it contacts oil and therefore early gas breakthrough occurs. In addition, low MRF causes poor displacement efficiency. On the other hand, by the similar token but the other way around, foam breakthrough is delayed with favorable displacement efficiency in the high-permeability layer. The intermediate-permeability layer has responses in between.

By combining all these together, Figure 4.15 shows the flowing fraction into each layer. As expected from Figure 4.14, fluids tend to be distributed into the layers evenly because of higher foam strength in the higher-permeability layer. It should be noted, however, that the overall performance should be evaluated based on both saturation profile and flowing fraction combined together. For example, that fact that the low-permeability layer admits more fluid (Figure 4.15) does not necessarily mean that the diversion process is successful because the saturation profile in the low-permeability layer exhibits poor displacement efficiency (Figure 4.14)). Put it differently,

although diversion into the low-permeability layer occurs, it does not contribute to improving sweep due to relatively high gas mobility.

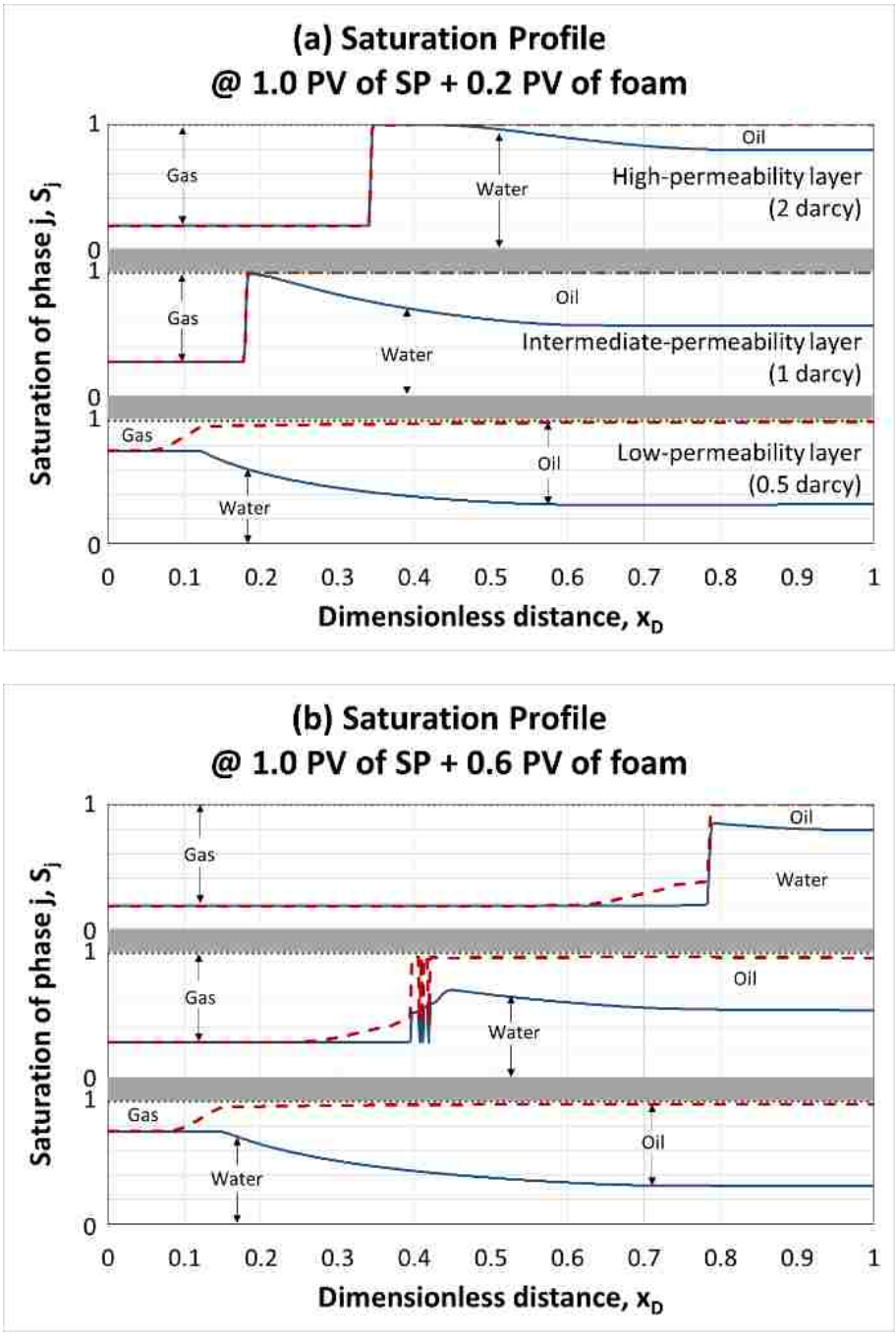

Figure 4.14: Case 4.7: displacement in a three-layer system with all effects combined

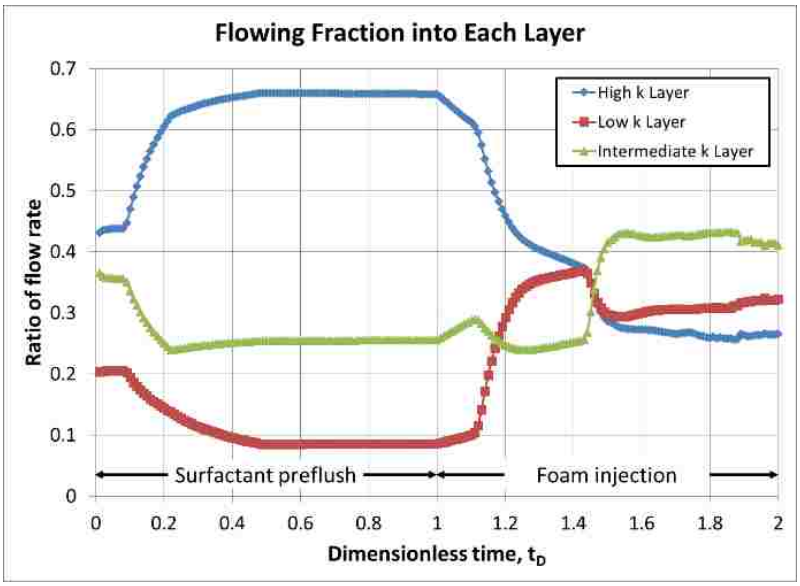

Figure 4.15: Case 4.7: flowing fraction into each layer vs. time

This example shows that the model developed in this study is capable of handling complicated cases where the applicability of foams for diversion process is not obvious at the first sight. To improve both diversion and sweep efficiency of injected fluids in heterogeneous systems, foam properties such as injection condition, MRF, S_w* and S_o* should be optimized at given initial conditions and petrophysical and formation properties.

CHAPTER 5
SENSITIVITY OF RESULTS TO MODEL INPUT PARAMETERS

This chapter deals with the sensitivity of modeling and simulation results to input parameters applied in the previous chapters.

5.1 Non-linear relative permeability functions (Case 5.1)

There are two issues involved in relative permeability functions used in the previous chapters: (i) the use of relative permeability which is only a function of that particular phase saturation; and (ii) the use of simple parameter values for Corey-type relative permeability (i.e., coefficient and exponent set to be 1). The former is an important issue because it essentially defines how easily different phases would migrate interacting each other. The latter is focused here, however, because the main question to be asked is how sensitively the results are affected by using non-linear relative permeability functions.

Table 5.1: Parameters for non-linear relative permeability

Input Parameters			
k_{rw}^{o} =	0.2	n_w =	4.2
k_{ro}^{o} =	0.94	n_o =	1.3
k_{rg}^{o} =	0.94	n_g =	1.3

In order to test the effect of non-linear relative permeability functions, this study borrows the relative permeability parameters from Ashoori et al. (2010) as summarized in Table 5.1 (cf. Table 3.1) where the functions are convex (i.e., the exponents (n_w, n_o, and n_g) greater than one) and the end-point relative permeability values (k_{rw}^{o}, k_{ro}^{o}, and k_{rg}^{o}) are less than one.. Except those

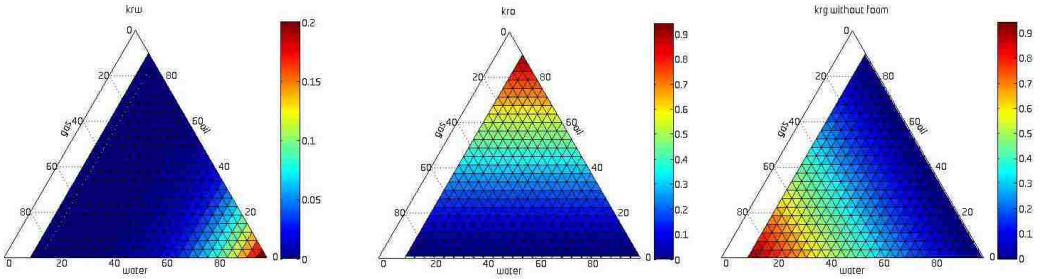

Figure 5.1: Relative permeability to water, oil and gas phases

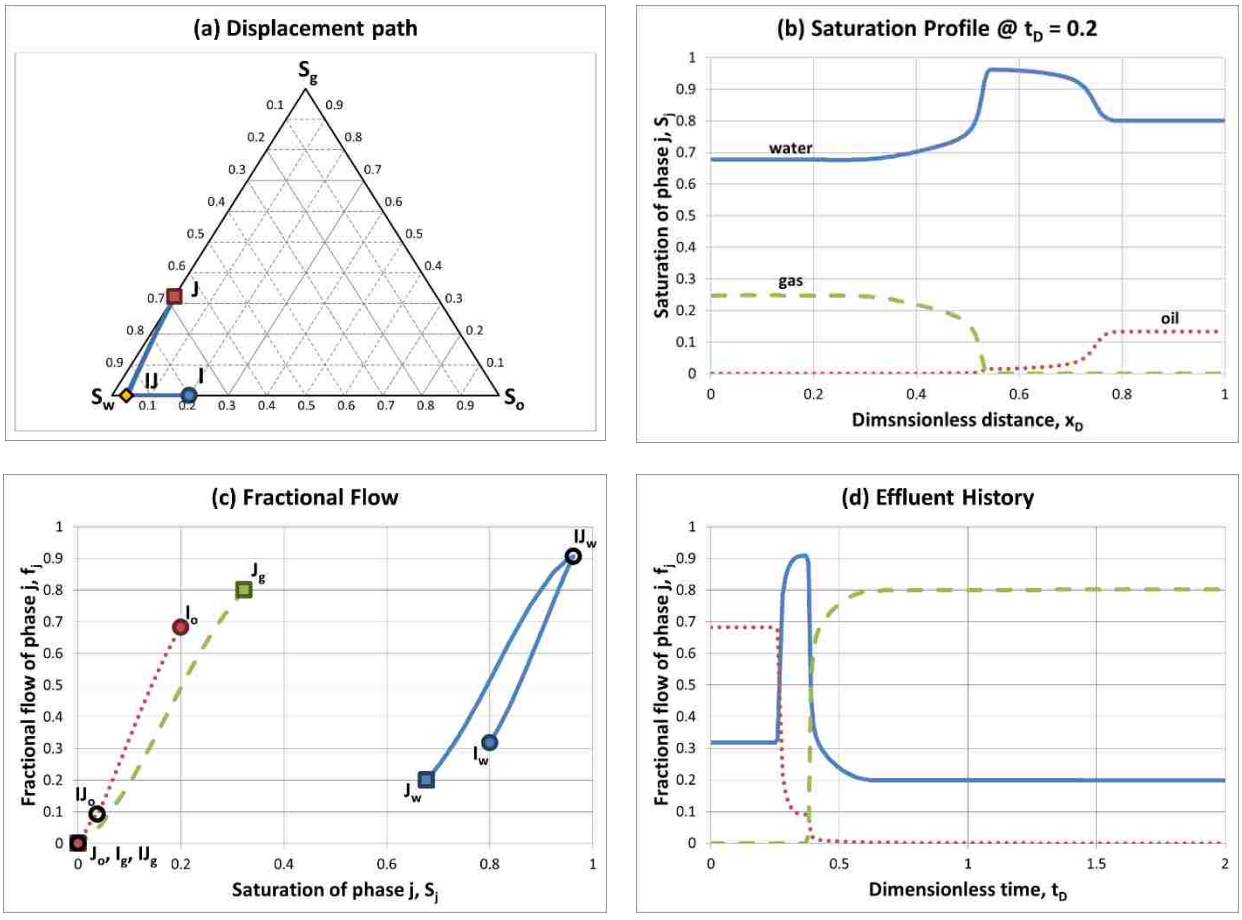

Figure 5.2: Case 5.1 with non-linear relative permeability functions: foam displacement at MRF = 100 with I:(S_w,S_o,S_g) = (0.8,0.2,0), J:(f_w,f_g) = (0.2, 0.8) and realistic relative permeability parameters from simulation results only

parameters, other inputs remain the same as those in Case 3.1 with MRF = 100 (cf. Figure 3.8). Figure 5.1 shows relative permeability values mapped in a ternary diagram.

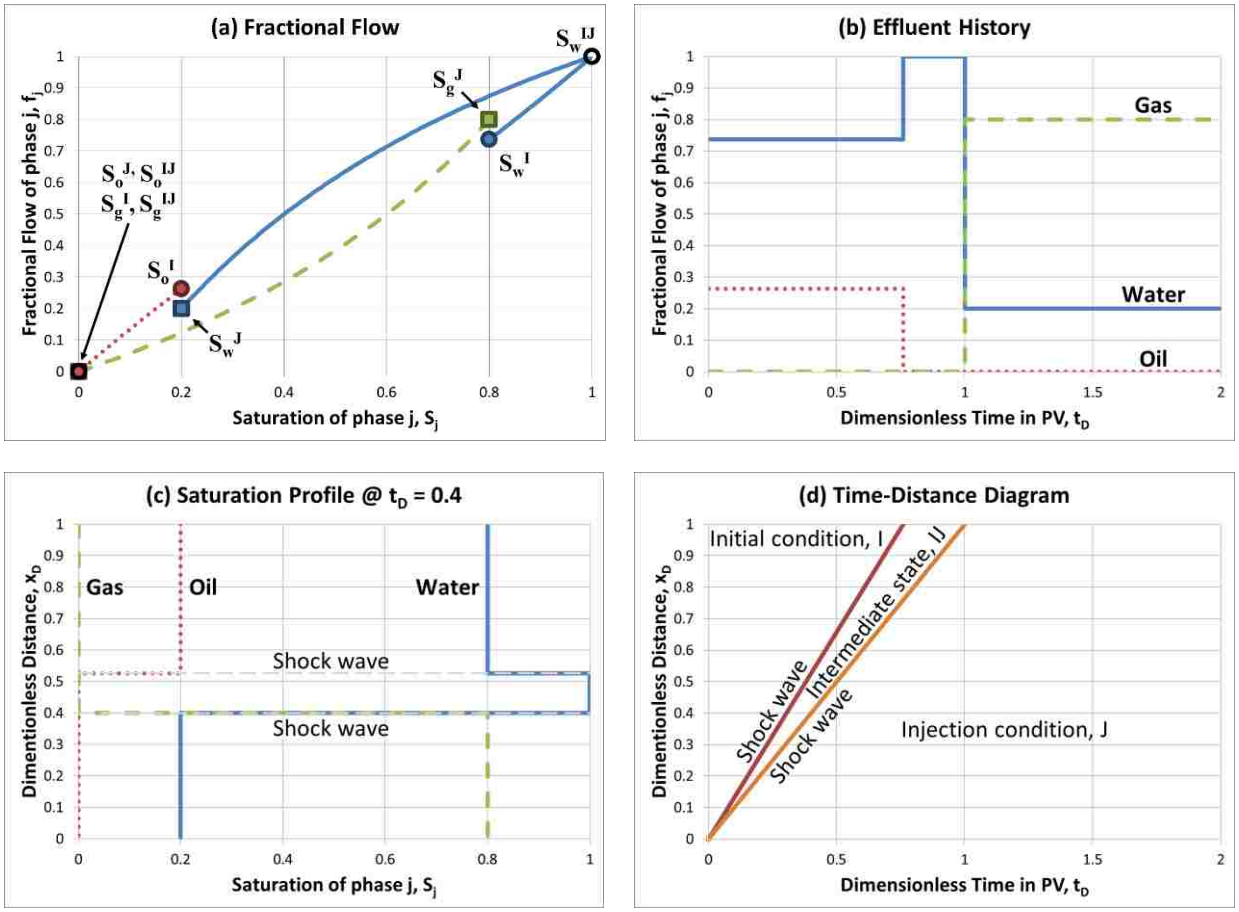

Figure 5.3: Results with linear relative permeability functions (identical to Case 3.1, Figure 3.8)

Figure 5.2 shows the results of Case 5.1 from numerical simulations compared to the similar case with linear relative permeability functions in Figure 5.3 (note that Figure 5.3 is identical to Figure 3.8 in Case 3.1). Unlike the displacement process with only two shock waves in Figure 5.3, the solution with non-linear relative permeability seems more complicated, consisting of shock waves and spreading waves. In addition, the flowing fraction of a phase may change significantly because the fractional flow is a direct function of relative permeability

functions. In spite of these differences, the nature of displacement process during three phase flow is well captured in both cases. This example shows that how much deviation one should expect by incorporating more realistic relative permeability is, in fact, case-specific.

5.2 Size of transition zone (ε_w and ε_o)

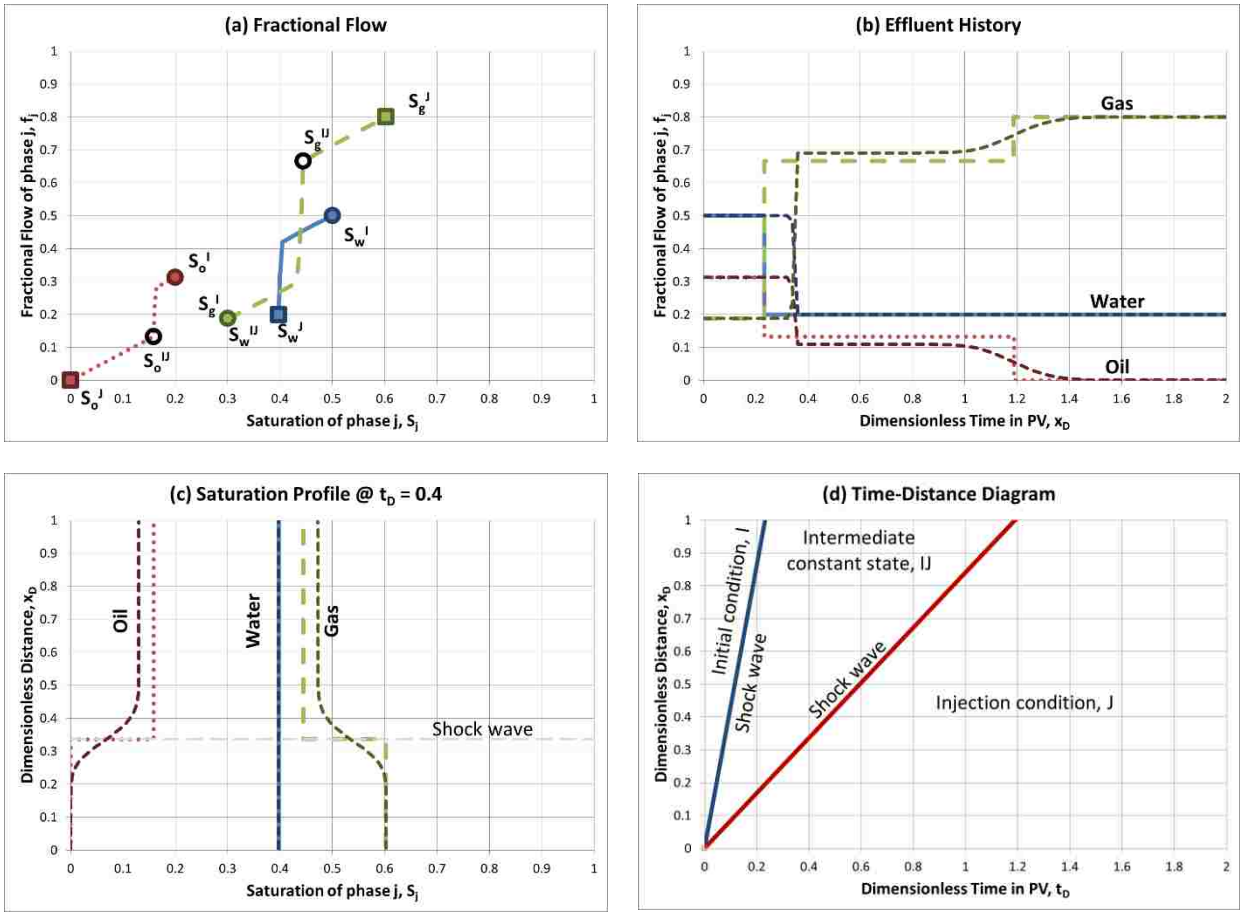

Figure 5.4: Case 5.2 with ε_w = 0.005: Foam displacement at MRF_{full}=100 with I:(S_w,S_o,S_g) = (0.5,0.2,0.3), J:(f_w,f_g) = (0.2, 0.8), S_w* = 0.4, S_o* = 1, and ε_w = 0.005

In all modeling and simulation attempts, the size of transition zone for foam sensitivity to water and oil saturations (ε_w and ε_o) has been set to be 0.05 arbitrarily. In order to investigate the effect of this transition length, another case with ε_w = 0.005 (more sharply changing MRF near

S_w*) is tried as shown in Figure 5.4, in comparison with Figure 5.5 with $\varepsilon_w = 0.05$ (Note that Figure 5.5 is identical to Figure 3.22 in Case 3.3). The results show that the size of ε_w may impact modeling and simulation results somewhat because the size of transition length affects phase mobility values near the discontinuity and thus distorts the wave velocities and saturation values. Figure 5.3 shows the results from both analytical solution and numerical simulation. The dotted lines in Figure 5.4(b) and 5.4(c) are obtained from simulation results.

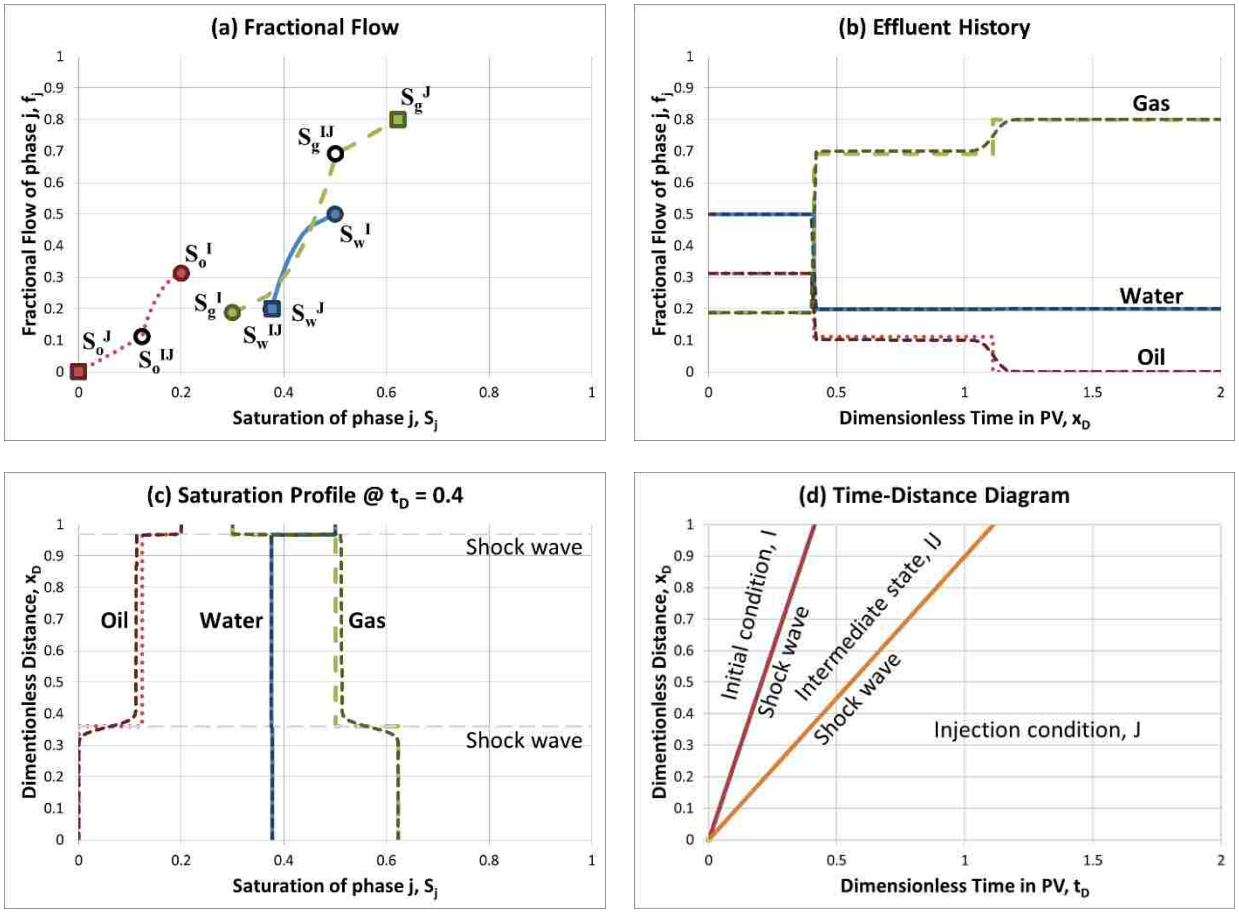

Figure 5.5: Results with $\varepsilon_w = 0.05$ (identical to Case 3.3, Figure 3.22)

As shown above, the results are similar to Case 3.3. However, small discrepancy occurs in the saturation at intermediate state, IJ. The constant state is (S_w, S_o, S_g) = (0.397, 0.158, 0.444)

from analytical solution while it is (S_w, S_o, S_g) = (0.397, 0.131, 0.472) from numerical simulation. Therefore, different characteristic velocities are observed between I and IJ. However, it does not affect the shock velocity at injection condition. As a result, slower breakthrough of IJ is observed from the result of numerical simulation (Figure 5.3(b)).

5.3 Effect of thickness and porosity on the flow in multi-layer system

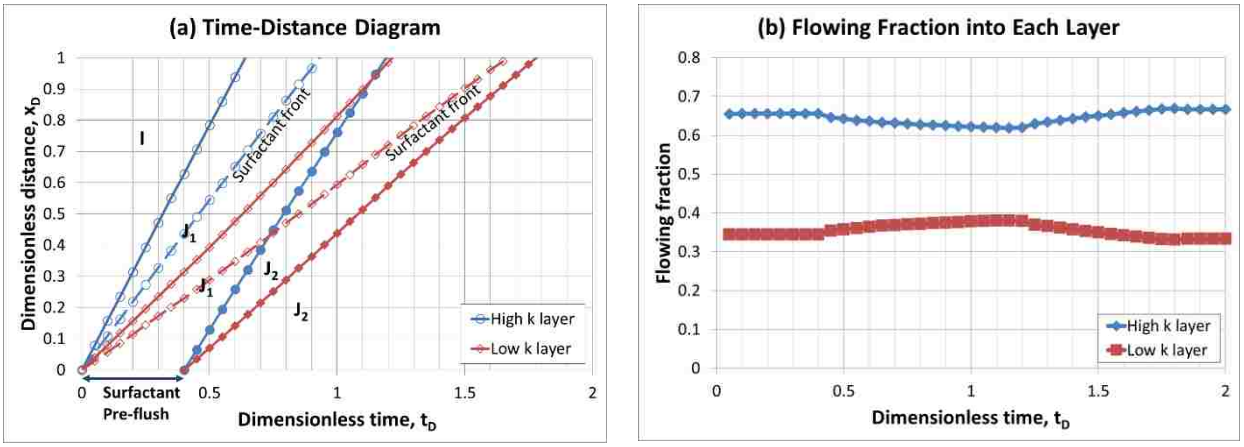

Figure 5.6: Base case with the same thickness and porosity (identical to Case 4.2, Figure 4.4)

In Chapter 4, the effect of foam properties such as MRF, S_w* and S_o* in a multi-layer system is covered by using the same thickness and porosity in each layer. Additional cases are presented here to see how injected fluids propagate where the layers have different void volumes by varying thickness and porosity values. For comparison, Case 4.2 is used as a base case as shown in Figure 5.6. Since the change in thickness and porosity does not affect fractional flow solutions expressed in dimensionless variables, only the results of time-distance diagram and flowing phase fractions are shown in this section.

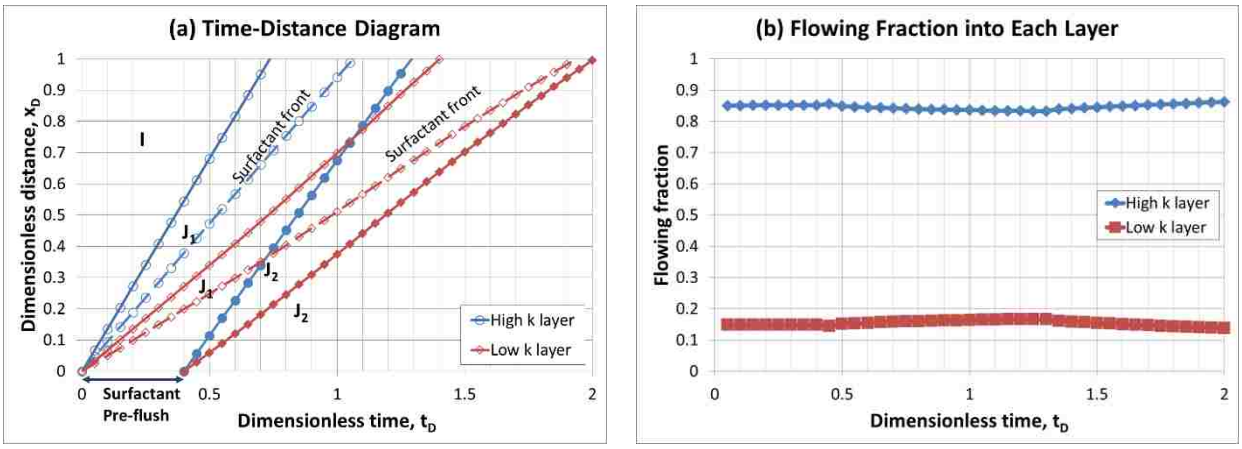

Figure 5.7: Results with varying thickness values (0.75 m for high k layer; 0.25 m for low k layer)

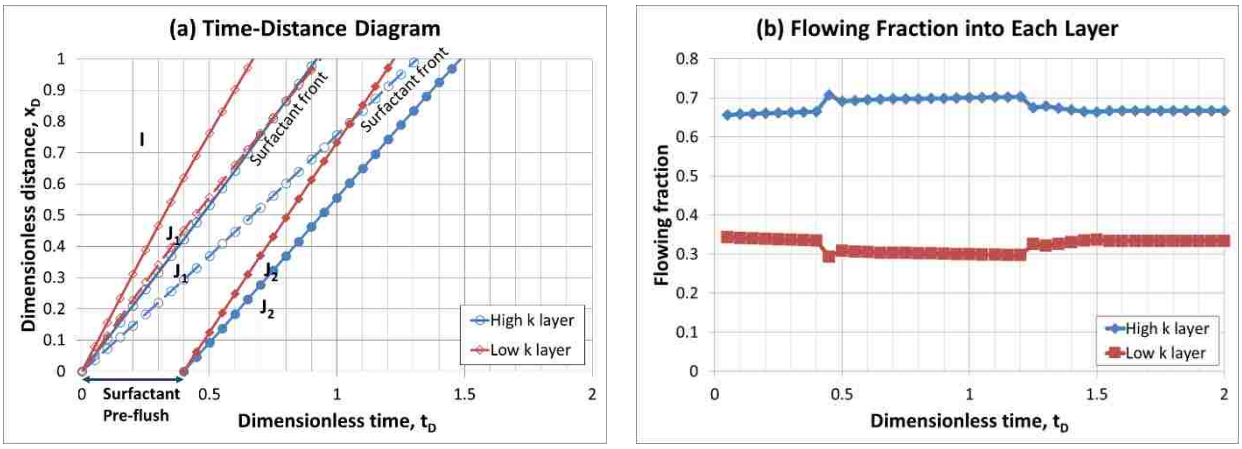

Figure 5.8: Results with varying porosity values (0.3 for high k layer; 0.1 for low k layer)

Figure 5.7 shows the case where the thickness of the high- and low-permeability layers are set to be 0.75 m and 0.25 m, respectively (cf. 0.5 m for both layers in Case 4.2). Because the pore volume of the high-permeability layer is three time higher than that of the low-permeability layer, more surfactant solutions are accepted by the high-permeability layer in general. The response does not seem to change significantly during foam injection either. This implies that the diversion process using foam becomes more difficult where there is a severe thief zone. Note that the

pressure gradient calculation in this case is caused by the change in cross-sectional area (cf. Darcy's equation), which essentially distorts injectivity into each layer.

Figure 5.8 shows the effect of porosity (i.e., porosity of 0.3 for the high permeability layer and porosity of 0.1 for the low permeability; cf. 0.2 for both layers in Case 4.2). Because porosity does not play any role in pressure gradient (cf. Darcy's equation) – this may not be necessarily correct in the real world because porosity and permeability are related – the steady-state injectivity during foam injection is almost the same as that in the base.

These two examples show how sensitively the outcome of foam-surfactant diversion processes can change in various occasions.

CHAPTER 6
CONCLUSIONS AND RECOMMENDATIONS

This chapter describes major conclusions obtained from Chapter 3 and Chapter 4. Possible recommendations for future study is also accompanied.

6.1 Conclusions

Foam displacement mechanisms in foam-assisted NAPL (non-aqueous phase liquid) remediation processes by using MoC (Method of Characteristics)-based three-phase fractional flow analysis are investigated in Chapter 3. The displacement mechanisms are shown to be strongly affected by effective foam viscosity represented by gas-phase mobility reduction factor (MRF), the phase saturations initially present in the media, and foam's sensitivity to oil and water represented by critical oil saturation (S_o*) and limiting water saturation (S_w*). The results from fractional flow solutions are compared with those from foam simulations for validation purposes. This first part of study can be summarized as follows:

- When different levels of MRF values are tried such as MRF = 1 (no foam), 10, 100, and 1000 to represent various injection foam strengths, the fractional flow solutions show that even a slight decrease in gas mobility (i.e., from MRF = 1 to MRF = 10) can improve sweep efficiency significantly, delaying the breakthrough of the injected gas phase. This seems to be great news because for successful foam-assisted remediation processes, creating very fine-textured and low-mobility foams may not be required necessarily. Comparing the results at MRF = 100 and 1000, the results show that although a higher MRF is more favorable in general, there is no significant benefits once the MRF is beyond a certain level.

- When it comes to foam-oil displacements, the effects of S_w* and S_o* are shown to be so crucial that they cannot be neglected. The results show that, in general, the more sensitive the foams are to water and oil saturations, the less effective the foam-assisted NAPL remediation processes are. Fractional flow analysis is able to show the quantitative interpretation if detailed design parameters are given.
- For the cases when the effects of both S_w* and S_o* are applied together, the displacement paths become very complicated and, as a results, the fractional flow analysis alone may not be able to find the solutions. In such cases, foam simulations based on the same material balance equations could be used to guide the analysis. Although time-consuming and labor-intensive, the tasks dealing with both S_w* and S_o* are doable. This study demonstrates how both fractional flow analysis and simulations can work together for complex displacement problems. Once confirmed, this model can be built into a multi-dimensional model for field-scale simulations.

Foam's ability to overcome subsurface heterogeneity is investigated in Chapter 4. The model deals with a horizontal multi-layered system in the absence of inter-layer vertical communications, which shares the same inlet pressure (varying with time) and fixed outlet pressure. Surfactant pre-flush and following foams are allowed to be distributed into each layer depending on the resistance of individual layers. Foam properties are characterized by mobility reduction factor (MRF), limiting water saturation (S_w*), and critical oil saturation (S_o*), while rock and fluid properties are characterized by porosity (ϕ), absolute permeability (k), relative permeabilities (k_r), and surfactant adsorption (D_{sf}). This study can be summarized as follows:

- If foam's sensitivity to water and oil saturations are not considered, foam can overcome permeability contrast only when the ratio of mobility reduction factors compensates the ratio of absolute permeabilities. If mobility reduction factors are almost the same for different layers, then injected foams are likely to be distributed primarily following the permeability ratio. The fact that foams tend to be more stable in the higher-permeability layers due to lower capillary pressure environment is a favorable condition.
- If foam's sensitivity to water saturation is taken into consideration, foam has a better chance to overcome the heterogeneity when the higher-permeability layers are more sensitive to water saturations (i.e., when $S_{w,H}$*is lower than $S_{w,L}$*, equivalently). Because higher-permeability layers tend to have lower S_w*, foam's sensitivity to water saturation works favorably for overcoming heterogeneity. Also, it causes faster saturation velocity of injected foam.
- Foam's sensitivity to oil also plays an important role. If lower-permeability layers have higher oil saturation and destabilize foams, it is likely to help following foams diverted more into the lower-permeability layers.
- If the system consists of multiple layers, it is complicated to understand exactly how much fluid will be introduced into each layer and what type of displacement efficiency will be achieved during surfactant and foam injection. The overall performance is obviously very specific to foam characteristics as well as rock and fluid fluids. The methodology introduced in this study can be applied to such complex cases successfully.

6.2 Recommendations

Based on the tasks performed in this study, the following topics can be recommended for future study:

- Experimental verifications (Chapter 3): Coreflood experiments can be conducted to verify modeling and simulation results presented in this study. If so, additional experiments should be performed in order to measure mobility reduction factor, foam's sensitivity to water and oil saturations, surfactant adsorption, three-phase relative permeability, and so on. Because how foam migrates in presence of oil is very difficult to measure, the use of high-tech equipment such as CT scanning and NMR imaging is believed to be helpful.
- Parallel coreflood experiments (Chapter 4): Modeling and simulation results in non-communicating multilayer systems can be compared with the results from parallel coreflood experiments. Because foam does not reach its steady-state texture immediately, the length of cores should be long enough to see the diversion effect more clearly.
- Field application of surfactant/foam processes and history matching: Because the ultimate goal of this study is to make surfactant/foam process successful for subsurface environmental remediation, any impediments to reach the goal is worth investigating. There are many issues involved including, not limited to, foam rheological properties in multi-dimensional space, quantifying the interactions between foams and different types of oils, field-scale simulation and matching the history of field trial, optimizing foam injection strategy such as foam injection velocity, foam quality, and surfactant pre-flush, to name a few.

REFERENCES

Afsharpoor, A., Lee, G. S., and Kam, S. I. (2010). Mechanistic simulation of continuous gas injection period during surfactant-alternating-gas (SAG) processes using foam catastrophe theory. *Chemical Engineering Science*, 65(11), 3615–3631.

Aronson, A. S., Bergeron, V., Fagan, M. E., and Radke, C. J. (1994). The influence of disjoining pressure on foam stability and flow in porous media. *Colloids and Surfaces A: Physicochemical and Engineering Aspects*, 83(2), 109–120.

Ashoori, E., Heijden, T. L. M. V. D., and Rossen, W. R. (2010). Fractional-Flow Theory of Foam Displacements With Oil. *SPE*, 15(2), 260-273.

Bikerman, J. J. (1973). *Foams*. Springer-Verlag. Berlin, Germany. pp 33-64, 184-213.

Bergeron, V., Fagan, M. E., and Radke, C. J. (1993). Generalized entering coefficients: a criterion for foam stability against oil in porous media. *Langmuir*, 9(7), 1704–1713.

Bernard, G. G., Holm, L. W., and Jacobs, W. L. (1965). Effect of Foam on Trapped Gas Saturation and on Permeability of Porous Media to Water. *SPEJ*. 5(4), 295-300.

Buckley, S. E. and Leverett, M. C. (1942). Mechanism of Fluid Displacement in Sands. *Trans.*, AIME, 146, 107-116.

Chambers, K. T. and Radke, C. J. (1991). Capillary Phenomena in Foam Flow Through Porous Media In *Interfacial Phenomena in Petroleum Recovery*. ed. Morrow, N .R., Marcel Dekker, NewYork.

Chen, Q., Gerritsen, M. G., and Kovscek, A. R. (2010). Modeling Foam Displacement With the Local-Equilibrium Approximation: Theory and Experimental Verification. *SPEJ*, 15(1), 21–24.

Cheng, L., Reme, A. B., Shan, D., Coombe, D. A., and Rossen, W. R. (2000). Simulating Foam Processes at High and Low Foam Qualities. SPE/DOE Improved Oil Recovery Symposium, 3-5 April, Tulsa, Oklahoma.

Crow, W. L, Anderson, E. P., and Minugh, E. M. (1987). Subsurface Venting of Vapors Emanating from Hydrocarbon Product on Ground Water. *Ground Water Monitoring & Remediation*, 7(1), 51-57.

Dake, L. P. (1978). *Fundamentals of Reservoir Engineering*. New York: Elsevier Scientific Publishing Company.

Derjaguin, B. V. and Obukhov, E. V. (1936). Anomalien dünner Flüssigkeitsschichten III. *Acta Physicochim*. URSS, 5(1), 1-22.

Derjaguin, B. V. and Kussakov, M. M. (1939a). Anomalous Properties of Thin Polymolecular Films V. *Acta Physicochim*. URSS, 10(1), 25-44.

Derjaguin, B. V. and Kussakov, M. M. (1939b). Anomalous Properties of Thin Polymolecular Films V. *Acta Physicochim*. URSS, 10(2), 153-174.

Dholkawala, Z.F., Sarma, H.K., and Kam, S.I. (2007). Application of Fractional Flow Theory to Foams in Porous Media. *SPEJ*, 57(1-2), 152-165.

Falls, A. H., and Schulte, W. M. (1992a). Theory of Three-Component, Three-Phase Displacement in Porous Media. *SPE*, 7(3), 377–384.

Falls, A. H., and Schulte, W. M. (1992b). Features of Three-Component, Three-Phase Displacement in Porous Media. *SPE*, 7(4), 426–432.

Falls, A. H., Hlrasakl, G. J., Patzek, T. W., Gauglltz, D. A., Miller, D. D., and Ratulowskl, T. (1988). Development of a Mechanistic Foam Simulator: The Population Balance and Generation by Snap-Off. *SPE*RE, 3, 884-893

Farajzadeh, R., Krastev, R., and Zitha, P. L. J. (2008). Properties of Foam Films Stabilized by AOS Surfactant. *Colloids and Surfaces A: Engineering Aspects*, 324, 35-40

Foundain, J. C. (1998) Technologies for Dense Nonaqueous Phase Liquid Source Zone Remediation, GWRTAC Technoloty Evaluation Report, TE-98-02.

Friedmann, F., Chen, W. H., and Gaugntz, P. A. (1991). Experimental and Simulation Study of High-Temperature Foam Displacement in Porous Media. *SPERE*, 6(1), 37-45.

Goloub, T.P., Koopal, L.K., Bijsterbosch, B.H., and Sidorova, M.P. (1996). Adsorption of Cationic Surfactants on Silica. Surface Charge Effects, *Langmuir* (12) 3188-3194.

Grigg, R.B., and Bai, B. (2005). Sorption of Surfactant Used in CO_2 Flooding onto Five Minerals and Three Porous Media, Presented at the SPE International Symposium on Oilfield Chemistry, 2-4 February.

Haley, J. L., Hanson B., Enfield C., and Glass, J. (1991). Evaluating the Effectiveness of Ground Water Extraction Systems, *Ground Water Monitoring & Remediation*, 11(3), 119-124.

Helfferich, F. G. and Klein, G. ed. (1970). *Multicomponent Chromatography: Theory of Interference*. New York City: Marcel Dekker.

Helfferich, F. G. (1981). Theory of Multicomponent, Multiphase Displacement in Porous Media. *SPE*, 21(1), 51-62.

Hirasaki, G. J., Miller, C. A., Szafranski, R., Lawson, J. B., and Akiya, N. (1997). Surfactant/Foam Process for Aquifer Remediation. SPE International Symposium on Oilfield Chemistry, 18-21 February, Houston, Texas.

Hirasaki G. J., Jackson, R. E., Jin, M., Lawson, J. B., Londergan, J., Meinardus, H., Miller, C. A., Pope, G. A., Szafranski, R., and Tanzil, D. (2000). Field Demonstration of the Surfactant/Foam Preocess for Remediation of a Heterogeneous Aquifer Contaminated with DNAPL. In *NAPL Removeal: Surfactant, Foams, and Microemulstions*, ed. Fiorenza, S., Miller, C. A., Oubre, C. L. and Ward, C. H. Boca Raton: Lewis Publishers.

Jackson, R. E. (1993). Surfactant-enhanced remediation of DNAPL zones in granular aquifer systems. *Remediation Journal*, 4(1), 77-91.

Jimenez, A. I. and Radke, C. J. (1989). Dynamic stability of foam lamellae flowing through a periodically constricted pore In *Oil Field Chemistry: Enhanced Recovery and Production Stimulation*, ed. Borchardt, J. K. and Yen, T. F., 396, 460-479. Washington, DC: Symposium Series, ACS.

Kam, S. I. and Rossen, W. R. (2003). A Model for Foam Generation in Homogeneous Media. *SPEJ*, 8, 417-425.

Khatib, Z. I., Hlrasaki, G. J., and Falls, A. H. (1988). Effects of Capillary Pressure on Coalescence and Phase Mobilities in Foams Flowing Through Porous Media. *SPEJ*, 3(3), 919–926.

Koczo, K., Lobo, L. A., and Wasan, D. T. (1992). Effect of Oil on Foam Stability: Aqueous Foams Stabilized by Emulsions. *Journal of Colloid and Interface Science*, 150(2), 492–506.

Kovscek, A. R. and Radke, C. J. (1994). Fundamentals of foam transport in porous media, In *Foams: Fundamentals and applications in the Petroleum Industry*. ed. Schramm, L. L., ACS Advances in Chemistry Series, N. 242, ACS.

Kovscek, a. R., Patzek, T. W., and Radke, C. J. (1995). A mechanistic population balance model for transient and steady-state foam flow in Boise sandstone. *Chemical Engineering Science*, 50(23), 3783–3799

Kovsek, A. R., Patzek, T. W., and Radke, C. J. (1997). Mechanistic Foam Flow Simulation in Heterogeneous and Multidimensional Porous Media. *SPEJ*. 2(4): 511-526.

Lake, L. (1989). *Enhanced Oil Recovery*. Englewood Cliffs, New Jersey: Prentice Hall

Lau, E. C. and Coombe, D. A. (1994). History Matching the Steam/Foam Injecton Process in a Thick Athabasca Tar Sand Reservoir, *J. Can. Pet. Tech.*, 33(1), 56-63.

Law, D. H.-S., Yang, Z. M., and Stone, T. W. (1992). Effect of the Presence of Oil on Foam Performance: A Field Simulation Study. *SPEJ*, 7(2): 228-236.

Lee, H. O., Heller, J. P., and Hoefer, A. M. W. (1991). Change in Apparent Viscosity of CO2 Foam With Rock Permeability. *SPE*. 6(4): 421-428.

Lee, S and Kam, S. I. (2013). Enhanced Oil Recovery by Using CO_2 Foams: Fundamentals and Field Applications In *Enhanced Oil Recovery Field Case Studies*. ed. Sheng, J., Elsevier.

Londergan, J. T., Meinardus, H. W., Mariner, P. E., Jackson, R. E., Brown, C. L., Dwarakanath, V., Pope, G. A., and Taffinder, S. (2001). DNAPL Removal from a Heterogeneous Alluvial Aquifer by Surfactant-Enhanced Aquifer Remediation. *Ground Water Monitoring & Remediation*, *21*(4), 57–67.

Lundegard, P. D., and LaBrecque, D. (1995). Air sparging in a sandy aquifer (Florence, Oregon, U.S.A.): Actual and apparent radius of influence. *Journal of Contaminant Hydrology*, 19, 1-27.

Ma, K., Lopez-salinas, J. L., Puerto, M. C., Miller, C. A., Biswal, S. L., and Hirasaki, G. J. (2013). Estimation of Parameters for the Simulation of Foam Flow through Porous Media. Part 1: The Dry-Out Effect. *Energy & Fuels*, 27, 2363–2375.

Mackay, D. M. and Cherry, J. A. (1989). Groundwater contamination: pump-and-treat remediation. *Environmental Science & Technology*, *23*(6), 630–636.

Mamun, C. K., Rong, J. G., Kam, S. I., Liljestrand, H. M., and Rossen, W. R. (2002). Extending Foam Technology from Improved Oil Recovery to Environmental Remediation. SPE Annual Technical Conference and Exhibition, 29 September-2 October, San Antonio, Texas.

Mannhardt, K., and Svorstøl, I. (1999). Effect of oil saturation on foam propagation in Snorre reservoir core. *Journal of Petroleum Science and Engineering*, 23(3), 189–200.

Mayberry, D. J., Afsharpoor, A., and Kam, S. I. (2008). The Use of Fractional-Flow Theory for Foam Displacement in Presence of Oil. *SPE*, 11(4), 707-718.

Miller, R. (1996). Report: In-well Vapor Stripping – Technology Overview Source: GWRTAC, TO-97-01.

Mohammadi, S. S., Coombe, D. A., and Stevenson, V. M. (1993). Test of Steam Foam Process for Mobility Control in South Casper Creek Reservoir, *J. Can. Pet. Tech.*, 32(10), 49-54.

Mulligan, C.N., Yong, R.N. and Gibbs, B.F. (2001). Remediation Technologies for Metal-Contaminated Soils and Groundwater: an evaluation, *Engineering Geology*, 60(1-4), 193-207.

Myers, T. J. and Radke, C. J. (2000). Transient Foam Displacement in the Presence of Residual Oil: Experiment and Simulation Using a Population-Balance Model. *Ind. Eng. Chem. Res.*, 39, 2725-2741.

Nikolov, A. D., Wasan, D. T., Huang, D. W., and Edwards, D. A. (1986). The Effect of Oil on Foam Stability: Mechanisms and Implications for Oil Displacement by Foam in Porous Media. SPE Annual Technical Conference and Exhibition, 5-8 October, New Orleans, Louisiana.

NRC. (1994). *Alternatives for Ground-water Cleanup*, National Academy Press, Washington D.C.

Oolman, T., Godard, S. T., Pope, G. A., Jin, M., & Kirchner, K. (1995). DNAPL Flow Behavior in a Contaminated Aquifer: Evaluation of Field Data. *Ground Water Monitoring & Remediation*, 15(4), 125–137.

Pankow, J. F. and Cherry, J. A. (1996). *Dense Chlorinated Solvents and other DNAPLs in Groundwater: History, Behavior, and Remediation*, Waterloo Press, Portland, Oregon.

Patzek, T. W. and Myhill, N. A. (1989) Simulation of the Bishop Steam Foam Pilot. SPE California Regional Meeting, 5-7 April, Bakersfield, California.

Peters, R. W., Enzien, M. V., Michelsen, D. L. and Frand, J. R. (1996). Solubilization of NAPLs in Foam Enhanced Remediation. *Proc.*, Fourth Great Lakes Geotechnical and Geoenvironmental Conference on In-Situ Remediation of Contaminated Sites, ed. Reddy, K. R., 255-261. Chicago: University of Illinois at Chacago.

Pope, G. A. (1980). The Application of Fractional Flow Theory to Enhanced Oil Recovery. *SPE*, 20(3), 191-205.

Prud'Homme, R. K. and Khan, S. (Eds.) (1996). *Foams: Theory, Measurements and Applications*. New York: Marcel Dekker.

Ramirez, W. F., Shuler, P. J., and Friedman, F. (1980). Convection, Dispersion, and Adsorption of Surfactants in Porous Media. *SPEJ*, 20(6), 430-438.

Roof, J.G. (1970). Snap-Off of Oil Droplets in Water-Wet Pores. *SPEJ*, 10(1), 85-90.

Rosman, A., and Kam, S. I. (2009). Modeling Foam-diversion Process Using Three-phase Fractional Flow Analysis in a Layered System. *Energy Sources, Part A*, 936–955.

Rossen, W. R., and Zhou, Z. H. (1995). Modeling Foam Mobility at the "Limiting Capillary Pressure." *SPE Adv. Technol.*, 3(1). 146-153.

Rossen, W. R. (1996), Foams in Enhanced Oil Recovery. In *Foams: Theory, Measurements and Application*, ed. Prud'Homme, R. K. and Khan, S. New York: Marcel Dekker.

Rossen, W. R., Zeilinger, S. C., Shi, J.-X., and Lim, M. T. (1999). Simplified Mechanistic Simulation of Foam Processes in Porous Media. *SPEJ*, 4(3), 279-287.

Rothmel, R. K., Peters, R. W., Martin, E. ST., and Deflaun, M. F. (1998). Surfactant Foam/Bioaugmentation Technology for In-Situ Treatment of TCE-DNAPLs. *Envirion. Sci. Technol.*, 32(11), 1667-1675.

Roostapour, A. and Kam, S.I. (2012). Modeling foam delivery mechanisms in deep vadose-zone remediation using method of characteristics. *Journal of Hazardous Materials*. 243, 37-51.

Roostapour, A. and Kam, S.I. (2013). Anomalous Foam-Fractional-Flow Solutions at High-Injection Foam Quality. *SPEREE*, 16(1), 40-50.

Schwille, F. (1988). *Dense Chlorinated Solvents in Porous and Fractured Media: Model Experiments*. Lewis Publishers, Chelsea, Michigan.

Schramm, L.L. (Ed.) (1994). *Foams: Fundamentals and Applications in the Petroleum Industry*. 242. Washington, DC: Advances in Chemistry Series, ACS.

Shrivastava, V. K., Coombe, D. A., Singhal, A. K., and Belgrave, J. D. M. (1999). Numerical Simulation of Foam Flooding For Sweep Improvement. J. Can. Pet. Tech., 38(13), 1-12

Staudinger, J., Roberts, P. V., and Hartley J. D. (1997). A Simplified Approach for Preliminary Design and Process Performance Modeling of Soil Vapor Extraction Systems. *Environmental Progress*, 16(3), 215-227.

Surguchev, L. M., Coombe, D. A., Hanssen, J. E., and Svorstøl, I. (1995). Simulation of WAG and Gas Injection with Potential Sweep Improvement by Application of Foam, 8th European IOR Symposium, Vienna, Austria.

Svorstøl, I., Vassenden, F., and Mannhardt, K. (1996). Laboratory Studies for Design of a Foam Pilot in the Snorre Field. SPE/DOE Improved Oil Recovery Symposium, 21-24 April, Tulsa, Oklahoma.

Taber, J.J. (1969). Dynamic and Static Forces Required to Remove a Discontinuous Oil Phase from Porous Media Containing Both Oil and Water, *SPEJ*, 9(1), 3-12.

Trogus, F.J., Sophany, T., Schechter, R.S., and Wade, W.H. (1977). Static and Dynamic Adsorption of Anionic and Nonionic Surfactants, *SPEJ*, 337-344.

U.S. EPA. 1990. Subsurface Contamination Reference Guide. EPA/540/2-90/011.

U.S. EPA. 2004. DNAPL Remediation: Selected Projects Approaching Regulatory Closure. EPA 542-R-04-016.

Zanganeh, M. N., Kam, S. I., LaForce, T. C., and Rossen, W. R. (2011). The Method of Characteristics Applied to Oil Displacement by Foam. *SPE*, 16(1), 8-23.

Zitha, P. L. J. and Du, D. X. (2010). A New Stochastic Bubble Population Model for Foam Flow in Porous Media. *Transp. Porous Med.*, 83, 603-621.

APPENDIX: LETTERS OF PERMISSION

JOHN WILEY AND SONS LICENSE
TERMS AND CONDITIONS

Apr 07, 2014

This is a License Agreement between Seungjun Lee ("You") and John Wiley and Sons ("John Wiley and Sons") provided by Copyright Clearance Center ("CCC"). The license consists of your order details, the terms and conditions provided by John Wiley and Sons, and the payment terms and conditions.

All payments must be made in full to CCC. For payment instructions, please see information listed at the bottom of this form.

License Number	3363820679523
License date	Apr 07, 2014
Licensed content publisher	John Wiley and Sons
Licensed content publication	Remediation
Licensed content title	Surfactant-enhanced remediation of DNAPL zones in granular aquifer systems
Licensed copyright line	Copyright © 1993 Wiley Periodicals, Inc., A Wiley Company
Licensed content author	Richard E. Jackson
Licensed content date	Dec 12, 2006
Start page	77
End page	91
Type of use	Dissertation/Thesis
Requestor type	University/Academic
Format	Print and electronic
Portion	Figure/table
Number of figures/tables	2
Original Wiley figure/table number(s)	Figure 1 and 4
Will you be translating?	No
Title of your thesis / dissertation	MODELING OF FOAM FLOW IN POROUS MEDIA FOR SUBSURFACE ENVIRONMETAL REMEDIATION
Expected completion date	Aug 2014
Expected size (number of pages)	120

Total 0.00 USD

Terms and Conditions

Terms and Conditions are not available at this time.

If you would like to pay for this license now, please remit this license along with your payment made payable to "COPYRIGHT CLEARANCE CENTER" otherwise you will be invoiced within 48 hours of the license date. Payment should be in the form of a check or money order referencing your account number and this invoice number RLNK501271933.

Once you receive your invoice for this order, you may pay your invoice by credit card. Please follow instructions provided at that time.

Make Payment To:
Copyright Clearance Center
Dept 001
P.O. Box 843006
Boston, MA 02284-3006

For suggestions or comments regarding this order, contact RightsLink Customer Support:customercare@copyright.com or +1-877-622-5543 (toll free in the US) or +1-978-646-2777.

Gratis licenses (referencing $0 in the Total field) are free. Please retain this printable license for your reference. No payment is required.

SOCIETY OF PETROLEUM ENGINEERS LICENSE
TERMS AND CONDITIONS

Apr 07, 2014

This is a License Agreement between Seungjun Lee ("You") and Society of Petroleum Engineers ("Society of Petroleum Engineers") provided by Copyright Clearance Center ("CCC"). The license consists of your order details, the terms and conditions provided by Society of Petroleum Engineers, and the payment terms and conditions.

License Number	3363830006033
License date	Apr 07, 2014
Licensed content publisher	Society of Petroleum Engineers
Licensed content publication	SPE Reservoir Engineering
Licensed content title	Effects of Capillary Pressure on Coalescence and Phase Mobilities in Foams Flowing Through Porous Media
Licensed content author	Z.I. Khatib, Shell Development Co.;G.J. Hirasaki, Shell Development Co.;A.H. Falls, Shell Development Co. et al
Licensed content date	1988
Volume number	3
Issue number	03
Type of Use	Thesis/Dissertation
Requestor type	non-commercial/non-profit
SPE member	yes
SPE member number	3526890
Format	print and electronic
Portion	figures/tables/images
Number of figures/tables/images	1
Will you be translating?	no
Distribution	10
Order reference number	
Title of your thesis / dissertation	MODELING OF FOAM FLOW IN POROUS MEDIA FOR SUBSURFACE ENVIRONMETAL REMEDIATION
Expected completion date	Aug 2014
Estimated size (number of pages)	120
Billing Type	Credit Card
Credit card info	Visa ending in 2574
Credit card expiration	02/2015

Total 12.00 USD

Terms and Conditions

STANDARD TERMS AND CONDITIONS FOR REPRODUCTION OF MATERIAL

1. The Society of Petroleum Engineers, Inc. (“SPE”) holds the copyright for this material. By clicking "accept" in connection with completing this licensing transaction, you agree that the following terms and conditions apply to this transaction (along with the Billing and Payment terms and conditions established by Copyright Clearance Center, Inc. ("CCC"), at the time that you opened your RightsLink account and that are available at any time at).

2. SPE hereby grants to you a non-exclusive license to use this material. Licenses are for one-time use only with a maximum distribution equal to the number that you identified in the licensing process; any form of republication must be completed within six months from the date hereof (although copies prepared before then may be distributed thereafter); and any electronic posting is limited to the period identified in the licensing process.

3. You may not alter or modify the material in any manner (except that you may use, within the scope of the license granted, one or more excerpts from the copyrighted material, provided that the process of excerpting does not alter the meaning of the material or in any way reflect negatively on SPE or any writer of the material or their employer), nor may you translate the material into another language.

4. Total excerpts from the license material may not exceed thirty percent (30%) of the total text. Not more than five (5) excerpts, figures, tables, or images may be used from any given paper. Multiple permission requests may not be used to exceed these limits.

5. SPE reserves all rights not specifically granted in the combination of (i) the license details provided by you and accepted in the course of this licensing transaction, (ii) these terms and conditions and (iii) CCC's Billing and Payment terms and conditions.

6. While you may exercise the rights licensed immediately upon issuance of the license at the end of the licensing process for the transaction, provided that you have disclosed complete and accurate details of your proposed use, no license is finally effective unless and until full payment is received from you (either by SPE or by CCC) as provided in CCC's Billing and Payment terms and conditions. If full payment is not received on a timely basis, then any license preliminarily granted shall be deemed automatically revoked and shall be void as if never granted. Further, in the event that you breach any of these terms and conditions or any of CCC's Billing and Payment terms and conditions, the license is automatically revoked and shall be void as if never granted. Use of materials as described in a revoked license, as well as any use of the materials beyond the scope of an unrevoked license, may constitute copyright infringement and SPE reserves the right to take any and all action to protect its copyright in the materials

13. This Agreement shall be governed and interpreted by the laws of the State of Texas, United States of America. Regardless of the place of performance or otherwise, the Agreement, and all schedules, amendments, modifications, alterations, or supplements thereto, will be governed by the laws of the State of Texas, United States of America. If any provisions of the Agreement are unenforceable under applicable law, the remaining provisions shall continue in full force and effect.

Other Terms and Conditions: None
v1.1

If you would like to pay for this license now, please remit this license along with your payment made payable to "COPYRIGHT CLEARANCE CENTER" otherwise you will be invoiced within 48 hours of the license date. Payment should be in the form of a check or money order referencing your account number and this invoice number RLNK501271945.

Once you receive your invoice for this order, you may pay your invoice by credit card. Please follow instructions provided at that time.

Make Payment To:
Copyright Clearance Center
Dept 001
P.O. Box 843006
Boston, MA 02284-3006

For suggestions or comments regarding this order, contact RightsLink Customer Support:customercare@copyright.com or +1-877-622-5543 (toll free in the US) or +1-978-646-2777.

Gratis licenses (referencing $0 in the Total field) are free. Please retain this printable license for your reference. No payment is required.

ELSEVIER LICENSE
TERMS AND CONDITIONS

Apr 07, 2014

This is a License Agreement between Seungjun Lee ("You") and Elsevier ("Elsevier") provided by Copyright Clearance Center ("CCC"). The license consists of your order details, the terms and conditions provided by Elsevier, and the payment terms and conditions.

All payments must be made in full to CCC. For payment instructions, please see information listed at the bottom of this form.

Supplier	Elsevier Limited The Boulevard,Langford Lane Kidlington,Oxford,OX5 1GB,UK
Registered Company Number	1982084
Customer name	Seungjun Lee
Customer address	1826 S Brightside View Dr APT B Baton Rouge, LA 70820
License number	3363830238714
License date	Apr 07, 2014
Licensed content publisher	Elsevier
Licensed content publication	Elsevier Books
Licensed content title	Enhanced Oil Recovery Field Case Studies
Licensed content author	S. Lee,S.I. Kam
Licensed content date	2013
Number of pages	39
Start Page	23
End Page	61
Type of Use	reuse in a thesis/dissertation
Intended publisher of new work	other
Portion	figures/tables/illustrations
Number of figures/tables/illustrations	1
Format	both print and electronic
Are you the author of this Elsevier chapter?	Yes
How many pages did you author in this Elsevier book?	35

Will you be translating?	No
Title of your thesis/dissertation	MODELING OF FOAM FLOW IN POROUS MEDIA FOR SUBSURFACE ENVIRONMETAL REMEDIATION
Expected completion date	Aug 2014
Estimated size (number of pages)	120
Elsevier VAT number	GB 494 6272 12
Permissions price	0.00 USD
VAT/Local Sales Tax	0.00 USD / 0.00 GBP
Total	0.00 USD
Terms and Conditions	

INTRODUCTION

1. The publisher for this copyrighted material is Elsevier. Byclicking "accept" in connection with completing this licensingtransaction, you agree that the following terms and conditions apply to thistransaction (along with the Billing and Payment terms and conditionsestablished by Copyright Clearance Center, Inc. ("CCC"), at the timethat you opened your Rightslink account and that are available at any time at http://myaccount.copyright.com).

Licensing material from an Elsevier book: A hyper-text link must be includedto the Elsevier homepage at http://www.elsevier.com . Allcontent posted to the web site must maintain the copyright information line onthe bottom of each image.

Posting licensed content on Electronic reserve: In addition to the above the following clausesare applicable: The web site must be password-protected and made available onlyto bona fide students registered on a relevant course. This permission isgranted for 1 year only. You may obtain a new license for future websiteposting.

For journal authors: the following clauses are applicable inaddition to the above: Permission granted is limited to the author acceptedmanuscript version* of your paper.

*Accepted Author Manuscript (AAM) Definition: An accepted authormanuscript (AAM) is the author's version of the manuscript of an article thathas been accepted for publication and which may include any author-incorporatedchanges suggested through the processes of submission processing, peer review,and editor-author communications. AAMs do not include other publishervalue-added contributions such as copy-editing, formatting, technicalenhancements and (if relevant) pagination.

21. Other Conditions:

v1.7

If you would like to pay for this license now, please remit this license along with your payment made payable to "COPYRIGHT CLEARANCE CENTER" otherwise you will be invoiced within 48 hours of the license date. Payment should be in the form of a check or money order referencing your account number and this invoice number RLNK501271952.

Once you receive your invoice for this order, you may pay your invoice by credit card. Please follow instructions provided at that time.

Make Payment To:
Copyright Clearance Center
Dept 001
P.O. Box 843006
Boston, MA 02284-3006

For suggestions or comments regarding this order, contact RightsLink Customer Support:customercare@copyright.com or +1-877-622-5543 (toll free in the US) or +1-978-646-2777.

Gratis licenses (referencing $0 in the Total field) are free. Please retain this printable license for your reference. No payment is required.

SOCIETY OF PETROLEUM ENGINEERS LICENSE
TERMS AND CONDITIONS

Apr 07, 2014

This is a License Agreement between Seungjun Lee ("You") and Society of Petroleum Engineers ("Society of Petroleum Engineers") provided by Copyright Clearance Center ("CCC"). The license consists of your order details, the terms and conditions provided by Society of Petroleum Engineers, and the payment terms and conditions.

License Number	3363830537135
License date	Apr 07, 2014
Licensed content publisher	Society of Petroleum Engineers
Licensed content publication	SPE Reservoir Engineering
Licensed content title	Change in Apparent Viscosity of CO2 Foam With Rock Permeability
Licensed content author	H.O. Lee, New Mexico Petroleum Recovery Research Center;J.P. Heller, New Mexico Petroleum Recovery Research Center;A.M.W. Hoefer, New Mexico Petroleum Recovery Research Center et al
Licensed content date	1991
Volume number	6
Issue number	04
Type of Use	Thesis/Dissertation
Requestor type	academic/educational
SPE member	yes
SPE member number	3526890
Format	print and electronic
Portion	figures/tables/images
Number of figures/tables/images	1
Will you be translating?	no
Distribution	10
Order reference number	
Title of your thesis / dissertation	MODELING OF FOAM FLOW IN POROUS MEDIA FOR SUBSURFACE ENVIRONMETAL REMEDIATION
Expected completion date	Aug 2014
Estimated size (number of pages)	120
Billing Type	Credit Card
Credit card info	Visa ending in 2574

Credit card expiration	02/2015
Total	12.00 USD

Terms and Conditions

STANDARD TERMS AND CONDITIONS FOR REPRODUCTION OF MATERIAL

1. The Society of Petroleum Engineers, Inc. (“SPE”) holds the copyright for this material. By clicking "accept" in connection with completing this licensing transaction, you agree that the following terms and conditions apply to this transaction (along with the Billing and Payment terms and conditions established by Copyright Clearance Center, Inc. ("CCC"), at the time that you opened your RightsLink account and that are available at any time at).

2. SPE hereby grants to you a non-exclusive license to use this material. Licenses are for one-time use only with a maximum distribution equal to the number that you identified in the licensing process; any form of republication must be completed within six months from the date hereof (although copies prepared before then may be distributed thereafter); and any electronic posting is limited to the period identified in the licensing process.

3. You may not alter or modify the material in any manner (except that you may use, within the scope of the license granted, one or more excerpts from the copyrighted material, provided that the process of excerpting does not alter the meaning of the material or in any way reflect negatively on SPE or any writer of the material or their employer), nor may you translate the material into another language.

4. Total excerpts from the license material may not exceed thirty percent (30%) of the total text. Not more than five (5) excerpts, figures, tables, or images may be used from any given paper. Multiple permission requests may not be used to exceed these limits.

5. SPE reserves all rights not specifically granted in the combination of (i) the license details provided by you and accepted in the course of this licensing transaction, (ii) these terms and conditions and (iii) CCC's Billing and Payment terms and conditions.

6. While you may exercise the rights licensed immediately upon issuance of the license at the end of the licensing process for the transaction, provided that you have disclosed complete and accurate details of your proposed use, no license is finally effective unless and until full payment is received from you (either by SPE or by CCC) as provided in CCC's Billing and Payment terms and conditions. If full payment is not received on a timely basis, then any license preliminarily granted shall be deemed automatically revoked and shall be void as if never granted. Further, in the event that you breach any of these terms and conditions or any of CCC's Billing and Payment terms and conditions, the license is automatically revoked and shall be void as if never granted. Use of materials as described in a revoked license, as well as any use of the materials beyond the scope of an unrevoked license, may constitute copyright infringement and SPE reserves the right to take any and all action to protect its copyright in the materials

13. This Agreement shall be governed and interpreted by the laws of the State of Texas, United States of America. Regardless of the place of performance or otherwise, the Agreement, and all schedules, amendments, modifications, alterations, or supplements thereto, will be governed by the laws of the State of Texas, United States of America. If any provisions of the Agreement are unenforceable under applicable law, the remaining provisions shall continue in full force and effect.

Other Terms and Conditions: None
v1.1

If you would like to pay for this license now, please remit this license along with your payment made payable to "COPYRIGHT CLEARANCE CENTER" otherwise you will be invoiced within 48 hours of the license date. Payment should be in the form of a check or money order referencing your account number and this invoice number RLNK501271955.

Once you receive your invoice for this order, you may pay your invoice by credit card. Please follow instructions provided at that time.

Make Payment To:
Copyright Clearance Center
Dept 001
P.O. Box 843006
Boston, MA 02284-3006

For suggestions or comments regarding this order, contact RightsLink Customer Support:customercare@copyright.com or +1-877-622-5543 (toll free in the US) or +1-978-646-2777.

Gratis licenses (referencing $0 in the Total field) are free. Please retain this printable license for your reference. No payment is required.

SOCIETY OF PETROLEUM ENGINEERS LICENSE
TERMS AND CONDITIONS

Apr 07, 2014

This is a License Agreement between Seungjun Lee ("You") and Society of Petroleum Engineers ("Society of Petroleum Engineers") provided by Copyright Clearance Center ("CCC"). The license consists of your order details, the terms and conditions provided by Society of Petroleum Engineers, and the payment terms and conditions.

License Number	3363830684010
License date	Apr 07, 2014
Licensed content publisher	Society of Petroleum Engineers
Licensed content publication	SPE Proceedings
Licensed content title	Laboratory Studies for Design of a Foam Pilot in the Snorre Field
Licensed content author	I. Svorstol, I. Svorstol;F. Vassenden, F. Vassenden;K. Mannhardt, K. Mannhardt et al
Licensed content date	1996
Type of Use	Thesis/Dissertation
Requestor type	academic/educational
SPE member	yes
SPE member number	3526890
Format	print and electronic
Portion	figures/tables/images
Number of figures/tables/images	1
Will you be translating?	no
Distribution	10
Order reference number	
Title of your thesis / dissertation	MODELING OF FOAM FLOW IN POROUS MEDIA FOR SUBSURFACE ENVIRONMETAL REMEDIATION
Expected completion date	Aug 2014
Estimated size (number of pages)	120
Billing Type	Credit Card
Credit card info	Visa ending in 2574
Credit card expiration	02/2015
Total	12.00 USD
Terms and Conditions	

STANDARD TERMS AND CONDITIONS FOR REPRODUCTION OF MATERIAL

1. The Society of Petroleum Engineers, Inc. (“SPE”) holds the copyright for this material. By clicking "accept" in connection with completing this licensing transaction, you agree that the following terms and conditions apply to this transaction (along with the Billing and Payment terms and conditions established by Copyright Clearance Center, Inc. ("CCC"), at the time that you opened your RightsLink account and that are available at any time at).

2. SPE hereby grants to you a non-exclusive license to use this material. Licenses are for one-time use only with a maximum distribution equal to the number that you identified in the licensing process; any form of republication must be completed within six months from the date hereof (although copies prepared before then may be distributed thereafter); and any electronic posting is limited to the period identified in the licensing process.

3. You may not alter or modify the material in any manner (except that you may use, within the scope of the license granted, one or more excerpts from the copyrighted material, provided that the process of excerpting does not alter the meaning of the material or in any way reflect negatively on SPE or any writer of the material or their employer), nor may you translate the material into another language.

4. Total excerpts from the license material may not exceed thirty percent (30%) of the total text. Not more than five (5) excerpts, figures, tables, or images may be used from any given paper. Multiple permission requests may not be used to exceed these limits.

5. SPE reserves all rights not specifically granted in the combination of (i) the license details provided by you and accepted in the course of this licensing transaction, (ii) these terms and conditions and (iii) CCC's Billing and Payment terms and conditions.

6. While you may exercise the rights licensed immediately upon issuance of the license at the end of the licensing process for the transaction, provided that you have disclosed complete and accurate details of your proposed use, no license is finally effective unless and until full payment is received from you (either by SPE or by CCC) as provided in CCC's Billing and Payment terms and conditions. If full payment is not received on a timely basis, then any license preliminarily granted shall be deemed automatically revoked and shall be void as if never granted. Further, in the event that you breach any of these terms and conditions or any of CCC's Billing and Payment terms and conditions, the license is automatically revoked and shall be void as if never granted. Use of materials as described in a revoked license, as well as any use of the materials beyond the scope of an unrevoked license, may constitute copyright infringement and SPE reserves the right to take any and all action to protect its copyright in the materials

7. You must include the appropriate copyright and permission notice and disclaimer in connection with any reproduction of the licensed material.The copyright information is found on the front page of the paper immediately under the title and author. This statement will then be followed with the disclaimer, “Further reproduction prohibited without

permission." Examples:1) Copyright 1990, Society of Petroleum Engineers Inc.Copyright 1990, SPE. Reproduced with permission of SPE. Further reproduction prohibited without permission.2) Copyright 2010, IADC/SPE Drilling Conference and ExhibitionCopyright 2010, IADC/SPE Drilling Conference and Exhibition. Reproduced with permission of SPE. Further reproduction prohibited without permission.3) Copyright 2008, Offshore Technology ConferenceCopyright 2008, Offshore Technology Conference. Reproduced with permission of OTC. Further reproduction prohibited without permission.4) Copyright 2005, International Petroleum Technology ConferenceCopyright 2005, International Petroleum Technology Conference. Reproduced with permission of IPTC. Further reproduction prohibited without permission.If for any reason, the copyright on the paper is missing or unclear, please follow Example 1 above, using SPE as the default copyright holder. SPE administers copyright for OTC, IPTC and other joint events on behalf of all parties in those events.

8. SPE makes no representations or warranties with respect to the licensed material and adopts on its own behalf the limitations and disclaimers established by CCC on its behalf in its Billing and Payment terms and conditions for this licensing transaction.

9. You hereby indemnify and agree to hold harmless SPE and CCC, and their respective officers, directors, employees and agents, from and against any and all claims arising out of your use of the licensed material other than as specifically authorized pursuant to this license.

10. This license is personal to you, but may be assigned or transferred by you to a business associate (or to your employer) if you give prompt written notice of the assignment or transfer to SPE. No such assignment or transfer shall relieve you of the obligation to pay the designated license fee on a timely basis (although payment by the identified assignee can fulfill your obligation).

11. This license may not be amended except in a writing signed by both parties (or, in the case of SPE, by CCC on SPE's behalf).

12. SPE hereby objects to any terms contained in any purchase order, acknowledgment, check endorsement or other writing prepared by you, which terms are inconsistent with these terms and conditions or CCC's Billing and Payment terms and conditions. These terms and conditions, together with CCC's Billing and Payment terms and conditions (which are incorporated herein), comprise the entire agreement between you and SPE (and CCC) concerning this licensing transaction. In the event of any conflict between your obligations established by these terms and conditions and those established by CCC's Billing and Payment terms and conditions, these terms and conditions shall control.

13. This Agreement shall be governed and interpreted by the laws of the State of Texas, United States of America. Regardless of the place of performance or otherwise, the Agreement, and all schedules, amendments, modifications, alterations, or supplements thereto, will be governed by the laws of the State of Texas, United States of America. If any

provisions of the Agreement are unenforceable under applicable law, the remaining provisions shall continue in full force and effect.

Other Terms and Conditions: None
v1.1

If you would like to pay for this license now, please remit this license along with your payment made payable to "COPYRIGHT CLEARANCE CENTER" otherwise you will be invoiced within 48 hours of the license date. Payment should be in the form of a check or money order referencing your account number and this invoice number RLNK501271958.

Once you receive your invoice for this order, you may pay your invoice by credit card. Please follow instructions provided at that time.

Make Payment To:
Copyright Clearance Center
Dept 001
P.O. Box 843006
Boston, MA 02284-3006

For suggestions or comments regarding this order, contact RightsLink Customer Support:customercare@copyright.com or +1-877-622-5543 (toll free in the US) or +1-978-646-2777.

Gratis licenses (referencing $0 in the Total field) are free. Please retain this printable license for your reference. No payment is required.

VITA

Seungjun Lee was born in August 1980 in Seoul, South Korea, as the son of Gwangwon Lee and Younghee Kwon. He received his B.S. degree from the Department of Geo-environment Engineering at Han Yang University, South Korea, in 2006 and M.S. degree in the Department of Petroleum Engineering at the University of Texas at Austin in December 2009. He joined the Craft and Hawkins Department of Petroleum Engineering at Louisiana State University for PhD study in 2010. His research interests are EOR and subsurface remediation using chemicals such as surfactants, polymers and foams. He had two years of military service (2001-2003) as an administrator at an armored company in the 32nd division, and has been married to Minjung Kim since 2008.